Doctoral Dissertation (Shinshu University)

Research on nanofiber-based multifunctional composites with shape memory and piezoelectric effects for energy harvesting

March 2021

GUAN XIAOYU

CONTENTS

Abstract

Smart piezoelectric and shape memory materials are widely used in many fields such as sensing, energy harvesting, automobile, aerospace and health monitoring. In recent years, both piezoelectric materials and shape memory polymer-based composites have attracted increasing attention owing to the favorable shape memory and piezoelectric effects. Among these applications, the popularity of flexible energy harvesters receives extensive investigation because of their high flexibility, which enables them applied in in wearable and implantable devices. Flexibility and functionality are key issues for their applications. However, most reported flexible composites only exhibit one kind of smart performance, and there are few reports on flexible multifunctional nanofibers for energy harvesting. Herein, multifunctional nanofibers from lead zirconate titanate (PZT) particles and shape memory polyurethane (SMPU) are prepared by electrospinning and melt spinning in this study. The resulting fibers and nanofibers obtained both piezoelectric and shape memory effects. To improve the dispersion, PZT particles were modified by silane coupling agents. The developed PZT/SMPU composite fibers are weaved into plain woven and coated with PVA films. The interdigitated electrodes are made on the surface of PZT/SMPU composite textiles and nanofibers to take

advantage of the piezoelectric effect along the longitudinal direction. The PZT/SMPU textiles and nanofibers were used to harvest energy from sinusoidal vibrations. The modified PZT 60% textiles can generate 55.6 mV, and the PZT 80 wt% nanofibers sample can produce a voltage of 120.3 mV (peak-to-peak). Due to the shape memory effect, the PZT/SMPU nanofibers can be easily deformed into desired shapes, which revealed their ability to realize energy harvesting in complex structures.

A large number of shape-memory polymers have been reported. The variations in recovery properties of shape-memory fibers, foams and nanofibers are discussed, and several reasons for the variations of recovery properties are also investigated. However, the aligned SMPU nanofibers are not presented yet. To understand the influence of aligned structures of SMPU nanofibers on the shape memory and mechanical performance, unidirectional SMPU nanofibers are fabricated by a specified spinning technique. Shape memory performance is improved, and the mechanical and shape memory properties with nanofiber directions are clarified. The results show that when the nanofiber alignment degree is 0° (parallel to the tensile direction), the aligned SMPU nanofibers exhibit eight times larger shape recovery stress, enhanced tensile strength (increased to 135%) and elastic modulus (increased to 313%), compared with random SMPU nanofibers. The aligned SMPU nanofibers with an alignment degree of 0° exhibit excellent shape memory properties with shape recovery rates larger

than 93%, shape fixity larger than 90%, and a dramatic increase of maximum shape recovery stress. Shape memory properties were influenced and controlled by nanofibers with different alignment degrees. Moreover, the developed aligned nanofibers exhibited good ability against stress relaxation and creep under constant strain or stress conditions in cyclic loading. The deformation processes and mechanisms of developed materials were discussed systematically based on both static and cyclic mechanical behavior and shape memory tests. Favorable shape memory properties such as high shape recovery rates, recovery stresses together with good biocompatibility endow the aligned SMPU nanofibers with wide applications. Therefore, the aligned SMPU nanofibers prepared in this study can be used as a potential smart scaffold and tissue repair material.

In addition to the pristine SMPU, the aligned structure of nanofibers also affects the mechanical, shape memory and piezoelectric properties in the composite system. It is imperative to analyze the influence of structures and alignment degrees on the piezoelectric effect. Thus, a multifunctional flexible energy harvester based on aligned PZT/SMPU nanofibers is presented. Due to its shape memory properties, it can be used with surfaces with curved and/or complex structures. Mechanical and thermomechanical analysis and energy harvesting tests were performed on random and aligned nanofibers to investigate the influence of nanofiber orientation and its shape memory properties. The results showed that compared with

random nanofibers, 0° aligned PZT/SMPU nanofibers (the direction of nanofibers is parallel to the tensile direction) demonstrate high mechanical, shape memory and energy harvesting properties. In particular, the energy harvesting properties such as output voltages increase by 5.4 times.

In addition, owing to the shape memory effect, the PZT/SMPU energy harvester can be deformed into various curved shapes in order to match complex structures while maintaining its original piezoelectric characteristics, which results in enhanced energy harvesting from curved surfaces. The developed energy harvester exhibits better piezoelectricity as a result of its nanofiber arrangement. Additionally, it offers a flexible ability to match various surfaces with complex structures, contributing to more effective energy harvesting.

Finally, due to the flexibility from the nanofiber structure and polymer matrix, flexible energy harvesters based on aligned nanofibers can improve the energy harvesting efficiency from body movement and keep the “right feeling” like clothes for humans. Herein, a flexible energy harvester based on PZT/SMPU nanofibers is prepared and made into wearable energy harvesters. The fabricated PZT/SMPU wearable energy harvesters transfer mechanical energy into electricity from the human body such as the wrist, fingers and neck. They exhibit various output voltages owing to different body motions, including bending, twisting and applying pressure. The results indicate that there is an optimal alignment to the degree of

nanofibers applicable to different types of human motion. The PZT/SMPU energy harvester with 0°, 45° and 90° alignment degrees generate output voltages as high as 23 mV, 55 mV and 36 mV, respectively, during the twisting and release cycles. This corresponds to the consistency between the directions of nanofiber alignment and strain. These results provide insights and methods for the optimal arrangement of nanofibers in wearable devices, which facilitates to improve the energy harvesting efficiency from the movement of different body parts.

Chapter 1: General introduction

1.1 Polymer-based composites

To date, composite materials have been used in many fields, including biology [1, 2], engineering [3, 4], aerospace [5, 6], sports [7], and energy harvesting [8-10], because of the excellent performances obtained from the combination of matrices and fillers [11]. Many researchers have combined fillers and matrices to create materials with new functions and improve the material performance [12-14]. The composites materials are divided into three types including polymer matrix composites, ceramic matrix composites and metal matrix composites, according to the concept of the matrix [15].

Polymers play an important role in composite materials for different applications ranged from daily necessities to industrial products. Due to the flexibility [16], lightweight [17], high strength [18] and various functional properties [19], polymer-based composites have attracted a lot of attention, and their applications are expanded into many advanced fields such as buildings [20], energy storage devices [21], civil infrastructure [22], military [23] and aerospace [24], etc. Polymer composites have been prepared from natural polymers or fibers instead of synthetic materials, due to their eco-friendliness [25]. These composites produced from biological materials such as wood [26], cellulose [27] and crops [28], can decrease the waste in the synthesis process [29]. Different methods are employed to prepare various functional polymer-based composites for many applications, including electrospinning [30], melt-extrusion [31], solution mixing [32], latex technology [33], and in situ methods [34].

1.2 Nanofillers for polymer-based composites

Nanocomposites made from a series of organized functional nano-components [35] have rapidly become a hot topic and attracted increasing attention. In general, nanofillers (nanoparticles, nanorods, nanotubes, nanosheets, nanofibers, nanowhiskers and nanolayers) are uniformly dispersed in the polymer matrix [33], which leads to the formation of nanocomposites. Due to their great specific surface area [36], high surface energy [33] and small size [33], these nanofibers endow nanocomposites with multi-functional abilities [37], high fracture and mechanical properties [38]. Therefore, they can be applied in various areas such as sensors [39], actuators [40], energy storage [41], photocatalysts [42], electronics [43] and drug delivery [44].

Even a small amount of added nanofillers (lower than 10 wt%) can significantly improve the elastic modulus, tensile strength [44], electrical conductivity [45], gas barrier [46] and thermal conductivity [47] of nanocomposites. The dispersion of nanofillers in the polymer matrix and the interface between different phases are still key issues for nanocomposites with high content nanofillers. This is because a high amount of nanofillers in the polymer matrix can create a high conductive network. Nanocomposites composed of a high amount of nanofillers have distinct features such as energy storage [48], piezoelectricity [49], gas barrier [50] and flame retardant properties [51].

It has been reported that the mechanism of how aggregation [52] and homogeneous dispersion of nanofillers affect the performance of nanocomposites. This can be mainly

attributed to the poor interfacial load transfer, aggregation of fillers and interfacial interaction [53]. To increase the dispersion of nanofillers in the polymer matrix, surface modifications [54] are used to improve the interface between nanofillers and the polymer matrix. The surface treatment of polymer and nanofillers in nanocomposite includes enhanced interfacial interaction [55], grafting modification [56], induced surface roughness [54] and in-situ polymerization [57], which results in a well-dispersed nanocomposite system and high mechanical properties.

1.3 Nanofibers

Electrospinning is capable of fabricating a wide range of polymer fibers with a diameter from the nanoscale to macroscale [58]. Different from traditional fiber production processes like wet spinning and melt spinning, polymeric solutions are derived and stretched by the applied high electric field [59], which is deposited in the form of nanofibers mats. Electrospun nanofibers are light-weight, inexpensive, easy availability and self-assembly [60, 61], which depends on different fabrication parameters. It indicates that electrospinning is a cost-effective and energy-saving method to prepare nanofibers continuously [62]. The characteristics of polymeric solutions (the concentration and conductivity of the solution, and molecular weight) and fabrication parameters (the applied voltage, feed speed of solution, collector speed and displacements) significantly affect the surface morphology and functional properties of prepared nanofibers, such as diameters and orientation [63, 64]. Electrospun nanofibers exhibit many superior properties like a high surface area [65],

high adsorption capacity [66] and large porosity [67]. Such advantages enable them to apply in many potential areas such as sensors [68], wastewater treatment [69], medical protection [70] and biomaterials [71]. Traditional fiber-reinforced composites are prepared by physically combining more than two components such as carbon [72], Poly(Butylene Succinate) [73], and glass fibers [74], which can perform as structural supports to reinforce the matrix. However, nanofiber-based composites can be controlled and designed into random or uniaxial structures [75]. Moreover, they are endowed with flexibility and functional properties from the polymer matrix and functional fillers [76, 77]. Many nanofiber structures have been fabricated such as random, uniaxial and yarn architectures [78, 79], providing isotropic reinforcement or transmit signals along the nanofiber direction for nanofiber-based composites [80, 81].

1.4 Shape memory polymers

As one type of smart material, shape memory polymers (SMPs) have attracted wide attention since their discovery. Owing to the shape memory effect, SMPs are endowed with the ability to recover their original shape from a different temporary shape or expand its volume to match various designed complex structures [82]. The SMP can be actuated by some external stimulus including temperature [83, 84], chemicals [85], water [86], light [87] and magnetic fields [88], as multi-functional materials [89]. In particular, because of its excellent shape memory effects, biocompatibility [90] and biodegradability [91], SMP-based biomaterials possess different features and advantages like being self-fitting [92], self-healing [93], self-repairing [94], and having

shape fixation [95], which may provide wide opportunities for various applications in controlled drug delivery [96], alternative for treatments bone defects [97] and soft medical robotics [98]. Compared with the shape memory alloy, SMPs are desirable for industry manufacturing because of their flexibility, light weight, low cost and high recoverable properties [99], but the weak recovery stress may limit its applications in some fields.

Many previous reports focus on improving shape memory properties. Carbon nanotubes can improve mechanical performance, recovery stress as well as recovery strain [100]. Carbon nanofibers [101] and graphene nanosheets [102] are used to shorten recovery time. The recovery rate of composites is enhanced with the addition of silk fibroin [103].

SMPs consists of soft segments (polymer segments) and hard segments (cross-linking points or netpoints). There are more than two separate phases in the SMPs molecular network. The hard segments connect with soft segments via cross-linkages such as the physical, chemical and interlocked networks [104]. According to different hard segments, SMPs are divided into physically cross-linked SMPs and covalently cross-linked SMPs. Physically cross-linked SMPs have two transition temperatures to switch segments, namely the melting temperature or glass transition temperature [105, 106]. Physically cross-linked SMPs can be reshaped after fixing, while the original shape of covalently cross-linked SMPs is determined during processing [107]. Compared with the physically cross-linked SMPs, covalently cross-linked SMPs exhibit higher recovery properties due to stronger covalent bonds. It has been proved

that the content of hard segments influences the glass-transition temperature and mechanical properties [108].

1.5 Piezoelectric materials

Piezoelectricity refers to the ability of certain materials to generate surface charges in response to applied mechanical stress from environments (direct piezoelectric effect) or to produce a deformation under an applied electric voltage (reverse piezoelectric effect). This effect is related to an asymmetry in the unit cell of the crystal and the resultant generation of electric dipoles due to mechanical distortion [109]. The piezoelectric effect was first found in 1880 by Pierre and Jacques Curie. Given that, piezoelectricity has promoted the quick development of nanotechnology [110], information technology [111] and industrial technology [112]. Piezoelectric materials have the ability to convert mechanical energy and electric charges, making them smart materials with a wide range of applications in electronic devices [113], such as actuators [114], transducers [115], and sensors [116]. Piezoelectric ceramic is one of the most commonly-used piezoelectric materials. Among them, the lead zirconate titanate (PZT) is the most commercially- used for different applications due to its high piezoelectricity, stable piezoelectric effect and temperature stability [117]. Unfortunately, the great brittleness and toxicity of PZT limit its widespread applications in biomaterials, implantable devices and eco-environments [118, 119]. Therefore, lead-free ceramic [120] and piezoelectric polymers [121] have attracted more attention due to their eco-friendliness and flexibility. They can be applied in wearable devices [122],

tissue regeneration [123] and bone tissue [124]. Except for the widely studied $BaTiO_3$ nanowires and polyvinylidene difluoride (PVDF) [125, 126], they are similar in structure to perovskite or polarized in specific phases. For instance, β-phase PVDF based composites are used to detect human motion [127], nerve regeneration [128], and convert mechanical energy from body movements and muscle contraction into electric charges [129].

Besides, multifunctional smart materials can meet multiple needs. Smart materials perform only one smart property at a time, and it is difficult and expensive to prepared. To combine the two effects in one material, PZT/shape memory alloy laminated composites [130, 131] have been prepared by some researchers, but the laminated composites are easily delaminated because of weak interfacial bonding between the different layers.

1.6 Energy harvester

Energy harvesting technology that converts waste energy like mechanical [132], solar [133], thermal energies [134] into electric charges from surrounding environments has received a great deal of attention. Energy harvesters meet the increasing demands of renewable energy sources [135], eco-friendly requirements, and can be used to power wearable electronics [136]. Among these technologies, piezoelectric effect based energy harvester that can generate electrical charges from applied mechanical force are changing human life today [137]. These technologies have been applied in many engineering fields such as sensing [138], energy harvesting [139],

microelectromechanical systems [140], and health monitoring [141]. Energy harvesters have become more powerful and miniature. Although pure PZT ceramics exhibit strong piezoelectric effect, traditional piezoelectric ceramics-based energy harvesters are brittle and hardly deformed into flexible shapes, which limits their applications [142]. To overcome these disadvantages, polymer-based piezoelectric composites [143], piezoelectric nanowires and piezoelectric polymers[144] have been developed to enhance the flexibility and piezoelectricity of the harvesters [145]. Polyurethane [146] and β-phase poly(vinylidene fluoride) (PVDF) [147, 148] are used as polymer matrices to produce piezoelectric composites, aiming to enhance the flexibility. Piezoelectric particles are generally coated with coupling agents to enhance the dispersion and interfacial bonding between piezoelectric fillers and polymer matrices [149, 150]. To enhance the piezoelectricity, conductive fillers such as carbon nanotubes [151] and nanographite [152] are added to combine with piezoelectric composites. Up to now, many efforts have been made to decrease the preparation production cost and size [153, 154], increase output voltages [155], enlarge operating temperature ranges [156] and ensure stable mechanical properties. These technologies offer very promising solutions to overcome the challenging issues about flexible energy harvesters, such as flexibility and piezoelectricity [157, 158]. Therefore, flexible energy harvesters can be used for the power sources of commercial electronics [159, 160].

1.7 Purpose of this research

This study aims to develop a new kind of textile or nanofibers-based smart materials

with the piezoelectric and shape memory effect by compounding PZT fillers into shape memory polyurethane (SMPU) polymer matrix, leading to the formation of 2D composite fibers and nanofibers. The multi-functional smart materials are hardly reported. PZT/SMPU composites with the piezoelectric and shape memory effect can be applied in energy harvesters and actuators. Because PZT particles are brittle and easy to aggregate, it is very difficult to disperse high-content PZT particles into the polymer matrix uniformly, even it has high and stable piezoelectricity. Therefore, it is difficult to prepare flexible composites with high-content PZT fillers. Moreover, most of them exhibit high toughness, which greatly limits their applications. Thus, PZT/SMPU composite fibers and nanofibers with high-content PZT particles are prepared. The prepared composites are endowed with the expected piezoelectric and shape memory effect while keeping the flexibility from the polymer matrix. These advantages could help us to explore promising applications with a wide range of either piezoelectric materials or shape memory polymers.

PZT particles were modified by the silane coupling agent to improve the dispersity in the SMPU matrix and the interfacial bonding. PZT/SMPU composite fibers were prepared by the melt spinning method. The pristine SMPU and PZT/SMPU composite nanofibers with random and uniaxial structures were prepared by the electrospinning technology. The developed composite fibers and nanofibers with high-content PZT have both the piezoelectric and shape memory effect. The surface morphology and mechanical tensile test were performed to investigate the modification effect and mechanical properties of PZT/SMPU composite fibers and nanofibers before and after

modification.

The thermomechanical analysis was employed to analyze the influence of particle modification, PZT particle content and the structure of nanofiber mats on the shape recovery properties, including shape recovery rates, shape recovery stress and shape fixity. The mechanism of how the alignment angle of nanofibers and the interface between the fillers and polymer matrix affect the mechanical and shape memory properties is systemically discussed.

The PZT/SMPU composite fibers are woven into plate weaving and prepared as textile-based energy harvesters. The nanofibers-based energy harvesters are made of random or aligned PZT/SMPU nanofibers. All the energy harvesters were employed to harvest energy from external sinusoidal vibrations. The effect of the alignment degree of nanofibers and modification effect is investigated to improve the energy harvesting properties. Besides, to analyze the energy harvesting properties of the PZT/SMPU energy harvester with complex structures, two methods of manufacturing the energy collector are pasted on two designed curved surfaces, namely non-pre-deformed and pre-deformed.

Reference

[1] A Nakamura, N Kaneko, VL Villemagne, et al. (2018) Nature 554: 249.

[2] Y Lin, J Dai, H Yang, L Wang, F Wang (2018) Chemical Engineering Journal 334: 1740.

[3] J Song, C Chen, S Zhu, et al. (2018) Nature 554: 224.

[4] M Li, Z-K Wang, T Kang, et al. (2018) Nano Energy 43: 47.

[5] Y Zhang, X Wang, M Cao (2018) Nano Research 11: 1426.

[6] M Cao, C Han, X Wang, et al. (2018) Journal of Materials Chemistry C 6: 4586.

[7] T Zhu, S Li, J Huang, M Mihailiasa, Y Lai (2017) Materials & Design 134: 342.

[8] X Chen, S Xu, N Yao, Y Shi (2010) Nano letters 10: 2133.

[9] C Chang, VH Tran, J Wang, Y-K Fuh, L Lin (2010) Nano letters 10: 726.

[10] J Zhao, H Li, C Li, et al. (2018) Nano Energy 45: 420.

[11] R Gangopadhyay, A De (2000) Chemistry of materials 12: 608.

[12] Y Guo, G Xu, X Yang, et al. (2018) Journal of Materials Chemistry C 6: 3004.

[13] Y Li, G Xu, Y Guo, et al. (2018) Composites Part A: Applied Science and Manufacturing 107: 570.

[14] RJ Young, M Liu, IA Kinloch, et al. (2018) Composites Science and Technology 154: 110.

[15] JP Jose, S Thomas, J Kuruvilla, S Malhotra, K Goda, MS Sreekala (2012) Polymer Composite: Macro-and Microcomposites. Weinheim: Wiley-VCH Verlag GmbH Co. KGaA 1: 3.

[16] H Peng (2008) Journal of the American Chemical Society 130: 42.

[17] T Liang, C Yan, S Zhou, Y Zhang (2017) Materials Research Express 4: 115306.

[18] X Sun, H Sun, H Li, H Peng (2013) Advanced Materials 25: 5153.

[19] J Chen, R Ramasubramaniam, C Xue, H Liu (2006) Adv. Funct. Mater. 16: 114.

[20] M Španić, M Hadzima-Nyarko, D Morić (2012) Elektronički časopis Građevinskog fakulteta Osijek-e-GFOS 3: 74.

[21] J Yang, Y Liu, S Liu, L Li, C Zhang, T Liu (2017) Materials Chemistry Frontiers 1: 251.

[22] L Hollaway (2003) Construction and Building Materials 17: 365.

[23] J Stanzione, G Palmese, J Sadler, J La Scala (2018) ABSTRACTS OF PAPERS OF THE AMERICAN CHEMICAL SOCIETYAMER CHEMICAL SOC 1155 16TH ST, NW, WASHINGTON, DC 20036 USA,

[24] TS Williams (2019).

[25] Z Sydow, K Bieńczak (2019) Journal of Natural Fibers 16: 1189.

[26] H Jiang, DP Kamdem (2004) Journal of vinyl and Additive Technology 10: 70.

[27] S Ummartyotin, H Manuspiya (2015) Renewable and Sustainable Energy Reviews 41: 402.

[28] FJ Areal, L Riesgo (2015) Ecological Indicators 52: 498.

[29] Y Huang, S Kormakov, X He, et al. (2019) Polymers 11: 187.

[30] X Lu, C Wang, Y Wei (2009) Small 5: 2349.

[31] L Huihong, P Lisha, L Qiang, et al. (2010) e-Polymers 10.

[32] G Sui, D Liu, Y Liu, W Ji, Q Zhang, Q Fu (2019) Polymer 182: 121838.

[33] Y Dong, Q-Q Ni, L Li, Y Fu (2014) Materials Letters 132: 206.

[34] X He, Q Shi, X Zhou, C Wan, C Jiang (2005) Electrochimica acta 51: 1069.

[35] S Cordier, F Grasset, Y Molard, et al. (2015) Journal of Inorganic and Organometallic Polymers and Materials 25: 189.

[36] Y Sun, S Yuan, K Xiong, et al. (2014) International journal of materials research 105: 599.

[37] Y Zhang, X Meng, J Wang, L Wang, Z Xiao (2019) Journal of Thermal Analysis and Calorimetry 135: 3223.

[38] Y Dong, F Xu, X Shi, et al. (2009) Materials Science and Engineering: A 504: 49.

[39] MI Azmer, F Aziz, Z Ahmad, et al. (2017) Talanta 174: 279.

[40] T Chung, J Han, YS Kim (2019) Nano convergence 6: 1.

[41] MSH Firoz, MM Hosen, MM Islam (2017) ACTA CRYSTALLOGRAPHICA A-FOUNDATION AND ADVANCESINT UNION CRYSTALLOGRAPHY 2 ABBEY SQ, CHESTER, CH1 2HU, ENGLAND,

[42] J Zhang, L Feng, J Wei, X Guo, W Cao (2006) Chinese Science Bulletin 51: 2050.

[43] S Han, MK Kim, B Wang, DS Wie, S Wang, CH Lee (2016) Advanced Materials 28: 10257.

[44] R Govindan, E Girija (2014) Journal of Materials Chemistry B 2: 5468.

[45] S Barthwal, B Singh, N Singh (2019).

[46] M Joshi, B Adak, B Butola (2018) Prog. Mater. Sci. 97: 230.

[47] Z Zabihi, H Araghi (2016) Physics Letters A 380: 3828.

[48] J Ru, D Min, M Lanagan, S Li, G Chen (2019) Applied Physics Letters 115: 213901.

[49] JS Dodds, FN Meyers, KJ Loh (2013) Smart Struct. Syst 12: 55.

[50] T Ebina, R Ishii, T Aizawa, H Yoshida (2017) Journal of the Japan Petroleum Institute 60: 121.

[51] Q Wang, J Guo, D Xu, et al. (2015) Cellulose 22: 3799.

[52] AH Esbati, S Irani (2018) Mechanics of Materials 118: 106.

[53] J-M Park, D-S Kim, S-J Kim, P-G Kim, D-J Yoon, KL DeVries (2007) Composites

Part B: Engineering 38: 847.

[54] S Ha, S Ryu, S Park, K Rhee (2007) Materials Science and Engineering: A 448: 264.

[55] C Zhou, M Tao, J Liu, T Liu, X Lu, Z Xin (2019) ACS Applied Polymer Materials 1: 381.

[56] H Yan, X-h Zhang, L-q Wei, X-g Liu, B-s Xu (2009) Powder technology 193: 125.

[57] A Esteves, M Neves, A Barros-Timmons, E Bourgeat-Lami, L Liz-Marzán, T Trindade (2006) Journal of nanoscience and nanotechnology 6: 414.

[58] CS Kong, WS Yoo, NG Jo, HS Kim (2010) Journal of Macromolecular Science®, Part B: Physics 49: 122.

[59] CP Carroll, E Zhmayev, V Kalra, YL Joo (2008) Korea-Australia Rheology Journal 20: 153.

[60] W Serrano-Garcia, WADM Jayathilaka, A Chinnappan, et al. (2019) Science China Technological Sciences: 1.

[61] CL Zhang, KP Lv, HP Cong, SH Yu (2012) Small 8: 648.

[62] G Gururajan, S Sullivan, T Beebe, D Chase, J Rabolt (2011) Nanoscale 3: 3300.

[63] LR Manea, A Bertea, E Nechita, CV Popescu, I Sandu (2016) Effect of the distance between electrodes on the electrospun fibers diameter Rev. Chim (Bucharest) 67: 1284.

[64] LR Manea, A Bertea, E Nechita, CV Popescu, I Sandu (2016) REVISTA DE CHIMIE 67: 1607.

[65] G Li (2017) Journal of Materials Science: Materials in Electronics 28: 12320.

[66] Y Lu, Y Fang, X Xiao, et al. (2018) Colloids and Surfaces A: Physicochemical and

Engineering Aspects 553: 210.

[67] A Morie, T Garg, AK Goyal, G Rath (2016) Artificial cells, nanomedicine, and biotechnology 44: 135.

[68] K Chen, W Chou, L Liu, Y Cui, P Xue, M Jia (2019) sensors 19: 3676.

[69] A Camiré, J Espinasse, B Chabot, A Lajeunesse (2018) Environmental Science and Pollution Research: 1.

[70] X Xu, Q Yang, J Bai, T Lu, Y Li, X Jing (2008) Journal of nanoscience and nanotechnology 8: 5066.

[71] G Zhou, G Zhang, Z Wu, et al. (2013) Journal of Nanomaterials 2013.

[72] G Tang, D Chang, D Wang, et al. (2012) Polymer-Plastics Technology and Engineering 51: 377.

[73] J Li, G Ben, J Yang (2014) Science and Engineering of Composite Materials 21: 289.

[74] R Giridharan (2019) Composites Part B: Engineering 167: 342.

[75] C Subramanian, R Weiss, MT Shaw (2013) Industrial & Engineering Chemistry Research 52: 15088.

[76] S Li, J Huang (2016) Advanced Materials 28: 1143.

[77] IS Gunes, C Pérez-Bolivar, F Cao, GA Jimenez, P Anzenbacher, SC Jana (2010) Journal of Materials Chemistry 20: 3467.

[78] J Xie, X Li, J Lipner, et al. (2010) Nanoscale 2: 923.

[79] J Joseph, SV Nair, D Menon (2015) Nano letters 15: 5420.

[80] D Edmondson, S Jana, D Wood, C Fang, M Zhang (2013) Analyst 138: 7135.

[81]J Lee, Y Deng (2012) Macromolecular research 20: 76.

[82]R Xiao, J Guo, DL Safranski, TD Nguyen (2015) Soft Matter 11: 3977.

[83]LB Wang, J Hua, ZB Wang (2019) Polymer Testing 76: 481. Doi:10.1016/j.polymertesting.2019.04.011

[84]VL Le, VT Le, NS Goo (2019) J. Intell. Mater. Syst. Struct. 30: 2625. Doi:10.1177/1045389x19873403

[85]L Sun, WM Huang, Z Ding, et al. (2012) Materials & Design 33: 577. Doi:10.1016/j.matdes.2011.04.065

[86]L Xia, M Zhang, H Gao, GX Qiu, ZX Xin, WX Fu (2019) Polymer Testing 77: 8. Doi:10.1016/j.polymertesting.2019.105910

[87]HY Li, D Guo, H Tzou (2017) J. Intell. Mater. Syst. Struct. 28: 3079. Doi:10.1177/1045389x17704984

[88]J Puig, C Hoppe, L Fasce, et al. (2012) The Journal of Physical Chemistry C 116: 13421.

[89]K Otsuka, X Ren (2005) Prog. Mater. Sci. 50: 511. Doi:10.1016/j.pmatsci.2004.10.001

[90]S Dogan, S Boyacioglu, M Kodal, O Gokce, G Ozkoc (2017) Journal of the mechanical behavior of biomedical materials 71: 349.

[91]H Lv, D Tang, Z Sun, et al. (2020) Colloid and Polymer Science 298: 103.

[92]F Senatov, MY Zadorozhnyy, K Niaza, et al. (2017) European Polymer Journal 93: 222.

[93]K Chang, H Jia, S-Y Gu (2019) European Polymer Journal 112: 822.

[94] A Anis, S Faiz, M Luqman, et al. (2013) Polymer-Plastics Technology and Engineering 52: 1574.

[95] J Ban, L Mu, J Yang, S Chen, H Zhuo (2017) Journal of Materials Chemistry A 5: 14514.

[96] JG Hardy, M Palma, SJ Wind, MJ Biggs (2016) Advanced Materials 28: 5717. Doi:10.1002/adma.201505417

[97] JH Yu, H Xia, A Teramoto, QQ Ni (2017) J. Biomed. Mater. Res. Part A 105: 1132. Doi:10.1002/jbm.a.36009

[98] C De Marco, CC Alcântara, S Kim, et al. (2019) Advanced Materials Technologies 4: 1900332.

[99] HY Kim, Y Ikehara, JI Kim, H Hosoda, S Miyazaki (2006) Acta Mater. 54: 2419. Doi:10.1016/j.actamat.2006.01.019

[100] S Hashmi, HC Prasad, R Abishera, HN Bhargaw, A Naik (2015) Materials & Design 67: 492.

[101] H Lu, Y Liu, J Gou, J Leng, S Du (2010) Applied Physics Letters 96: 084102.

[102] H Jiu, H Jiao, L Zhang, S Zhang, Y Zhao (2016) Journal of Materials Science: Materials in Electronics 27: 10720.

[103] Y Sun, Y Luo, Y Dong, Y Fu (2017) Materials Letters 193: 26.

[104] WS Baker, ER Kaswell (1961) MCGRAW-HILL BOOK CO INC NEW YORK,

[105] JW Cho, YC Jung, YC Chung, BC Chun (2004) Journal of applied polymer science 93: 2410.

[106] M Ebara (2015) Science and technology of advanced materials 16: 014804.

[107] N Sabahi, W Chen, C-H Wang, JJ Kruzic, X Li (2020) JOM 72: 1229.

[108] FL Ji, JL Hu, SSY Chui (2012) Polymer Engineering & Science 52: 1015.

[109] H Czichos, T Saito, LE Smith (2011) Springer handbook of metrology and testing. Springer Science & Business Media,

[110] C Falconi (2019) Nano Energy 59: 730.

[111] S-K Kim, S-C Shin, K No (2004) IEEE transactions on magnetics 40: 2637.

[112] X-H Wang, I-W Chen, X-Y Deng, Y-D Wang, L-T Li (2015) Journal of Advanced Ceramics 4: 1.

[113] J Yang, A Wang, S Zhang, J Liu, Z Zhong, L Chen (2019) Physical Chemistry Chemical Physics 21: 132.

[114] C Bowen, M Lopez-Prieto, S Mahon, F Lowrie (2000) Scripta materialia 42: 813.

[115] Z Yang, S Guo, J Yang (2008) IEEE transactions on ultrasonics, ferroelectrics, and frequency control 55: 1380.

[116] YK Fetisov (2014) IEEE Sens. J. 14: 1817.

[117] A Amin, H-Y Lee, B Kelly (2007) Applied physics letters 90: 242912.

[118] JF Choo, NS Goo (2014) Journal of Central South University 21: 2572.

[119] MM Akmal, A Warikh, A Ralib (2019) Materials Research Express 6: 115708.

[120] K Lam, X Wang, H Chan (2006) Sensors and Actuators A: Physical 125: 393.

[121] KK Sappati, S Bhadra (2018) Sensors 18: 3605.

[122] SS Won, M Sheldon, N Mostovych, et al. (2015) Applied Physics Letters 107:

202901.

[123] N Barroca, S Vieira, O Da Cruz e Silva, et al. (2012) JOURNAL OF TISSUE ENGINEERING AND REGENERATIVE MEDICINEWILEY-BLACKWELL 111 RIVER ST, HOBOKEN 07030-5774, NJ USA,

[124] C Ribeiro, DM Correia, S Ribeiro, V Sencadas, G Botelho, S Lanceros-Méndez (2015) Engineering in Life Sciences 15: 351.

[125] J Wu, N Qin, D Bao (2018) Nano Energy 45: 44.

[126] N Jaitanong, R Yimnirun, H Zeng, G Li, Q Yin, A Chaipanich (2014) Materials Letters 130: 146.

[127] H Khan, A Razmjou, M Ebrahimi Warkiani, A Kottapalli, M Asadnia (2018) Sensors 18: 418.

[128] Y Cheng, Y Xu, Y Qian, X Chen, Y Ouyang, W-E Yuan (2020) Nano Energy 69: 104411.

[129] X Hu, Z Ding, L Fei, Y Xiang (2019) Journal of materials science 54: 6401.

[130] N Choudhary, D Kharat, D Kaur (2011) Surface and Coatings Technology 205: 3387.

[131] I-J Kim, H-W Lee (2001) Scripta materialia 44: 525.

[132] C Liu, N Zhang, J Li, et al. (2019) Nano Energy 65: 104011.

[133] I Rodriguez, F Ramiro-Manzano, P Atienzar, et al. (2007) Journal of Materials Chemistry 17: 3205.

[134] Y Yang, H Zhang, G Zhu, S Lee, Z-H Lin, ZL Wang (2013) ACS nano 7: 785.

[135] RM Ferdous, AW Reza, MF Siddiqui (2016) Renewable and Sustainable

Energy Reviews 58: 1114.

[136] S Khalid, I Raouf, A Khan, N Kim, HS Kim (2019) International Journal of Precision Engineering and Manufacturing-Green Technology: 1.

[137] X Wang (2012) Nano Energy 1: 13.

[138] K Shin, D Kim, H Park, et al. (2020) IEEE Trans. Ind. Electron. 67: 637. Doi:10.1109/tie.2019.2912788

[139] I Chinya, A Sasmal, S Sen (2020) J. Alloy. Compd. 815: 8. Doi:10.1016/j.jallcom.2019.152312

[140] M Soliman, A Kochhar, H Abdelsalam, et al. (2019) IEEE Trans. Circuits Syst. I-Regul. Pap. 66: 4439. Doi:10.1109/tcsi.2019.2927999

[141] A Marzani, N Testoni, L De Marchi, M Messina, E Monaco, A Apicella (2019) Struct. Health Monit.: 18. Doi:10.1177/1475921719889029

[142] A Jain, AK Sharma, A Jain (2015) Polymer Engineering & Science 55: 1589.

[143] JA Krishnaswamy, FC Buroni, E Garcia-Macias, R Melnik, L Rodriguez-Tembleque, A Saez (2020) Smart Materials and Structures 29: 13. Doi:10.1088/1361-665X/ab547d

[144] RL Hadimani, DV Bayramol, N Sion, et al. (2013) Smart Materials and Structures 22: 6. Doi:10.1088/0964-1726/22/7/075017

[145] YJ Hwang, S Choi, HS Kim (2019) Sens. Actuator A-Phys. 300: 6. Doi:10.1016/j.sna.2019.111672

[146] AO Sanches, DHF Kanda, LF Malmonge, MJ da Silva, WK Sakamoto, JA Malmonge (2017) Polymer Testing 60: 253.

[147] X Lu, H Qu, M Skorobogatiy (2017) ACS nano 11: 2103.

[148] X Guan, Y Zhang, H Li, J Ou (2013) Sensors and Actuators A: Physical 194: 228.

[149] S-J Chang, W-S Liao, C-J Ciou, J-T Lee, C-C Li (2009) Journal of Colloid and Interface Science 329: 300.

[150] S Dalle Vacche, F Oliveira, Y Leterrier, V Michaud, D Damjanovic, J-AE Månson (2014) Journal of materials science 49: 4552.

[151] Y Gao, Q Zhai, R Barrett, NS Dalal, HW Kroto, SF Acquah (2013) Carbon 64: 544.

[152] W Sakamoto, P Marin-Franch, D Das-Gupta (2002) Sensors and Actuators A: Physical 100: 165.

[153] SY Chung, S Kim, JH Lee, et al. (2012) Advanced Materials 24: 6022.

[154] X Ma, X Zhang (2017) Smart Materials and Structures 26: 085001.

[155] Z Wen, L Deng, X Zhao, Z Shang, C Yuan, Y She (2015) Microsystem Technologies 21: 331.

[156] Y Sun, J Chen, X Li, Y Lu, S Zhang, Z Cheng (2019) Nano Energy 61: 337.

[157] W Kim, S Pyo, M-O Kim, Y Oh, D-S Kwon, J Kim (2019) Nanotechnology 30: 275401.

[158] J-H Yang, H-S Cho, S-H Park, S-H Song, K-S Yun, JH Lee (2016) Smart Materials and Structures 25: 035012.

[159] CK Jeong, JH Han, H Palneedi, et al. (2017) Apl Materials 5: 074102.

[160] J Xie, Y Wang, R Dong, K Tao (2020) Sensors 20: 458.

Chapter 2: Preparation of PZT / SMPU composites

2.1 Introduction

The composite fibers and yarns, as the main flexible material, have attracted more attention to the increasing demand of fibers-based composites with unique properties. Various composite fiber-based composites exhibit multi-functional properties, suggesting potential applications such as fiber-reinforced composite, smart textile, sensor, wearable energy harvester, and electromagnetic shields. It is a convenient method to compound different polymers and functional fillers into composite fibers. The wet-spinning [1], gel-spinning [2], melt spinning [3] and electrospinning [4] have been applied to prepare various composite fibers due to their low-energy consumption [5] and easy processing. Among these methods, melt spinning is a fast and cost-effective method [6] to produce composite fibers. However, the addition of fillers results in many problems [7] like higher viscosity and dispersion [8]. Especially, nanoparticles within the composite fiber are easy to aggregate in the mixture during the melt spinning process because of their small diameter and high aspect ratio. Therefore, it is necessary to increase the continuity of the polymer matrix during melt spinning while maintaining the endowed properties of composite fibers.

In the past few decades, electrospinning has become a key manufacturing method to produce nanofibers directly [9] with the diameters from nanoscale to microscale, due to the simplicity and low consumption for fabricating continuous nanofibers [10], and this one dimensional nanostructure plays a vital role in design of new nanomaterials,

such as nano-fabrication [11], biomaterials [12], microelectromechanical systems [13] and so on. Thus, electrospinning possesses critical attention and wide range of applications. In general, these nanofibers are randomly deposited on the collector, and formed nanofibers films. The disordered structure of nanofibers resulting in the limit of high strength and some request of applications. In recent years, in order to overcome the shortcomings of random nanofibers, several researches are reported to fabricate aligned nanofibers by some approaches, such as controlling the rotation speed of collector [14,15], depositing nanofibers in magnetic field [16,17], employed modifying collector setup [18,19] and using near field electrospinning method [20,21]. This kind of highly ordered structure endow the aligned nanofibers in a variety of protentional applications including biomaterials [22,23], sensor [24], energy harvester [25] and engineering [26]. There are many researches focus on the piezoelectric polymer based energy harvester, but the study on composite nanofibers with both piezoelectric and shape memory effects are hardly reported.

In this study, a kind of composite fibers with both the shape memory and piezoelectric effect is developed. It is a great challenge to produce composite fibers with a high content of piezoelectric ceramic (more than 50%) without sacrificing the fiber performance. To increase the distribution of fillers in the polymer matrix and the interfacial bonding, silane coupling agents are used to modify the surface of particles. The developed PZT/SMPU composite fibers are made into 2D plain-woven fabric.

The random and aligned pristine SMPU and PZT/SMPU nanofibers are fabricated by electrospinning technology with a specified device. The PZT particles are modified

by a silane coupling agent to obtain better dispersion of PZT fillers to meet complicated and variable requirements. The optimal method to prepare PZT/SMPU composites is discussed and the characterization of the developed materials is clarified.

2.2 Materials and methods

2.2.1 Modification of PZT particles

An easy modification method [27] was employed to improve the distribution of PZT particles in SMPU matrix. The PZT particles (HIZIRCO ALT, Hayashi Chemical Industry Co., Ltd., Japan) were modified by coating silane coupling agents onto their surfaces. PZT particles with a specified ratio were refluxed in a mixture that consisted of an acetone and silane coupling agent (KBM-503, Shin-Etsu Chemical Co., Ltd., Japan). This mixture was dispersed using an ultrasonic device (Sonifier 250, Branson Ultrasonics Corp., USA.), and then was dried at 70 °C to remove the acetone solution completely.

2.2.2 Preparation of PZT/SMPU fibers and textiles

The non-modified and modified PZT particles were placed separately in a THF solution, and dispersed with an ultrasonic device for 15 min (Figure 2-1). Then, SMPU particles (MM6520, SMP Technologies Inc., Japan) were added to the mixed solution that was being stirred at 600 rpm. After stirring for 24 h, the stirring speed was lowered to 400 rpm, and THF was evaporated at room temperature until the ratio of SMPU to

solvent was 1:7. Then, the mixture was cast on a teflon film by an auto film applicator (PI-1210, TESTER SANGYO CO,. LTD., Japan). The film would cure after evaporating THF again for three days. After evaporation, the film was cut into small pieces, and they were dried in the vacuum desiccator for melt spinning.

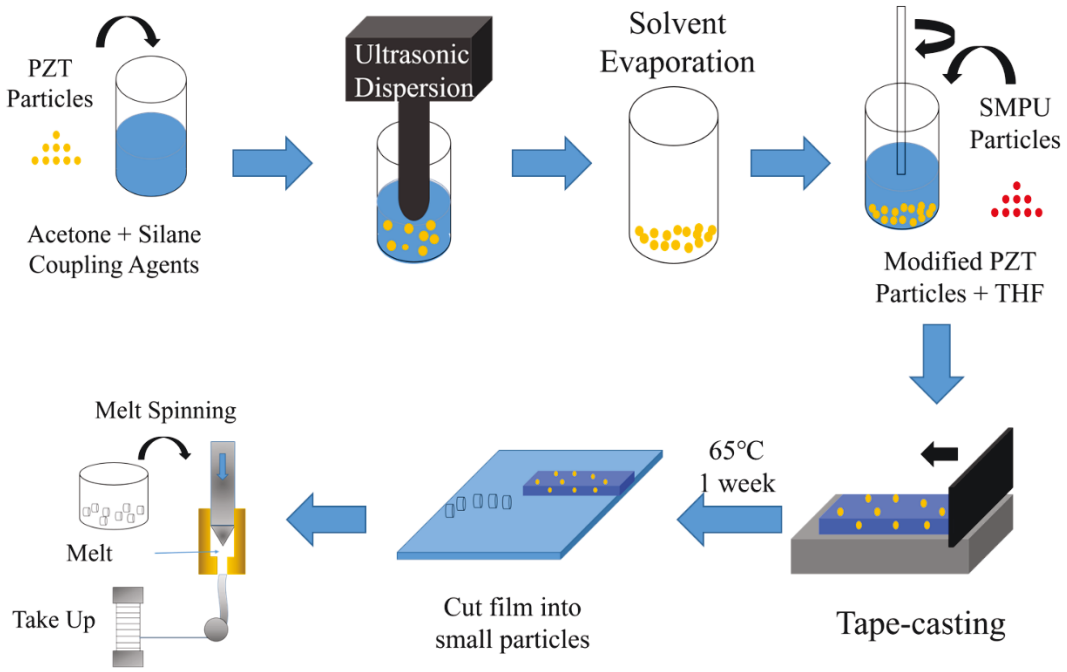

Figure 2-1. Schematic diagram showing preparation of PZT/SMPU composite fibers

The composite fiber was prepared from PZT/SMPU using a melt spinning method by the twin-screw extruder machine (DSM Xplore Compounder 15, Xplore Instruments BV, Netherlands) at 190°C. The whole spinning process was under nitrogen protection. Both pure and composite fibers were spun using a spinning head with a diameter of 0.1 mm attached to an extruder. The as-spun fibers were collected by rollers at a winding speed of 40 m/min.

2.2.3 Preparation of random and aligned nanofibers

The random and aligned nanofibers were prepared by an electrospinning method. For SMPU nanofibers, A mixed solvent of tetrahydrofuran (THF)/dimethylformamide (DMF) (1:1) was prepared, SMPU pellets (MM6520, SMP Technologies Inc., Japan) were added as a solute, at a ratio of material to solvent 1:7. The random and aligned SMPU nanofibers were prepared by an electrospinning device (NANON-02, MECC Co., Ltd., Japan). For the unidirectional SMPU nanofibers, a voltage of 13 kV was applied on the spinneret, which is 75 mm from the collector at the speed of 19.63 m/min. The spinneret moved at a speed of 2 cm/min with a feed rate of 0.6 ml/h. For comparison, random SMPU nanofibers were also prepared, where the collector speed was 3.93 m/min. After preparation, all the samples stood at room temperature for 48 h and were then dried at 70 °C in an oven for 1 week.

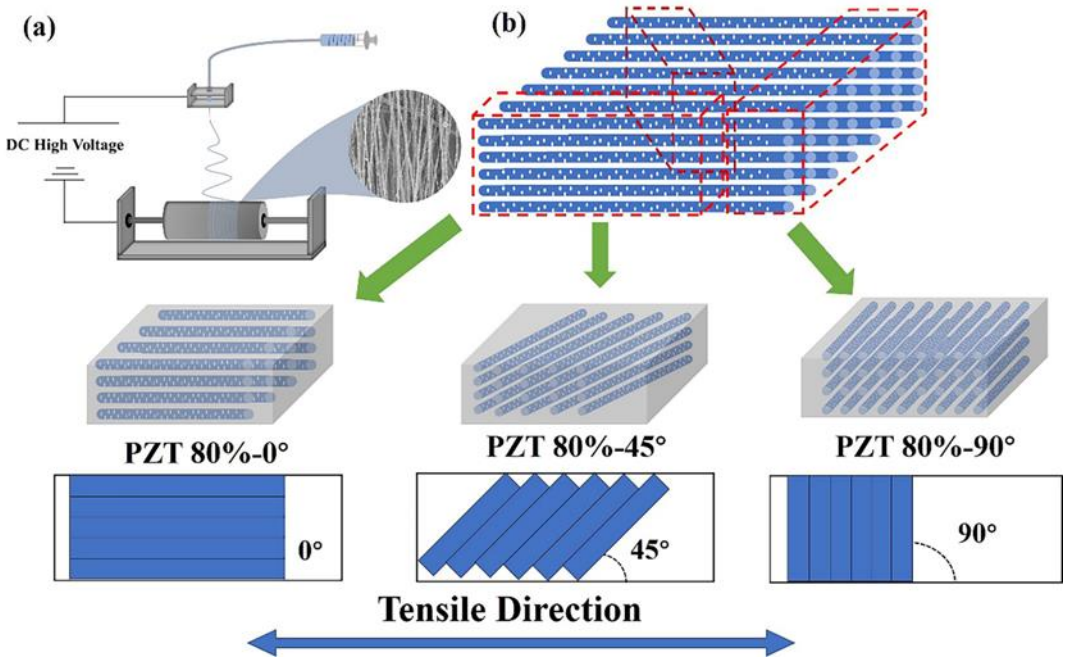

Figure 2-2. (a) Schematic diagram of the fabrication process, (b) Aligned nanofibers cut from nanofibers mats and placed at different alignment degrees.

For PZT/SMPU nanofibers, the modified PZT particles were poured into a solution of tetrahydrofuran (THF)/dimethylformamide (DMF) (6:4), and dispersed with an ultrasonic device, and then SMPU pellets were added while being stirred. The weight percentage concentration of the PZT particles was 80 wt%. The THF was evaporated until the weight ratio of SMPU to solvent (THF and DMF) was 1:7. After evaporation, the mixture was aspirated into a syringe to prepare the nanofibers. A schematic diagram of the preparation method is shown in Figure 2-2a. Aligned PZT/SMPU nanofibers were prepared by an electrospinning device (NANON-02, MECC Co., Ltd., Japan). A voltage of 20 kV was applied to the spinneret, which was 75 mm away from the collector at the speed of 19.63 m/min. The spinneret moved at the speed of 10 mm/min with a feed rate of 1 ml/h. For the random PZT/SMPU nanofibers, the speed of collector was changed to 3.93 m/min. After the fabrication, all the samples stood at room temperature for 48 h and then dried at 70 °C in an oven for 1 week.

In the analysis of influence of particles content and modification, the PZT/SMPU composite fibers and random PZT/SMPU nanofibers were divided into two groups depending on whether they were modified or not. The first group is the modified nanofibers, PZT 50%-M, PZT 60%-M, PZT 70%-M and PZT 80%-M. The second group is unmodified nanofibers, PZT 50%-U, PZT 60%-U, PZT 70%-U, and PZT 80%-U. All the percentages are weight percentages.

For the pristine SMPU nanofibers, the developed random and aligned nanofibers were divided into four groups: 0° (SMPU-0), 45° (SMPU-45), 90° (SMPU-90) and random nanofibers (SMPU-R), According to the alignment degree (see Figure 2-2b).

For the aligned PZT/SMPU nanofibers, the PZT/SMPU nanofibers were divided into four groups depending on their alignment angles: 0° (P/S-0), 45° (P/S-45), 90° (P/S-90) and random (P/S-R).

2.2.4 Microscopic morphology

Scanning electron microscopy (SU1510, Hitachi Co., Ltd., Japan) was used to take pictures of the nanofibers. A Schottky Field Emission Scanning Electron Microscope (FE-SEM) (SU5000, Hitachi Co., Ltd., Japan) was employed to observe the surface of composites. The surface microstructures of the modified PZT particles were analyzed with a transmission electron microscope (JEM2100, JEOL Ltd, Japan).

2.2.5 Chemical and bet surface area measurements

The rheometer (RHEOGRAPH 20, GOETTFERT Werkstoff-Prüfmaschinen GmbH, German) were employed to measure the viscosity of the SMPU polymer in the melt state. SMPU specimens were 20 g, under the condition of the atmosphere, which was heated to 190-205℃ melting, to measure the dynamic rheological behavior of the material in 190℃, 195℃ and 200℃ and the shear velocity was set to 8.

The chemical groups on the surface of the PZT particles before and after modification were characterized by Fourier Transform infrared spectroscopy (IR Prestige-21 spectrometer, Shimadzu, Japan). The modified and unmodified PZT particles were mixed with potassium bromide and then pressed into pellets.

The thermal properties of the SMPU were investigated with the differential scanning

calorimetry (DSC) (Thermo Plus DSC8230; Rigaku Corporation, Japan). The samples were purged with nitrogen gas and scanned from 0 ℃ to 220 ℃ at a scanning rate of 5 ℃/min.

The specific surface areas of the random and aligned nanofibers were investigated with an analyzer using the Brunauer Emmett Teller (BET) method (TriStar ii, Micromeritics Instrument Corp., USA). Before measurements, all the samples were dried at 65 °C in a vacuum for 30 min to remove all solvents.

The density of nanofibers were measured with a Specific Gravity Measurement kit (SMK-301, Shimadzu Scientific Instruments, Kyoto, Japan). Ethanol (liquid density 789 g/mL) was used as a measure of density.

2.3 Results and discussion

2.3.1 Surface morphology and characterization of PZT particles and PZT/SMPU composites

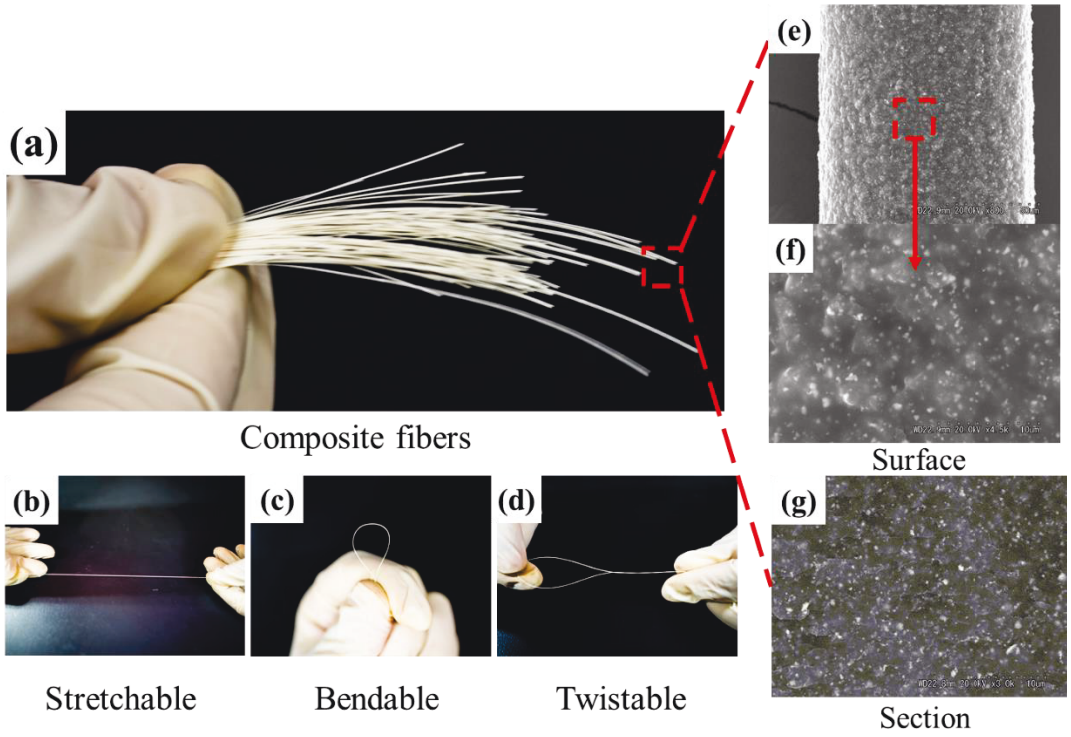

Figure 2-3. (a) The real images of PZT/SMPU composite fibers, (b-d) The images of PZT/SMPU composite fibers in stretching, bending and twisting stages. (e-g) The surface and section morphology of PZT/SMPU composite fibers.

PZT/SMPU composite fibers in Figure 2-3(a-d) exhibit superior flexibility, which means the prepared fiber can be stretched, bent and twisted many times. Figure 2-3(e-g) show the surface and cross section of the composite fibers with 50% PZT. The distribution of PZT fillers in the polymer is uniform, which illustrates the effect of modification and pre-dispersion on particle distribution.

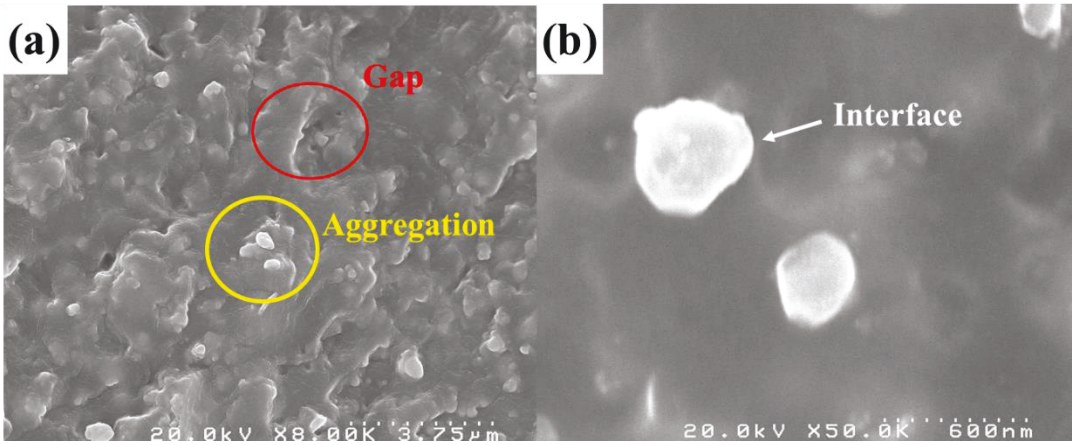

Figure 2-4. The cross-section morphology of PZT/SMPU composite fibers (a) before and (b) after modification.

Figure 2-4a shows the dispersion of PZT particles in the unmodified composites fibers. The aggregation of PZT particles and the gap between the fillers and SMPU matrix are obvious. In comparison, for modified samples (Figure 2-4b), the PZT distribution is more uniform than those of the sample before modification, and the aggregation of PZT particles is significantly reduced. Besides, gaps between the polymer matrix and PZT particles are substantially narrowed. The FESEM image demonstrates well-dispersion properties of PZT particles after modification, as well as a better connection between particles and the polymer matrix.

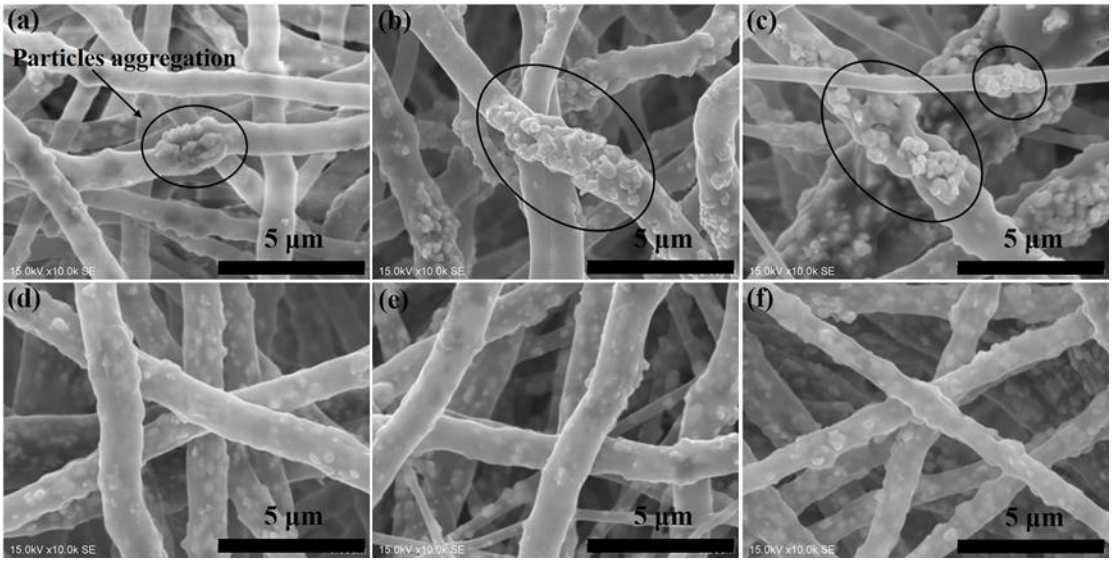

Figure 2-5. SEM images of unmodified samples: (a) PZT 60%-U, (b) PZT 70%-U, (c) PZT 80%-U. (d, e, f) SEM images of modified samples: (d) PZT 60%-M, (e) PZT 70%-M, (f) PZT 80%-M

To clarify the differences in morphology between modified and unmodified nanofibers, the microscopic structures of the unmodified and modified PZT/SMPU nanofibers are shown in Figure 2-5. In the unmodified samples (Figure 2-5(a-c)), PZT particles aggregate together, which results from the poor dispersion due to the small radius and large surface energy of particles, and strong interactive forces between particles. For this reason, a silane coupling agent was coated on the surface of PZT particles to improve the dispersion of PZT particles in the SMPU polymer matrix.

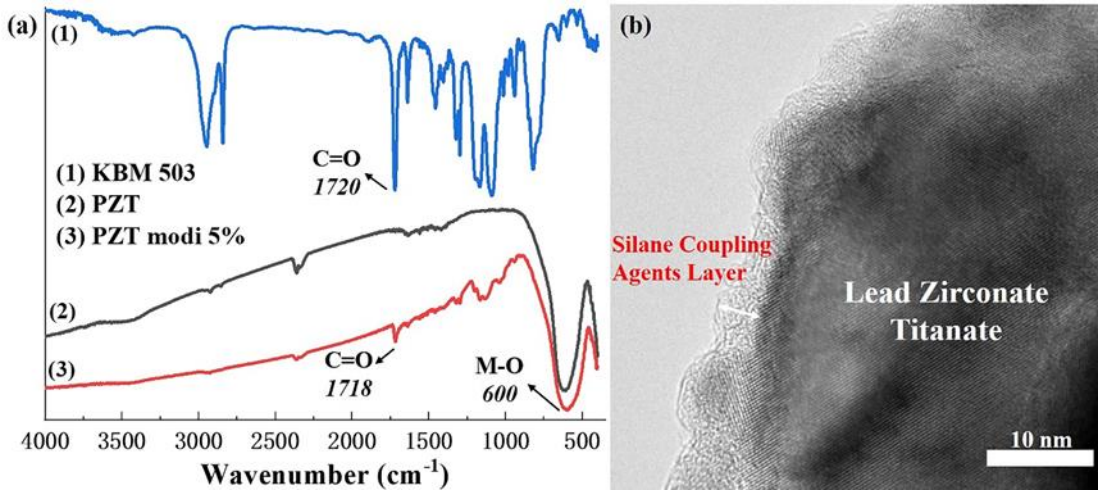

Figure 2-6. (a) FT-IR spectra of PZT particles and modified PZT particles with silane coupling agents KBM-503, (b) TEM images of modified PZT particles with silane coupling agents.

FT-IR spectroscopy and TEM is used to confirm the interaction between the PZT particles and silane coupling agents. The FT-IR spectra of the pure PZT particles and modified PZT particles (modified with the 5% of coupling agents) are shown in Figure 2-6a. The peaks occur at the wavenumber of 600 cm^{-1} in the FT-IR spectra of PZT and modified PZT particles, and represent the metal oxygen (M-O) bonds in PZT particles. Also, the peak of C=O groups from the KBM-503 silane coupling agents appears near 1720 cm^{-1}, which is a new absorption spectra compared with the spectra of pure PZT particles. This result proves that the silane coupling agents are coated on the surface of PZT particles. Besides, a TEM image (Figure 2-6b) also exhibits a thin layer of silane coupling agents on the surface of a PZT particle, and the thickness of the silane coupling agent layer is about 2 nm.

2.3.2 Chemical and surface area characterization

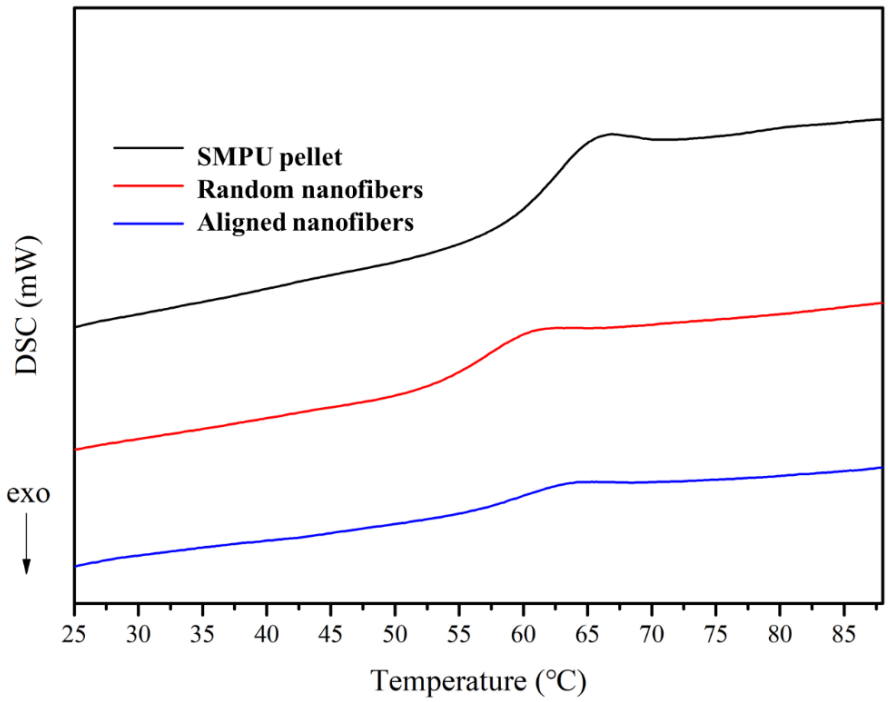

Figure 2-7. DSC curves of SMPU pellet, random and aligned SMPU nanofibers.

The results of DSC (Figure 2-7) demonstrate that the baseline of the measurement curve increases from about 60℃ to 65 ℃, corresponding to the glass transition temperature (T_g) of the SMPU matrix. The T_g of SMPU pellet, random and aligned SMPU nanofibers have no obvious shifts.

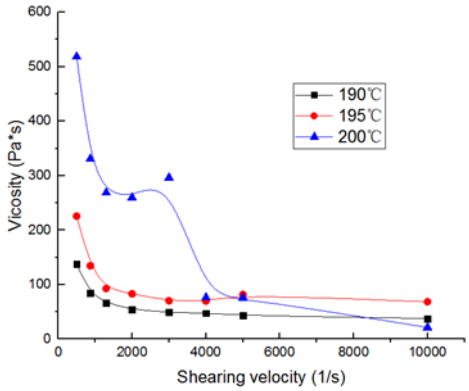

Figure 2-8. Viscosity vs Shearing velocity of SMPU at different temperature

As shown in Figure 2-8, the results of shear viscosity measurements of the SMPU melt at different temperatures in a capillary rheometer. SMPU presents a consistent trend at various temperatures. The shear viscosity decreases with the increasing shear rate and shows a typical shear thinning effect, which is an important feature of melt spinning polymers. Given that, to reduce the system viscosity, the shear rate can be increased appropriately within a specific range. The shear viscosity increases with the increasing temperature. The viscosity of SMPU also shows an increasing trend with increasing temperature at the same shear rate. It may be because the motion of the molecular chain is more intense with the increasing temperature, indicating the short relaxation time of the molecular chain. Hence, when the same shear stress is applied to the polymer, the molecular chain counteracts the influence of external force on the disentanglement of the molecular chain by its thermal motion. Finally, polymer shear stress increases.

Table 2-1. BET surface area and density of aligned and random SMPU and PZT/SMPU nanofibers

Materials	**BET surface area** m^2/g	**Density** g/cm^3
Random SMPU	0.79	0.78
Aligned SMPU	0.23	0.79
Random PZT/SMPU	1.05	3.06
Aligned PZT/SMPU	0.50	3.7

Table 2-1 shows the BET specific surface area and density of aligned and random

SMPU and PZT/SMPU nanofibers. Aligned nanofibers including SMPU and PZT/SMPU nanofibers have a lower BET specific surface area and higher density than those of random nanofibers, indicating that they have a higher volume of nanofibers in the same area.

2.4 Conclusions

The preparation of PZT/SMPU composite fibers and nanofibers are discussed in the chapter. PZT particles aggregate together before modification, which results from the poor dispersion due to the small radius and large surface energy of particles. In order to find out the optimal method to prepare PZT/SMPU composites, the saline coupling agents were used to improve the interfaces between the PZT particles and the SMPU matrix. Our results prove that the silane coupling agents are coated on the surface of PZT particles, as a bridge to bind the SMPU matrix and particles. Thus, the saline coupling agents improve the dispersion and interfaces between the fillers and polymer matrix. Besides, the results from BET surface area and density show that the aligned nanofibers (including SMPU and PZT/SMPU nanofibers) have lower BET surface area and higher density, compared with the random nanofibers, indicated that the aligned nanofibers have higher volume of nanofibers and more compact in the same area.

Reference

[1] MA Al Faruque, R Remadevi, JM Razal, M Naebe (2020) Journal of Applied

Polymer Science.

[2] X Zhang, T Liu, T Sreekumar, S Kumar, X Hu, K Smith (2004) Polymer 45: 8801.

[3] M Qu, DW Schubert (2016) Composites Science and Technology 136: 111.

[4] Y Zhao, L Wang, H Yu, et al. (2015) Journal of Applied Polymer Science 132.

[5] Z Dai, X Shi, H Liu, H Li, Y Han, J Zhou (2018) RSC advances 8: 1218.

[6] Z Yang, D Xu, J Liu, et al. (2015) Progress in Natural Science: Materials International 25: 437.

[7] L Marischal, A Cayla, G Lemort, C Campagne, É Devaux (2019) Polymers 11: 1827.

[8] S Kotomin, T Ignatenko, YA Kostrov (1995) Fibre Chemistry 26: 374.

[9] K Watanabe, T Maeda, A Hotta (2018) Composites Science and Technology 165: 18.

[10] YJ Yun, WG Hong, N-J Choi, et al. (2014) Nanoscale 6: 6511.

[11] X Wu, T Xiao, Z Luo, et al. (2018) Journal of nanobiotechnology 16: 1.

[12] W Tutak, S Sarkar, S Lin-Gibson, et al. (2013) Biomaterials 34: 2389.

[13] KS Teh (2017) Frontiers of Mechanical Engineering 12: 490.

[14] G-Y Liao, X-P Zhou, L Chen, X-Y Zeng, X-L Xie, Y-W Mai (2012) Composites science and technology 72: 248.

[15] MR Badrossamay, HA McIlwee, JA Goss, KK Parker (2010) Nano letters 10: 2257.

[16] D Yang, B Lu, Y Zhao, X Jiang (2007) Advanced materials 19: 3702.

[17] Y Liu, X Zhang, Y Xia, H Yang (2010) Advanced materials 22: 2454.

[18] J Rafique, J Yu, J Yu, et al. (2007) Applied Physics Letters 91: 063126.

[19] P Katta, M Alessandro, R Ramsier, G Chase (2004) Nano letters 4: 2215.

[20] D Sun, C Chang, S Li, L Lin (2006) Nano letters 6: 839.

[21] H Chen, AdBFB Malheiro, C van Blitterswijk, C Mota, PA Wieringa, L Moroni (2017) ACS applied materials & interfaces 9: 38187.

[22] H Xia, Y Xia (2018) Materials Science and Engineering: C 91: 228.

[23] W Wang, J He, B Feng, et al. (2016) Nanomedicine 11: 1055.

[24] T Sharma, S Naik, J Langevine, B Gill, JX Zhang (2014) IEEE Transactions on Biomedical Engineering 62: 188.

[25] C Jin, H Fan, Y Wang, H Hwang, Y Zhang, Q Wang (2017) Ceramics International 43: 14476.

[26] C Xu, R Inai, M Kotaki, S Ramakrishna (2004) Biomaterials 25: 877.

[27] X Guan, H Chen, H Xia, Y Fu, Y Qiu, Q-Q Ni (2020) J. Intell. Mater. Syst. Struct.: 1045389X20906477.

Chapter 3: Mechanical properties

3.1 Introduction

The mechanical properties are regarded as one of the important factors in the composite materials. Although pure PZT ceramics show strong piezoelectric effect, the brittleness of PZT materials limits their applications [1]. Because of low consumption, low weight, flexibility and easy availability from the polymer [2], energy harvesters based on the polymer matrix obtain favorable flexibility and less expensive manufactures [3] than pure PZT ceramics. The piezoelectric ceramic-based composite energy harvesters require high-percent piezoelectric materials to enhance the piezoelectricity [4]. However, a high volume fraction of PZT particles within the polymer matrix is easy to aggregate [5] and cause poor interface bonding [6], which greatly decreases overall mechanical properties [7]. The mechanical properties of PZT based composite energy harvesters still cannot meet the requirement of flexibility in engineering fields. To overcome these disadvantages, various fibers and particles are compounded into the composites to enhance mechanical properties, like short carbon fibers [8], carbon nanotubes [9], graphene [10] and nanoparticles [11]. In addition, the modification processes are used in the preparation of composites [12] to enhance the interfacial bonding and improve the distribution of particles during mixing [13].

The mechanical properties include static mechanical, cyclic mechanical and dynamic mechanical characteristics. Generally, the static mechanical properties are measured by the tensile process, exhibiting some parameters like elastic modulus, yield stress, tensile

strength and breaking strain. The cyclic mechanical tests are employed to measure the stress relaxation and creep of materials. Dynamic Mechanical Analysis (DMA) is widely used to characterize the storage modulus, loss modulus and damping properties of as a function of temperature and frequency.

In this chapter, the static and cyclic mechanical measurements are conducted and investigated to clarify the mechanical properties. The influence of the filler content and the effect of modification on the composite mechanical properties are also studied.

3.2 Materials and methods

3.2.1 Static tensile test

A static tensile was preformed to investigate mechanical properties of the nanofibers by a universal tensile machine (RTC1250A, A&D Co., Ltd, Japan) at a speed of 1 mm/min at room temperature. According to the standard of JIS K-6251-7, the samples were cut into dumbbell specimens, in which the nanofiber directions were aligned along the tensile direction at 0° (longitudinal), 45° or 90° (transverse) as shown in Figure 2-2b, respectively.

3.2.2 Cyclic mechanical measurement

To understand the stress and strain relaxation behaviors of SMPU nanofibers, mechanical cycle tests under constant strain and constant stress were conducted respectively to observe the hysteresis of the developed materials. For the constant stress

cycle test, 50% of the maximum stress is specified as the upper limit. For the constant strain cycle test, the upper limit of strain was set at 50% of strain in the elastic region, where the upper limit of SMPU-R and aligned nanofibers was 3.5% and 3%, respectively. Each sample was tested in 60 cycles of loading and unloading at a speed of 3 mm/min at room temperature.

3.2.3 Dynamic mechanical analysis (DMA)

The thermomechanical properties were evaluated by a dynamic mechanical analyzer (DMA, IT Keisoku Seigyo Co., Ltd., Japan) at a frequency of 10 Hz. The samples were cut into rectangles (10-mm length and 2-mm width), and the thickness of the nanofibers was varied from 0.15 mm to 0.3 mm. All the samples were tested in tensile mode, and the experimental temperature was preformed from 30 °C to 110 °C at the heating rate of 5 °C/min.

3.2.4 Morphology Characterization and alignment degree

The surface morphology of nanofibers was observed by scanning electron microscopy (SU1510, Hitachi Co., Ltd., Japan). The alignment degree of random and aligned nanofibers were calculated by Image J software.

3.3 Results and discussion

3.3.1 Static mechanical properties

3.3.1.1 Mechanical properties of PZT/SMPU composite fibers

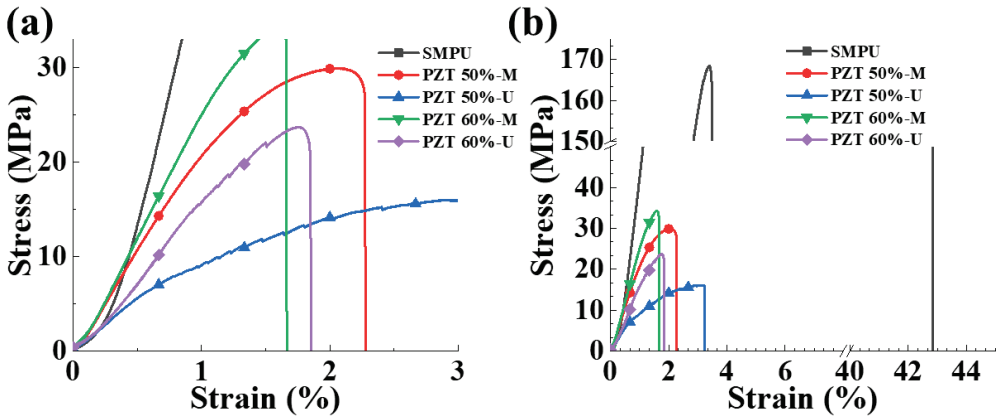

Figure 3-1. Comparison of strain-stress curves of pristine SMPU and PZT/SMPU composite fibers. (a) total graph. (b) enlarged graph of initial part.

The stress-strain curves for aligned PZT/SMPU nanofibers are shown in Figure 3-1. The yielding phenomenon was observed in all PZT/SMPU composite fibers without necking. After the yield limits, due to the strain-hardening phenomenon, the stresses slightly increase with the increase of strain in SMPU fibers. There is no obvious strain-hardening phenomenon in composite fibers. The tensile strength and breaking strain of composite fibers significantly decrease compared to SMPU fibers, while their elastic modulus is higher than that of SMPU fibers.

Table 3-1. Mechanical performances of pristine SMPU nanofibers and PZT/SMPU nanofibers

Materials	Elastic modulus (GPa)	Tensile strength (MPa)	Breaking strain (%)
SMPU	1.5	218.4	52.1
PZT 50%-U	1.1	16.0	3.2
PZT 50%-M	1.6	29.9	2.3
PZT 60%-U	1.1	23.7	1.8
PZT 60%-M	1.8	34.3	1.7

As demonstrated in Figure 3-1 and Table 3-1, the mechanical properties are dependent on the modification. Modified PZT/SMPU composite fiber has increased elastic modulus and tensile strength. Their elastic modulus enhances 1.63 times (from 1.1 GPa to 1.8 GPa), and tensile strength of PZT 60% increases by about 1.45 times. However, the breaking strain of PZT 50%-M and PZT 60%-M decreases by 28.1% and 5.5%, respectively. The above results indicate that the PZT particle modification improves the dispersion of fillers and interfacial bonding between fillers and the polymer matrix. The silane coupling agents act as a bridge to combine the SMPU matrix with particles, which augments mechanical properties. Additionally, similar behavior is observed from the mechanical properties of all composites fibers with different contents of PZT. The elastic modulus and tensile strength increase with the increasing content of PZT, indicating that the composite fibers become harder and stronger.

The tensile strength and breaking strain of pristine SMPU fibers are higher than those

of PZT/SMPU nanofibers. This can be attributed to the addition of PZT fillers, which hiders the movement of molecular chains and leaves a shorter strain until breaking. But after modification, the elastic modulus of the PZT 50%-M and PZT 60%-M improves by 6.7% and 20%, respectively, compared with SMPU fibers.

3.3.1.2 Effect of particles content and modification on the mechanical properties of random nanofibers

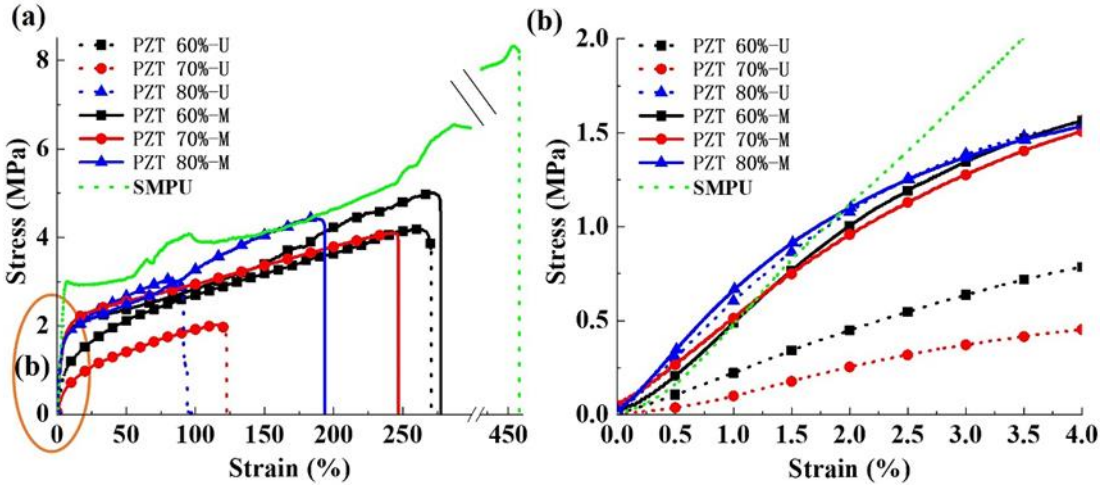

Figure 3-2. Comparison of strain-stress curves of pristine SMPU and PZT/SMPU nanofibers. (a) total graph. (b) enlarged graph of initial part.

The PZT/SMPU random nanofibers were divided into two groups depending on whether they were modified or not. The first group is the modified nanofibers, PZT 60%-M, PZT 70%-M and PZT 80%-M. The second group is unmodified nanofibers, PZT 60%-U, PZT 70%-U, and PZT 80%-U. All the percentages are weight percentages. The stress-strain curves for pristine SMPU and PZT/SMPU nanofibers are shown in Figure 3-1 at 25 ℃. Compared with the unmodified PZT/SMPU nanofibers, the elastic regions of modified nanofibers become larger after modification. The yielding

phenomenon is observed in all nanofibers with different PZT contents, but there is no occurrence of necking in PZT/SMPU nanofibers (Figure 3-2). After the yield limits, a strain-hardening phenomenon is observed that the strain become larger with the growth of stress slow down. All the modified nanofibers have lager break strain than those of unmodified nanofibers, this result indicate the PZT/SMPU nanofibers have good flexibility.

Table 3-2. Mechanical performances of pristine SMPU nanofibers and PZT/SMPU nanofibers

Materials	Yield stress [a)] (MPa)	Elastic modulus (MPa)	Tensile strength (MPa)	Break strain (%)
Pristine SMPU	2.80	23.89	8.24	375.8
PZT 60%-U	0.64	23.24	4.36	268.8
PZT 60%-M	1.26	46.75	4.81	283.1
PZT 70%-U	0.40	10.82	2.15	129.4
PZT 70%-M	1.22	91.67	4.01	242.6
PZT 80%-U	1.21	69.91	3.40	99.6
PZT 80%-M	1.28	74.83	4.26	203.5

[a)] Yield stresses are defined by the 0.2%-strain offset method.

In comparison of the unmodified PZT/SMPU nanofibers (Figure 3-2 and Table 3-2), the elastic moduli of modified PZT/SMPU nanofibers increase after modification, and also become higher than the elastic moduli of pristine SMPU nanofibers. The elastic moduli of the PZT 60%-M, PZT 70%-M and PZT 80%-M are improved by 26.52%,

626.67% and 0.33%, respectively. The increase of elastic modulus results from the better dispersion of fillers and better interfaces due to modification. The same phenomenon was observed in tensile strength in PZT/SMPU nanofibers. The Figure 3-2 and Table 3-2 show the enhancement in tensile strength of modified samples compared with that of unmodified nanofibers, the tensile stress of the PZT 60%-M, PZT 70%-M, and PZT 80%-M nanofibers increases by 10.32%, 86.51%, and 25.29%, respectively. Both tensile strength and elastic moduli of modified nanofibers are higher than those of unmodified nanofibers (Table 3-2). It can be explained by improved binding forces between the SMPU matrix and fillers after modification. The silane coupling agents act as a bridge to bind the SMPU matrix and particles. Thus, the saline coupling agents increase interfacial interactions and result in improvement in mechanical properties.

Additionally, a similar behavior is observed from yield stresses of all the PZT/SMPU nanofiber samples with different contents of PZT (Table 3-2). The yield stress of modified nanofibers is higher than that of unmodified nanofibers which results from modification. Compared with the unmodified nanofibers, the yield stress of the PZT 60%-M, PZT 70%-M, and PZT 80%-M nanofibers is improved by 96.88%, 205%, and 5.79%, respectively.

3.3.1.3 Effect of alignment degree on the mechanical properties of SMPU and PZT/SMPU nanofibers

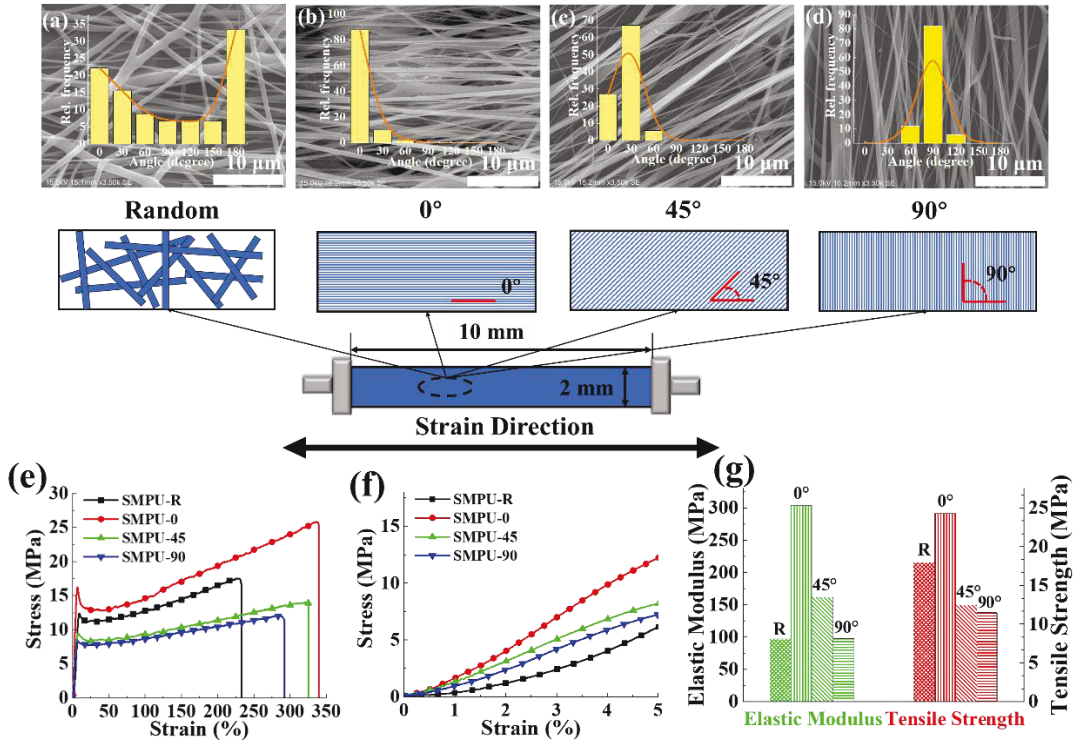

Figure 3-3. SEM images and mechanical properties of random and aligned SMPU nanofibers. (a–d) nanofiber orientation, (a) random nanofibers, (b) aligned nanofibers at 0°, (c) aligned nanofibers at 45°, (d) aligned nanofibers at 90°; (e) total strain–stress curves, and (f) the elastic region of the curves and (g) the elastic modulus and tensile strength.

According to the alignment degree, the random and aligned SMPU nanofibers developed are divided into four groups: 0° (SMPU-0), 45° (SMPU-45), 90° (SMPU-90) and random nanofibers (SMPU-R).

Figure 3-3 shows four types of samples with different nanofiber alignments, i.e., random, 0°, 45° and 90°, respectively. The random SMPU nanofibers are disordered in

the spatial orientation and form random nanofiber mats, resulting in a wide distribution of nanofiber angles (Figure 3-3a). In comparison, the aligned nanofibers are uniform across the collector and form well-aligned SMPU nanofiber mats, and the three prepared samples at different alignment angles with the main histograms of 0°, 45° and 90°, respectively.

The stress–strain curves for random and aligned SMPU nanofibers are shown in Figure 3-3e. The strain handing pheromone is observed in all the samples; the strains rise slowly with increasing stress after the yield limits, but there is no occurrence of necking. The break strains of random and aligned nanofibers are larger than 200%, indicating that all of the SMPU nanofibers have good flexibility.

Table 3-3. Mechanical performances of random and aligned SMPU nanofibers.

Materials	**Yield stress** * **(MPa)**	**Elastic modulus (MPa)**	**Tensile strength (MPa)**	**Break strain (%)**
SMPU-R	10.6	97.0	18.0	232.9
SMPU-0	13.0	303.7	24.3	325.0
SMPU-45	7.1	161.7	12.5	279.2
SMPU-90	6.6	97.9	11.5	275.9

* Yield stresses are defined by the 0.2%-strain offset method.

The mechanical properties of random and aligned SMPU nanofibers are shown in Figure 3-3f and g and Table 3-3. The mechanical properties of 0° alignment degree provide higher yield stress, elastic modulus, tensile strength and breaking strain than

randomly oriented SMPU nanofibers. Compared with SMPU-R, the yield stress, elastic modulus, tensile strength and breaking strain of SMPU-0 are increased by 22.6%, 213.1%, 35% and 39.5%, respectively (Table 3-3). When the alignment angle decreases from 90° to 0°, the volume of nanofibers along the strain direction becomes greater, which bear the main applied load during the tensile process, resulting in the promotion of the mechanical properties of aligned nanofibers. For the SMPU-90, when the transverse tensile is applied to the nanofibers, the tensile direction is perpendicular to the nanofiber direction; thus, the debonding and fractures of nanofibers in the off-axis direction lead to a decrease in break strains. These results indicate that the volume faction of nanofibers along the tensile direction plays an important role in mechanical properties.

Compared with the SMPU-R, stretching in the preparation process also contributes to the increment of tensile strength in SMPU-0 at temperatures below T_g. The aligned nanofibers are collected at high speed rotation with high tension in which the molecular chains are drafted along the longitudinal direction (rotation direction) at room temperature. This primary stretching in the preparation process endows the aligned nanofibers with higher stored energy than random nanofibers and cause an increase in elasticity and stiffness below T_g. Figure 3-8a shows that the storage modulus of aligned SMPU nanofibers is about five times higher than that of random SMPU nanofibers, especially for 0° sample. The increased storage modulus induces the hardness of nanofibers and leads to incremental strength.

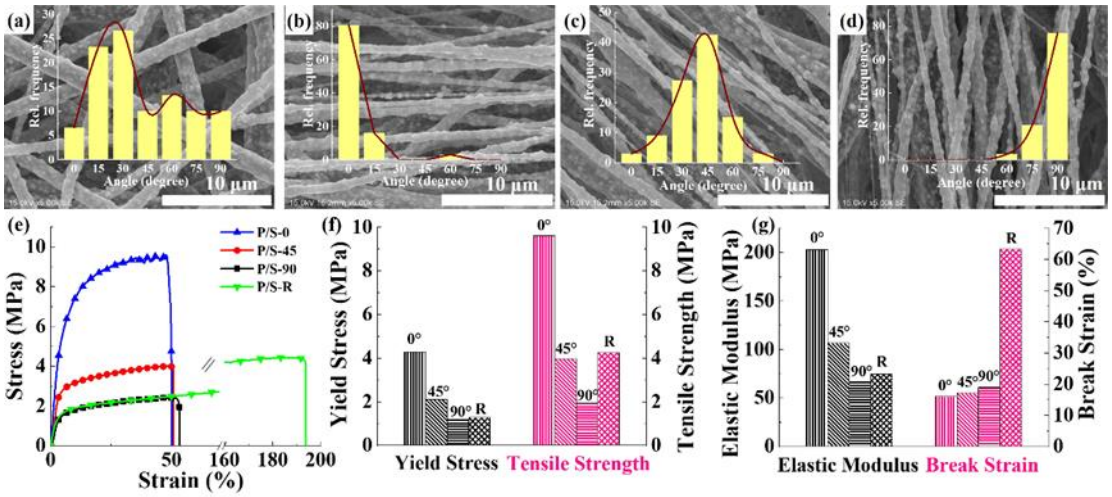

Figure 3-4. SEM images of PZT/SMPU nanofibers and variations of nanofiber orientation: (a) random nanofibers, (b) nanofibers aligned at 0°, (c) nanofibers aligned at 45°, (d) nanofibers aligned at 90°, (e) strain-stress curves of PZT/SMPU nanofibers, and (f-g) the yield stress, elastic modulus, tensile strength and break strain of PZT/SMPU nanofibers.

The PZT/SMPU nanofibers were divided into four groups depending on their alignment angles: 0° (P/S-0), 45° (P/S-45), 90° (P/S-90) and random (P/S-R).

Figure 3-4(a-d) clearly shows the microstructures of random and aligned PZT/SMPU nanofibers. By controlling the speed of the collector during the electrospinning process, the PZT/SMPU aligned nanofibers (Figure 3-4(b-d)) were aligned across the collector and uniformly oriented. In comparison, the random nanofibers (Figure 3-4a) were disordered in spatial orientation, and the resulting nanofibers deposited on the surface of the collector and formed a random nanofiber mat. A significant increment of aligned nanofibers was observed (Figure 3-4(b-d)) with increased rotation speed, and a large number of aligned nanofibers were distributed at the angles of 0°, 45° and 90°. From the SEM images and alignment degree histogram, we found that nanofibers were

distributed in the rotation direction, and formed high-density PZT/SMPU nanofiber mats. However, the random nanofibers were in a wide range of alignment degrees, with the nanofibers randomly distributed in different directions.

The stress-strain curves for aligned PZT/SMPU nanofibers are shown in Figure 3-4d. The effect of nanofiber direction on stress–strain response was significant at all alignment angles. When the alignment angle increased from 0° to 90°, the elastic modulus and tensile strength were sharply decreased. After the yield limits were exceeded, because of the strain-hardening phenomenon, the stresses increased slightly with increasing strain, but the strain-hardening range of the aligned nanofibers became small between the alignment angles of 0° and 90°. These results also demonstrated that the overall mechanical properties were improved when the aligned nanofibers were oriented close to the tensile direction, i.e., with an alignment angle of 0° and a sufficient ductile break strain of around 50%. The mechanical properties of random nanofibers (P/S-R) were similar to those of P/S-45, but the break strain of P/S-R was significantly higher than that of all the aligned nanofibers.

Table 3-4. Mechanical performances of aligned PZT/SMPU nanofibers

Materials	**Yield stress** * **(MPa)**	**Elastic modulus (MPa)**	**Tensile strength (MPa)**	**Break strain (%)**
P/S-0	4.3	203.1	9.6	51.5
P/S-45	2.1	106.6	4.0	55.1
P/S-90	1.2	66.8	1.9	60.9
P/S-R	1.3	74.8	4.3	203.5

* Yield stresses are defined by the 0.2%-strain offset method.

As demonstrated in Figure 3-4(e-f) and Table 3-4, the strain and strength of aligned nanofibers depended on the alignment angle of nanofibers in the tensile process. For the sample with an alignment angle of 0°, its tensile strength reached 9.6 MPa, almost 5 times as large as that of the sample with an alignment angle of 90°. Similar behavior was also observed for the yield stress and elastic modulus, which were significantly enhanced to 3.5 times in yield stress (from 1.2 MPa to 4.3 MPa) and about 3 times in elastic modulus (from 66.8 MPa to 203.1 MPa). Fiber orientation contributed to all of the results, and is a key parameter that affected the mechanical properties of the PZT/SMPU nanofibers. Because nanofibers are the main load-bearing objects during the tensile process, the volume of nanofibers along the loading direction determines the mechanical properties of materials. Therefore, increasing the alignment of nanofibers is an effective way to improve the mechanical properties of PZT/SMPU nanofibers.

The mechanical properties of random and aligned nanofibers were significantly different depending on the orientation of nanofibers. Yield stress, elastic modulus and tensile strength of the sample with an alignment angle of 0° (P/S-0) were greater than those of those of the sample of random nanofibers (P/S-R). In contrast, the random nanofibers P/S-R exhibited the best break strain to 203.5% compared with 51.5%, 55.1% and 60.9% for the aligned nanofibers of 0°, 45° and 90°, respectively. These results also indicated that the amount of nanofibers along the loading direction is a key issue for improving mechanical properties. The nanofibers along the loading direction act as the main load-bearing object.

3.3.2 Mechanical cycle analysis

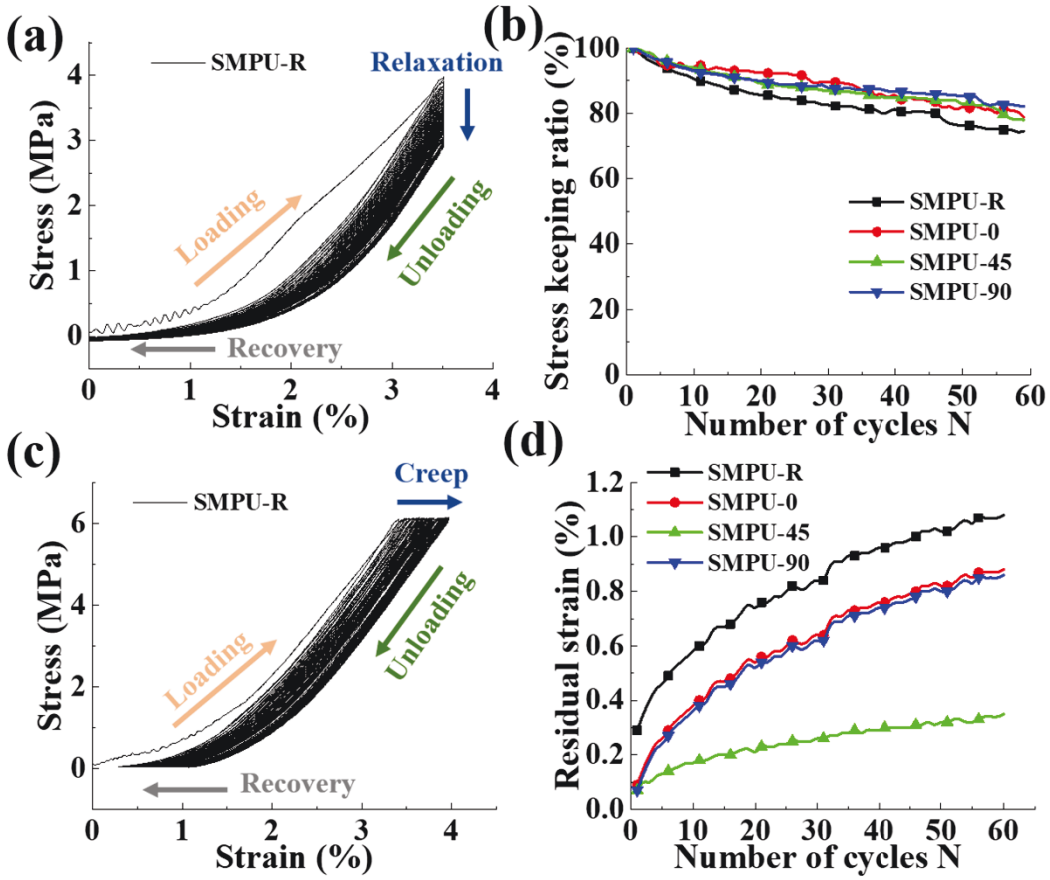

Figure 3-5. Representative cyclic mechanical testing results under constant strain or constant stress conditions. (a) stress–strain curves of SMPU-R under constant strain showing relaxation with increasing cycle numbers, (b) residual strains of SMPU nanofibers under a constant strain condition, (c) stress–strain curves of SMPU-R under constant stress conditions showing creep with increasing cycle numbers, (d) stress keeping ratios of SMPU nanofibers under a constant strain condition.

Figure 3-5a shows the stress–strain curve of SMPU-R in 60 cycles under a constant strain cycle loading, which includes the loading, relaxation, unloading, and recovery process. Hysteresis loops are observed in all cycles. The elastic modulus sharply

decreased in first cycle and reduced slowly afterward. The stress–strain curve loop of each cycle shift increased as the number of cycles increased. Figure 3-5b shows the stress keeping ratios of four types of SMPU nanofiber samples with increasing cycle numbers. Compared with the SMPU-R, the stress keeping ratios of aligned SMPU nanofibers declined slowly and stayed higher than 78% even after 60 cycles, which means the tensile stress relaxed slowly. These results indicate that the aligned nanofibers are of better dimensional stability and have higher elastic recovery ability during deformation than those of random nanofibers; the aligned structures of nanofibers have an influence on the remaining strain.

Figure 3-5c shows the stress–strain curves under a constant stress condition; the hysteresis loops shift slowly as the number of loading cycles increases where the slope change of loops showed no obvious change during this creep process. Figure 3-5d shows the relationship between cycle number and residual strain of random and aligned SMPU nanofibers. It is evident that the residual strain reduced slowly and tended to flatten due to the strain hardening phenomenon as the cycle number increased during loading cycles under constant stress.

The increment of residual strain in the aligned nanofibers (0° to 90°) between the first and last tensile cycle is 0.72%, 0.28% and 0.77%, respectively, which is lower than that of the random nanofibers. The lower residual strain during loading cycles suggests that the aligned SMPU nanofibers have good strain recovery ability during deformation. The total residual strains of aligned SMPU nanofibers in the 0°, 45° and 90° samples are only 0.82%, 0.35% and 0.94%, respectively, remaining higher than the 99%

recovery ratio even at 60 cycles. These results indicate that the aligned nanofibers are good candidates as reinforced structures to enhance mechanical properties even in cycle loading. The high stress keeping ratios and low residual strains of the aligned nanofibers are attributed to the storage modulus of the aligned nanofibers and related microstructure improvement during the electrospinning process. The aligned nanofibers have a better ability to recover from the deformed strain after unloading, which may be because of the contribution of the larger storage modulus than that of random nanofibers in the glassy state, resulting in lower residual strains. Long-term stability under cyclic loading is an important issue for support structures. The lower stress relaxation and limited creep of aligned SMPU nanofibers indicated that the aligned SMPU nanofibers have higher stability to against repeated stress and strain compared with the random SMPU nanofibers, and may be suitable for long-term and repeatable use.

3.3.3 Dynamic mechanical analysis

3.3.3.1 Dynamic mechanical properties of PZT/SMPU composite fibers

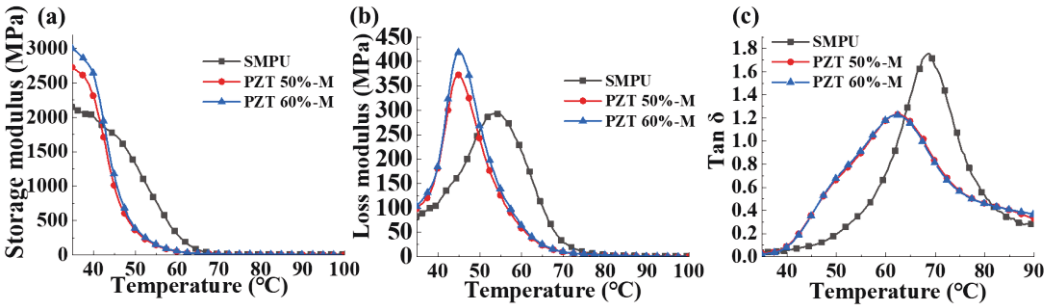

Figure 3-6. Dynamic mechanical properties of PZT/SMPU composite fibers, (a) Storage modulus, (b) Loss modulus, (c) Tan δ.

The results of Figure 3-6a show that the storage modulus of PZT/SMPU composite fibers are higher than that of SMPU fibers, and increased with the increasing of PZT content in the glassy state. These results indicated that the modification process and addition of PZT fillers enhance the storage modulus of PZT/SMPU composite fibers, corresponding to the increment of elastic modulus (Table 3-1).

The results of loss modulus (Figure 3-6b) show that the PZT 60%-M nanofibers have the largest loss modulus than those of other samples. The results of tan δ (Figure 3-7c) show that a slightly shift in the peaks of tan δ of pristine SMPU and PZT/SMPU composite fibers is found. It means the T_g of modified PZT/SMPU nanofibers is almost changed after modification.

3.3.3.2 Effect of particles content and modification on the dynamic mechanical properties of random nanofibers

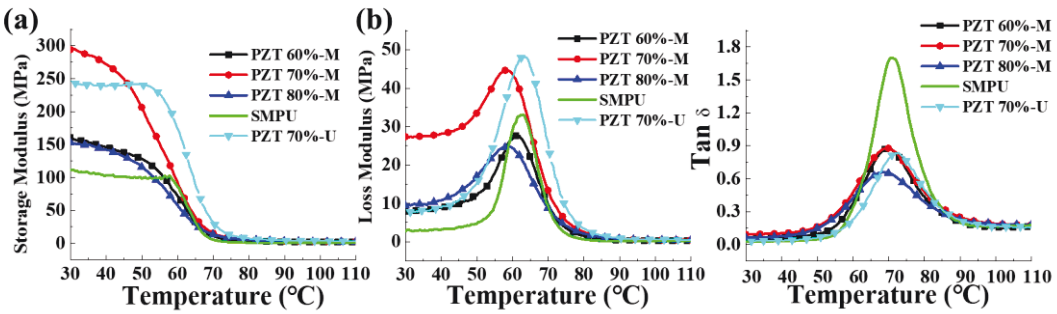

Figure 3-7. Dynamic mechanical properties of modified and unmodified PZT/SMPU nanofibers, (a) Storage modulus, (b) Loss modulus, (c) Tan δ.

As shown in Figure 3-7a, all storage modulus of PZT/SMPU nanofibers is higher than that of SMPU nanofibers. This can be attributed to the addition of PZT fillers, which can store more energy than pristine SMPU during tensile. Moreover, PZT 70%-

M has higher storage modulus than that of PZT 70%-U. This indicates that the filler modification enhances storage modulus, corresponding to the enhanced mechanical properties after modification.

The results of loss modulus (Figure 3-7b) show that the PZT 70%-M nanofibers have the largest loss modulus than those of other samples. The results of tan δ (Figure 3-7c) show that no obvious shift in the peaks of tan δ of pristine SMPU modified PZT/SMPU nanofibers is found. It means the T_g of modified PZT/SMPU nanofibers is almost not changed.

3.3.3.3 Effect of alignment degree on the dynamic mechanical properties of SMPU and PZT/SMPU nanofibers

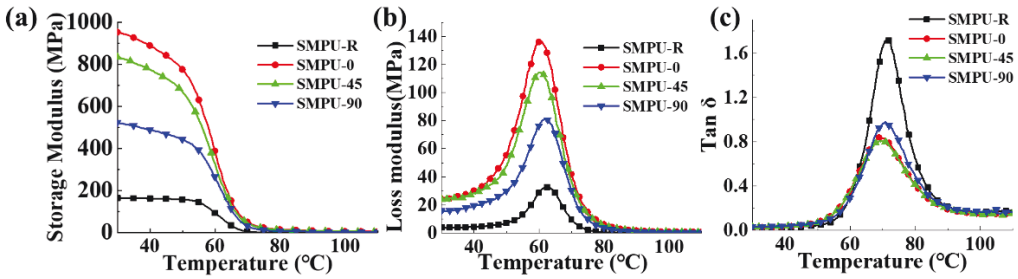

Figure 3-8. Dynamic mechanical properties of random and aligned SMPU nanofibers, (a) Storage modulus, (b) Loss modulus, (c) Tan δ.

The results of Figure 3-8a show that the storage modulus of aligned SMPU nanofibers are higher than that of random SMPU nanofibers, and increased with the decreasing of alignment degrees in the glassy state. Increased storage modulus induce the harder of nanofibers, led to the increment of strength, and reduces the degree of freedom for the movement of molecular chain. That why the SMPU-R have higher

tensile strength but lower breaking strain than that of SMPU-45 (Table 3-3). With the decreasing of alignment degrees, the storage modulus of aligned SMPU nanofibers are enhanced and reaches to the maximum value at 0 degree. It is indicated that the SMPU-0 can storage more energy during deformation.

The results of loss modulus (Figure 3-8b) show that the SMPU-0 have the largest loss modulus than those of other samples. The results of tan δ (Figure 3-8c) shows the tan δ of random SMPU nanofibers are higher than that of aligned SMPU at the temperature range at T_g and reach maximum 1.7, but all the tan δ of aligned nanofibers are less than 1. Since the tan δ represent the ratios of viscous to elastic response or energy dissipation of a material with an applied force, the lower tan δ at T_g indicated that the aligned SMPU nanofibers store more energy and reveal more elastic response. Therefore, decreased tan δ indicates that aligned SMPU nanofibers has more potential to store energy from load than dissipating it at above T_g, the stored energy during cooling process can be released after reheating to recovery the deformed strain.

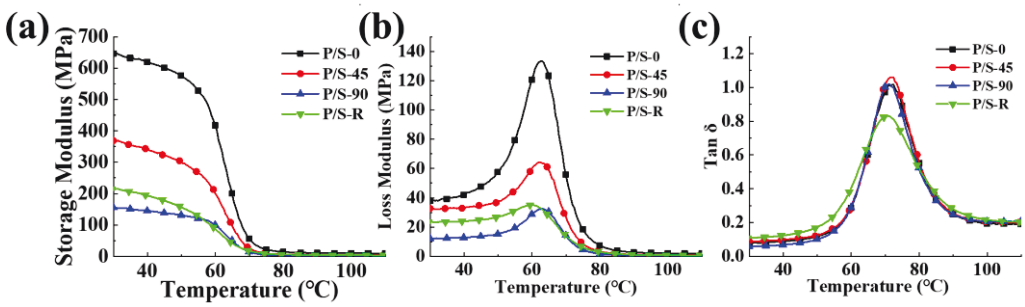

Figure 3-9. Dynamic mechanical properties of random and aligned PZT/SMPU nanofibers, (a) Storage modulus, (b) Loss modulus, (c) Tan δ.

Different with the dynamic mechanical analysis of SMPU nanofibers (Figure 3-8a), the storage modulus of random P/S-R nanofibers (Figure 3-9a) are higher than that of

P/S-90, and all the storage modulus of random and aligned SMPU nanofibers are decreased after PZT particles added. This phenomenon can be explained by the addition of PZT fillers. In the pristine SMPU nanofibers, the stored energy is more depend on the deformation of SMPU nanofiber, but the movement of SMPU polymer chain are hindered when PZT fillers added. That's why storage modulus of SMPU nanofibers are higher than those of PZT/SMPU nanofiber. In the random and aligned PZT/SMPU nanofibers, the P/S-R have larger breaking strain than that of other aligned PZT/SMPU nanofibers, so the added filler have little influence on the random PZT/SMPU nanofibers, leave a higher storage modulus than P/S-90.

The results of loss modulus (Figure 3-9b) show that the P/S-0 have the largest loss modulus than those of other samples. The results of tan δ (Figure 3-9c) show that no obvious shift in the peaks of tan δ of random and aligned PZT/SMPU nanofibers is found. It means the T_g of PZT/SMPU nanofibers is almost not changed.

3.4 Conclusions

The saline coupling agents that perform as a bridge between the SMPU matrix and particles significantly improve the dispersion of PZT fillers in SMPU matric and interfacial bonding. The elastic modulus and tensile strength of PZT 60%-M composite fibers increase by 63.6% and 44.7%, respectively, compared with unmodified PZT 60%-U.

The similar improvements are found in the mechanical properties of the modified nanofibers, including the tensile strengths (increased by at least 9.36%), yield stresses

(increased by at least 5.47%) and break strains (increased by at least 5.03%). Compared with the pristine SMPU nanofibers, the recovery stress of the PZT 60%-M, PZT 70%-M and PZT 80%-M increases by 26.15%, 76.99% and 21.2%.

By changing the nanofiber alignment degree in the aligned SMPU nanofibers, our results indicate that there exists an optimum alignment degree for aligned SMPU nanofibers to improve mechanical properties. SMPU-0 (with a nanofiber direction parallel to the strain direction) exhibited better mechanical properties than those of random SMPU nanofibers, including yield stress (increased by 123%), tensile stress (increased by 135%), elastic modulus (increased by 313%) and breaking strain (increased by 120%). The aligned nanofiber structures enhanced the durability of the developed materials in cycle tests, and showed a stress keeping rate of over 80% with a residual strain of less than 0.8, even at 60 tensile cycles.

Well aligned PZT/SMPU nanofibers were fabricated by electrospinning technology wherein the orientation of nanofibers was controlled and designed. The results indicate there exists an optimum alignment angle for the fabrication of aligned PZT/SMPU nanofibers. In terms of mechanical properties, the alignment angle of 0° in the loading direction endows the aligned nanofibers with superior mechanical properties, recovery rates and recovery stress. Compared with the random nanofibers (P/S-R), the 0° aligned nanofibers (the nanofiber direction is parallel to the tensile direction) exhibit superior mechanical and shape recovery properties, including yield stress (increased by 230%), tensile stress (increased by 123%), elastic modulus (increased by 171%) and recovery rates (increased by 5.1%).

Reference

[1] A Jain, AK Sharma, A Jain (2015) Polymer Engineering & Science 55: 1589.

[2] TQ Nguyen, H-H Kausch (2012) Flexible polymer chains in elongational flow: Theory and experiment. Springer Science & Business Media,

[3] Y Sun, J Chen, X Li, Y Lu, S Zhang, Z Cheng (2019) Nano Energy 61: 337.

[4] X Ji, Y Hou, Y Chen, Y Zhen (2019) Materials & Design 179: 107890.

[5] S Liu, E Senses, Y Jiao, S Narayanan, P Akcora (2016) ACS Macro Letters 5: 569.

[6] H Chen, H Xia, Q-Q Ni (2018) Composites Part A: Applied Science and Manufacturing 110: 183.

[7] J Ma, Q Meng, I Zaman, et al. (2014) Composites Science and Technology 91: 82.

[8] B Xiong, Z Wang, C Wang, Y Xiong, C Cai (2019) Intermetallics 106: 59.

[9] TH Nam, K Goto, T Kamei, et al. (2019) Journal of Composite Materials 53: 1241.

[10] H Wang, G Xie, M Fang, Z Ying, Y Tong, Y Zeng (2017) Composites Part B: Engineering 113: 278.

[11] R Ghorpade, C Rajan, N Chavan, S Ponrathnam (2015) Express Polymer Letters 9.

[12] NE Marcovich, MI Aranguren, MM Reboredo (2001) Polymer 42: 815.

[13] K Sonoda, J Juuti, Y Moriya, H Jantunen (2010) Composite Structures 92: 1052.

Chapter 4: Shape memory performance and shape recovery mechanism of pristine SMPU and PZT/SMPU composites

4.1 Introduction

In recent years, many fabrication methods such as foaming formation [1] and 3D printing [2] are used to construct 3D structures with SMPs according to various demands. Electrospinning is directly of great importance to the production of nanofibers [3] with diameters from the nanoscale to microscale for simplicity and low consumption [4]. These one-dimensional nanostructures are playing a vital role in the design of new biomaterials, such as wound healing [5], biocompatible electrically conductive devices [6,7], and bone tissue repair [8]. The electrospun nanofibers possess critical attention and a wide range of applications, in which the highly aligned nanofiber structures may possess different characterizations that are easy for engineering applications [9]. The aligned nanofiber scaffolds of SMPs were created for implantable devices and functional scaffolds [10-12]. Thus, nanofiber structures may have a great influence on shape memory properties and their applications. Although aligned nanofibers have been used in various fields of biomaterials, the research of shape memory materials still mainly focus on improving recovery rate [13], increasing the recovery stress and strain [14] and shorten recovery time [15]. But the development of aligned SMPU nanofibers and investigation the influence of alignment degree on the shape memory properties are hardly reported.

In our group, SMPU and its nanocomposites have been developed for various

applications such as sensing and actuation [16-19], electromagnetic wave shielding [20,21], scaffold structures [22,23] and artificial blood vessels [24] for its excellent shape memory performance and good biocompatibility. The SMPU based foam scaffolds exhibited a good compression recovery property and controllable size, promoting cell proliferation for self-healing [25]. These porous SMPU scaffolds may provide ideas and methods for scaffold design and tissue engineering, suggesting potential applications for bone defect repair. SMPUs also can be made into nanofibrous scaffold rods for cell growth in a controlled direction. Taking advantage of the shape memory effect, the SMPU based tubular scaffolds and artificial blood vessels with the ability of programmed deformation also extend SMPUs as a candidate material in tissue engineering [26].

In this chapter, the thermal mechanical analysis is conducted and investigated to clarify the shape memory recovery and fixing behavior. The mechanisms of how the alignment angle of nanofibers affect the shape memory properties are discussed systemically. In the terms of nanofibers, the alignment degrees of 0° (parallel to the tensile direction), 45° and 90° are analyzed to exhibit the dependence of both shape recovery rate and shape recovery stress on nanofiber direction, which may provide a reasonable design to use shape memory materials and expand SMP applications.

4.2 Materials and methods

4.2.1 Shape recovery rate test

The random and aligned SMPU and PZT/SMPU nanofibers were cut into a rectangle (10 mm length and 2 mm width). For the aligned nanofibers, the length direction of the sample was cut at 0° (nanofiber direction), 45°, and 90° (transverse), respectively.

To investigate the shape memory properties (shape recovery rate) of the random and aligned nanofibers, thermomechanical stress cycle tests were performed using a thermomechanical analyzer (TMA / SS6100, Hitachi High-Tech Science Corp., Japan) in a temperature range from about 15 °C to about 70 °C. Before they started to stretch, to keep them from buckling, the samples (10 mm long and 2 mm wide) were heated to about 70 °C (the glass transition temperature (T_g) of SMPU is 65 °C) under a prestress of 0.012 MPa. The tensile stress was then increased to 0.12 MPa over 10 min. The samples were cooled down to room temperature and kept for 5 min while stress was maintained at 0.12 MPa. Before the samples were reheated to about 70 °C again, the tensile stress was decreased to 0.012 MPa over 10 min. These steps were only one cycle of the recovery test, and all samples were measured in three cycles.

The shape recovery rates R_r(N) were calculated according to the following formula (1).

$$R_r(N) = \frac{\varepsilon_m(N) - \varepsilon_f(N)}{\varepsilon_m(N) - \varepsilon_f(N-1)} \times 100\% \quad (1)$$

where ε_m denotes the maximum strain under the loading condition, ε_f denotes the residual strain after shape recovery, and N denotes the number of cycles.

The rate of shape fixity R_f is defined by the following equation (2).

$$R_f(N) = \frac{\varepsilon_u(N)}{\varepsilon_m(N)} \times 100\%, \quad (2)$$

where ε_m denotes the maximum strain under loading condition above the T_g temperature, ε_u denotes the strain after unloading at room temperature, N denotes the number of cycles.

4.2.2 Shape recovery stress test

In the recovery stress measurement, first, the samples were heated to about 70 °C and kept at the original strain at the same time. Second, the strain was increased to 10% over 10 min, then the samples were cooled to room temperature and kept for 5 min at the same strain. Then, the strain was adjusted until the stress reached zero at room temperature. Finally, the samples were reheated to about 70 °C while the strain was kept at 10%, and the recovery data were recorded by a thermo-mechanical analyzer (TMA).

4.3 Results and discussion

4.3.1 Shape recovery rate

4.3.1.1 Shape recovery rate of PZT/SMPU composite fibers

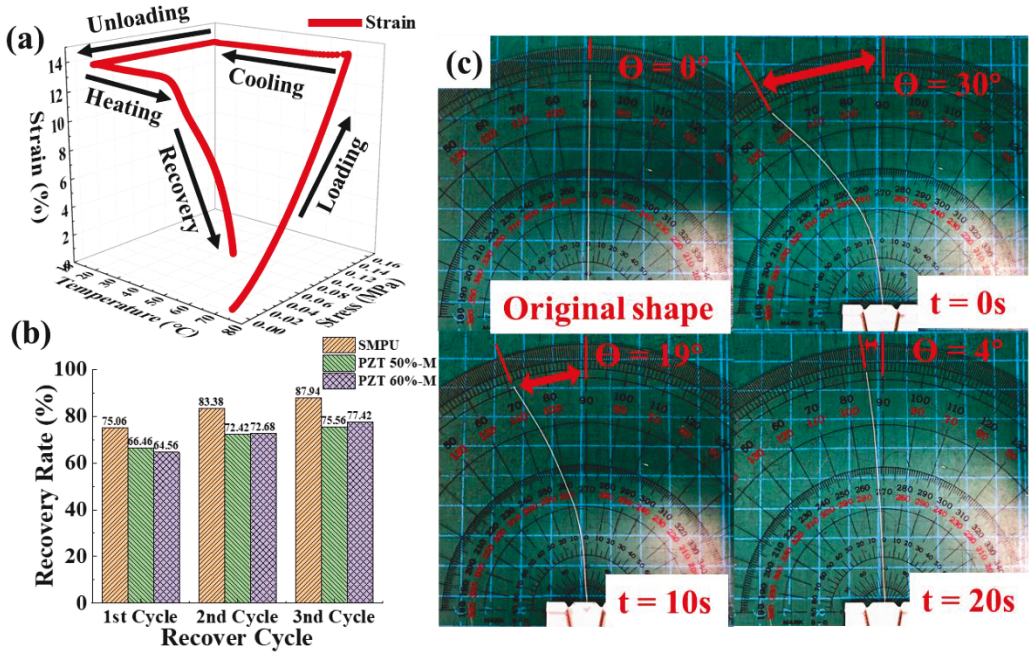

Figure 4-1. Shape recovery rates of SMPU and modified PZT/SMPU composite fibers. (a) 3D graph of shape memory cycles for PZT 60%-M composite fibers. (b) Comparison of recovery rates of SMPU and modified PZT/SMPU composite fibers. (c) Image of PZT 60%-M recovering.

To calculate the shape memory recovery rates of composite fibers, the pure SMPU and the modified PZT/SMPU composite fibers are all tested for three cycles, and the one cycle process shown in Figure 4-1a. Firstly, the fibers are heated about 70°C and stabilized for a few minutes to ensure that the temperature of nanofibers samples above its T_g temperature. Then the fibers are stretched at the same speed of 0.011 MPa/min

under the T_g temperature. Secondly, when the stress reaching 0.12 MPa, the fibers began to cooling down, and the stress still keep at 0.12 MPa. At the beginning stage of cooling, because of the elastic recovery and the principle of thermal expansion of fibers, the strain abruptly decreased and then changed to be steady. After the temperature of sample decreased to the room temperature, the stress began to decline to the pretension force. Finally, the fibers are reheated again. Due to the shape memory effects from SMPU, the strain of fibers began to decrease when the sample temperature above its T_g temperature. This result suggests that the PZT/SMPU composite fibers began to recover to their initial shape. The temperature of fibers is maintained above T_g temperature to complete the process of shape memory shape recovery. The image of PZT 60%-M composite fibers recovery process are shown in Figure 4-2c.

Table 4-1. Shape recovery rates of SMPU and PZT/SMPU composite fibers

Materials	**Recovery rate (%)**		
	1st cycle	**2nd cycle**	**3rd cycle**
SMPU	75.1	83.4	87.9
PZT 50%-M	66.5	72.4	75.6
PZT 60%-M	64.6	72.7	77.4

Compared with unmodified PZT/SMPU nanofibers, the shape recovery performance of PZT 50%-M and PZT 60%-M composite fibers increase to 66.5% and 64.6%, respectively, in the first cycle (Table 4-1). Even the PZT content reach 80%, the shape recovery rates are still no less than 60%. It is indicated that modified nanofibers have a good shape recovery ability.

Furthermore, after the first cycle, the recovery rates of the modified PZT/SMPU composite fibers are greater than 72% (Table 4-2), which is similar to the performance of pure SMPU. The recovery rates of PZT/SMPU composite fibers increase with the cycle number. PZT 50%-M and PZT 60%-M composite fibers obtain the recovery rates more than 75% in third cycle. The recovery rates in the third cycle increase slightly compared with those in the second cycle. This phenomenon is called "training" effect [27] which has been reported by many researchers [28,29].

4.3.1.2 Effect of PZT particles modification on the shape recovery rate of random nanofibers

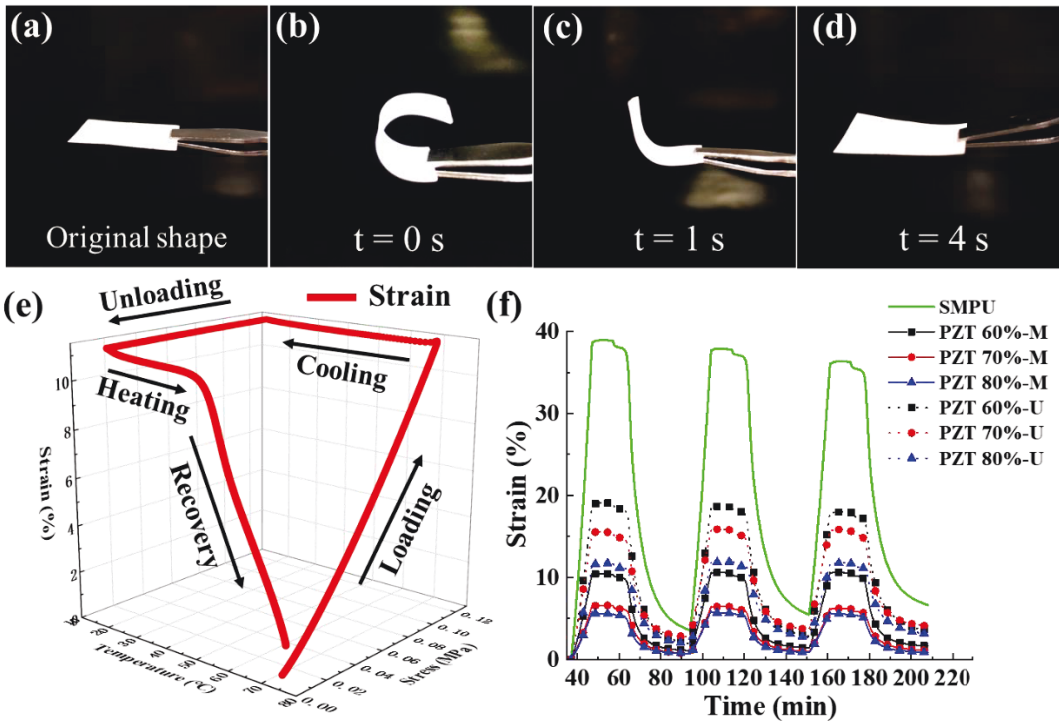

Figure 4-2. Shape recovery performance of pristine SMPU and PZT/SMPU nanofibers. (a-d) Image of sample recovering, (e) 3D graph of shape memory cycles for PZT 60%-M nanofibers, (f) Comparison of strain of different samples over three cycles.

To exhibit the shape memory effects of PZT/SMPU nanofibers (PZT 60%-M) visually, the recovery process of bending deformation is shown in Figure 4-2(a-d). The sample recoveries to the original shape (Figure 4-2a) due to the shape memory effect. When the sample is heated to above the T_g temperature, it is deformed into the designed shape, and then the sample is cooled down to below the T_g temperature to fix the deformed shape (Figure 4-2b). Then, the sample is heated to above the T_g temperature again, and starts recovering to the original shape (Figure 4-2(c-d)). From the above experiment, we can see the nanofibers have good shape recovery properties. It shows the ability that the PZT/SMPU nanofiber can be shaped easily just by a heating and cooling process.

In order to exactly calculate the shape memory recovery rates, the pure SMPU and the PZT/SMPU nanofibers were all tested for three cycles, and a three-dimensional graph of one cycle process of PZT 60%-M is shown in Figure 4-2e. In the loading stage, the sample are stretched under 0.12 MPa stress above the T_g temperature. In the cooling stage, the stress keeps at 0.12 MPa, and the sample is cooled from the T_g temperature to room temperature. At the beginning stage of cooling, the strain abruptly decreases and then becomes steady, because of the elastic recovery and thermal expansion. In the unloading stage, the sample is fixed at room temperature, and the stress begins to decline to 0.012 MPa. In the heating stage, the sample begins to recover to their initial shape when the sample temperature above the T_g temperature.

Table 4-2. Shape recovery performances of pristine SMPU and PZT/SMPU nanofibers

Materials	Recovery rate (%)			Average young's modulus above *T*g (KPa)
	1st cycle	2nd cycle	3rd cycle	
Pristine SMPU	90.9	94.4	96.2	4.2
PZT 60%-U	89.5	94.6	95.6	7.6
PZT 60%-M	89.7	96.6	97.5	12.4
PZT 70%-U	82.6	93.0	96.6	8.0
PZT 70%-M	85.7	94.1	96.8	18.4
PZT 80%-U	83.9	92.0	95.2	11.8
PZT 80%-M	84.8	94.0	96.5	20.1

Due to the different young's modulus of various PZT contents of PZT/SMPU nanofibers, the strains of nanofibers are different from the various PZT contents (Figure 4-2f). With the increase of PZT contents, both the strains of modified and unmodified PZT/SMPU nanofibers are decreased. Additionally, the strain above the T_g temperature of modified nanofibers are lower than that of unmodified sample, and the average young's modulus above the T_g temperature of the modified nanofibers was higher than that of the unmodified nanofibers (Table 4-2). The Young's modulus above the T_g temperature reflect the deformation of material, which depends on the interfaces between fillers and polymer. These result from the coupling agent enhancing the interfaces between the polymer matrices and PZT fillers, giving rise to the increase in

the Young's modulus above the T_g temperature.

Furthermore, above the T_g temperature, the strain of the materials increased owing to disentanglement of molecular chains, which caused large-scale deformation. Such large deformations are more likely to occur at the interfaces of the composites. Therefore, the improvement in the average value of the Young's modulus above the T_g indicates that the interfaces of the modified nanofibers are greater than those of the unmodified nanofibers.

Compared with unmodified PZT/SMPU nanofibers, the shape recovery performance of PZT 60%-M, PZT 70%-M, and PZT 80%-M nanofibers increase to 89.73%, 85.74%, and 84.8%, respectively in the first cycle (Table 4-2), and higher than those of PZT 60%-U, PZT 70%-U, and PZT 80%-U at the second and third cycle. Despite many previous studies on SMP nanofibers, which have tried to explain the changes in recovery rates, these effects are simply attributed to factors such as the restriction on movement of SMP soft segments induced by the added fillers. However, recently, a molecular mechanism of shape memory composites was proposed, which shows the fillers in the SMP matrix both promote and inhibit recovery performances. This mechanism can be used to explain the reason for the increase in shape memory recovery rates of the modified nanofibers. The interfaces in unmodified nanofibers are poor and modification of PZT particles enhance interfaces. According to the above mechanism, poor interfaces lead to weak "cross-link" effects of fillers and the enhancement of interfaces due to modification improve the "cross-link" effects of fillers. As a result, the modified nanofibers perform higher recovery rates.

Furthermore, after the first cycle, there is no obvious decrease of recovery rate among second and third cycle, the recovery rates of the modified PZT/SMPU nanofibers were greater than 94%, which is similar to the performance of pure SMPU. What's more, the recovery rates of PZT/SMPU nanofibers are increased with the increased cycle numbers, and the rate tends to be 100%. Different with the first cycle, there is significate decrease of the addition of PZT content to the recovery rate of PZT/SMPU nanofibers. Compared with the PZT 60%-M, the recovery rate of PZT 80%-M decreased by 4.93% in first cycle, but only decreased by 2.59% and 1% in second and third cycle. This phenomenon is called "training" effect which has been reported by many researchers. It is indicated that both the unmodified and unmodified PZT/SMPU nanofibers show good repeatability and shape memory recovery abilities after training cycle.

4.3.1.3 Effect of aligned structures on the shape recovery rate of SMPU and PZT/SMPU nanofibers

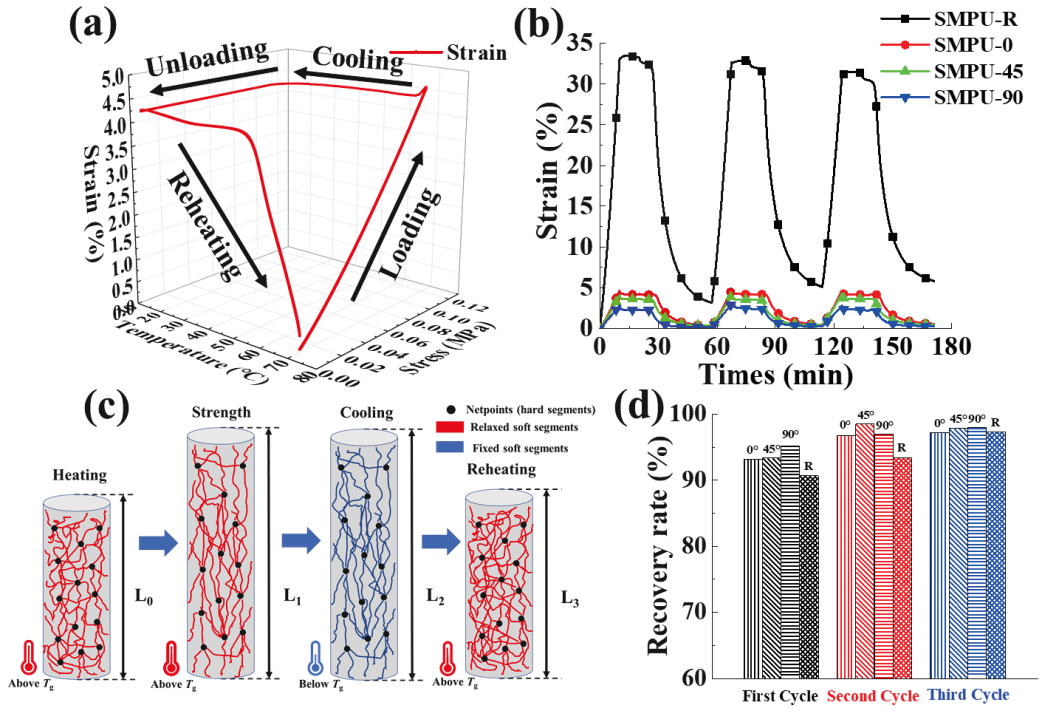

Figure 4-3. (a) 3D schematic of shape recovery measurement for SMPU-0 nanofibers, (b) comparison of the strains in different samples over three cycles, (c) the molecular mechanism of shape memory effect under thermal stimuli, (d) comparison of recovery rates of random and aligned SMPU nanofibers in three cycles.

To clarify the shape recovery ability of the developed materials, a 3D thermal testing program is designed, as shown in Figure 4-3a. The program includes heating, loading, cooling and recovery processes, and all samples are tested in three cycles to measure the shape recovery rates. The mechanism of SMPU can be shown schematically (Figure 4-3c), where the mobility of the soft segments between the netpoints (hard segments) increase and result in easy deformation after the SMPU is heated above T_g. The soft

segments store strain energy when external stress is applied, resulting in an entropy decrease, and stabilize the temporary shape by crystallization or other means [30] if the temperature is cooled to the glassy stage. When the nanofibers are reheated, the soft segments release the storage strain energy and recover to their original shapes using the stored energy, which causes the entropy state to return to the highest level [31].

Figure 4-3d and Table 4-3 show the shape recovery rates of random and aligned nanofibers, which strongly depended on the fiber orientation. In the first cycle, compared with the random SMPU nanofibers, the aligned SMPU nanofibers exhibited a slight promotion in recovery rates. The recovery rates of SMPU-0, SMPU-45 and SMPU-90 reached 93.8%, 92.3% and 95.7%, respectively, in the first cycle. As the test cycle is repeated, the shape recovery rates of all the samples improved, with values larger than 97% in the third cycle due to the training process and stress-induced polymer chain reorientation during the tensile process.

Table 4-3. Shape recovery rates of random and aligned SMPU nanofibers

Materials	**Recovery rate (%)**		
	1st cycle	**2nd cycle**	**3rd cycle**
SMPU-R	90.7	93.4	97.3
SMPU-0	93.2	96.8	97.2
SMPU-45	93.4	98.5	97.8
SMPU-90	95.2	97.0	97.9

For the SMPU, the netpoints (hard segments) between the soft segments act as the fixed phase to memorize the original shapes (Figure 4-3c), and determine the permanent shape and recovery rates of the SMPU. The aligned SMPU nanofibers are adjusted the

alignment degrees of nanofibers and do not significantly influence the volume of soft and hard segments. The difference in shape recovery rates (Table 4-3) between the random and aligned nanofibers in the first cycle is caused by the polymer chain slippage of soft segments during tensile at above T_g, and the orientation ratio of nanofibers along the loading direction. The four types of samples are stretched to different strains (Figure 4-3b) under the same stress (0.12 MPa) at above T_g during the tensile process. The strain in the random nanofibers reached 33% over three cycles, due to the random distribution of their nanofibers, which is much higher than the strain of the aligned nanofibers. In other words, the low strains in the aligned nanofibers indicated the reinforcement effects of nanofiber orientation due to their higher stiffness than that of random nanofibers at temperatures above T_g. The lower strains in response to the applied stress may be attributed to small chain slippage [32] and relative displacements of soft segments in aligned nanofibers, resulting in higher recovery rates.

Figure 3-3 shows the gaps between the nanofibers, which decrease when the nanofibers are aligned; the random nanofibers have more space between the nanofibers and a lower volume of nanofibers in the tensile direction, resulting in decreased recovery rates.

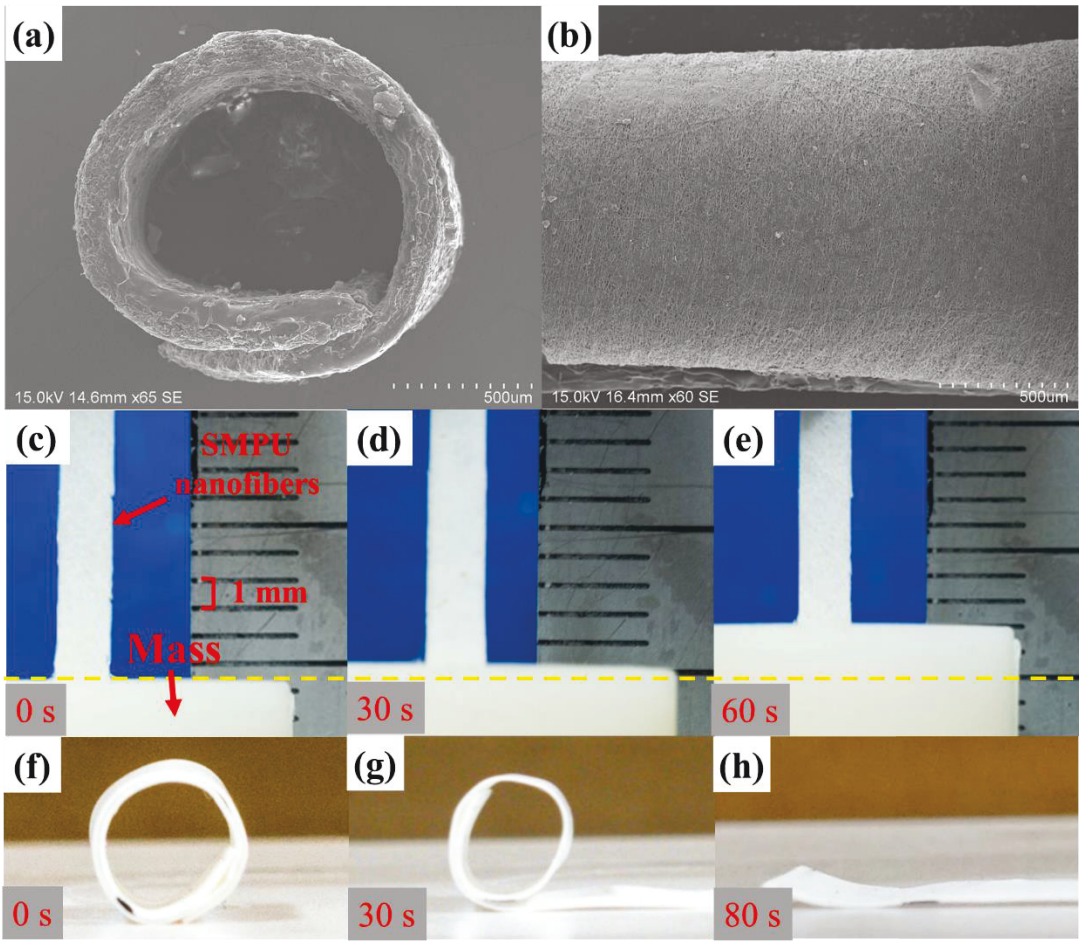

Figure 4-4. (a) cross-section and (b) surface of a tubular SMPU-0. Image of SMPU-0 nanofibers recovering, (c) temporary shape, (d) partially recovered, (e) fully recovered. Side view of an aligned SMPU tube recovering, (f) temporary shape, (g) partially recovered, (h) fully recovered.

Figure 4-4 (a-b) shows the cross-section and surface of an SMPU-0 nanofiber based tubular structure with a diameter of approximately 1 mm. To visually exhibit the recovery capability of aligned SMPU nanofibers in response to heat, images of the recovery process (temporary shape to original shape) of SMPU-0 are shown in Figure 4-4(c–e). The SMPU-0 nanofibers are elongated to 3 mm at about 70 °C (the T_g of the SMPU is 65 °C), then the sample is cooled to room temperature to fix the temporary

shape. One end of the nanofibers are fixed, and the other end have a 2.24-g mass applied to them (Figure 4-4c). Owing to the shape memory effect, the nanofibers are observed to slowly recover to their original shape after being reheated above T_g. Figure 4-4e shows the recovery strain of the SMPU-0 (nearly 3 mm), indicating that the SMPU-0 has good recovery rates and recovery stress. The same recovery behaviors are observed in the form of SMPU tubes (Figure 4-4(f–h)). The aligned SMPU nanofibers are deformed into tiny tubes (when above T_g) with a diameters of 5 mm, which is in the range of tubular scaffolds or blood vessels. The SMPU tubes keep their temporary shapes well at room temperature and recover to their initial shapes when the temperature is above T_g, responding to the temperature stimuli. These recovery processes indicated that the aligned nanofibers have excellent shape recovery properties.

Table 4-4. Shape recovery rates of random and aligned PZT/SMPU nanofibers

Materials	**Recovery rate (%)**		
	1st cycle	**2nd cycle**	**3rd cycle**
P/S-0	89.9	95.8	98.1
P/S-45	84.7	97.7	97.9
P/S-90	80.4	92.8	95.6
P/S-R	84.8	94.0	96.5

The rates of shape memory recovery rates of PZT/SMPU nanofibers are listed in Table 4-4. Of the aligned samples, P/S-0 has the highest maximum recovery stress

(0.39 MPa) and shows an excellent recovery rate (89.9%) in the first cycle but this was reduced for the alignment angles of 45° and 90°. For the random nanofibers, the P/S-R also showed a good recovery rate (84.8%) and a maximum recovery stress (0.14 MPa) that was between that of P/S-45 and P/S-90.

The shape recovery process results from the relaxation or shrinkage of the molecular chains in the SMPU matrix[33]. However, increasing the alignment angle decreased the amounts of nanofibers along the loading direction, and then reduced the number of molecular chains along the recovery direction. Therefore, for the aligned nanofibers, the alignment angles and loading direction are an important factor in shape recovery properties. Meanwhile, these results (Table 4-4) also confirmed that the recovery rates of all three kinds of aligned nanofibers changed slightly and obtained recovery rates over 95% in the third cycle, in which the recovery rate of P/S-0 reached 98.1% in the third cycle. This result is attributed to the training process in each cycle. Future strains after the first cycle are prevented by the fixity ratio contributed by the nanofibers, and approach a balanced state under constant stress in each loading. The good shape recovery rates (more than 95%) of the aligned nanofibers after training is consistent with results reported by many other researchers[34].

4.3.2 Shape recovery stress

4.3.2.1 Effect of particles content and modification on the shape recovery stress of random nanofibers

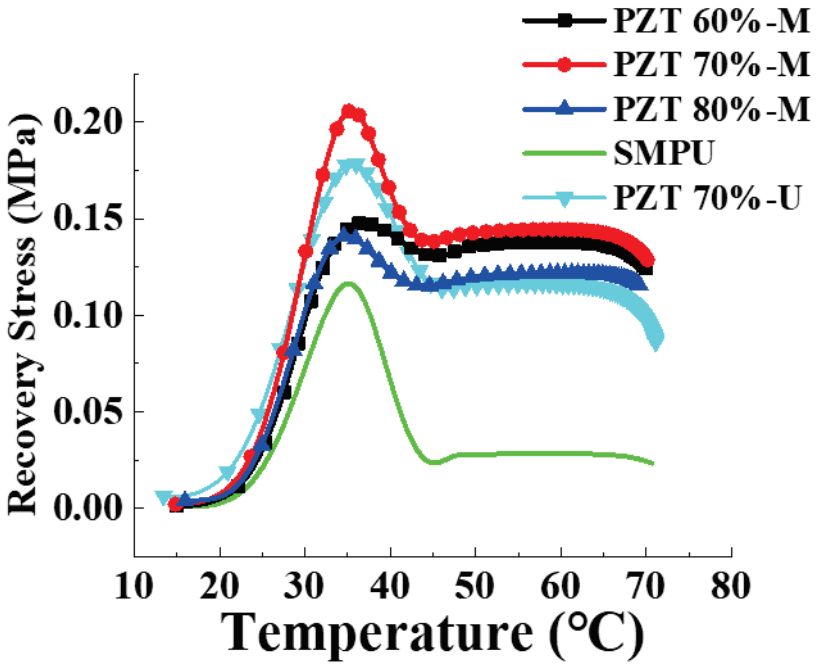

Figure 4-5. Recovery stress versus time for modified and unmodified PZT/SMPU nanofibers

The shape memory recovery stresses of modified and unmodified PZT/SMPU nanofibers are measured (Figure 4-5). The recovery stress of PZT/SMPU nanofibers first rapidly increase with temperature, due to the release of stored energy [35,36], and all the samples reach their peak values of recovery stress at about 35°C. With the temperature continuously increasing, the recovery stress of nanofibers decreases and keep a stable level in the T_g temperature region (about 55°C-70°C). The reason is the decrease of moduli with the increase in temperature.

The recovery stress of PZT/SMPU nanofibers is higher than that of SMPU nanofibers.

Especially, the recovery stress of PZT 70%-M is two times higher than that of SMPU nanofibers. The increment in the recovery stress of PZT/SMPU nanofibers is caused by the improvement of storage moduli (Figure 3-7a) and elastic moduli (Table 3-2) from modification. In the tensile process, more energy is stored because of the higher storage moduli, so in the recovery process, the more stored energy would be released. These results also indicate that the modified nanofibers PZT 70%-M have higher recovery stress than that of unmodified samples PZT 70%-U. Not only the modified nanofibers have higher storage modulus, the better interfaces also help the molecular chain for recovering and transferring recovery stress, compared with unmodified nanofibers.

4.3.2.2 Effect of alignment degree on the shape recovery stress of SMPU and PZT/SMPU nanofibers

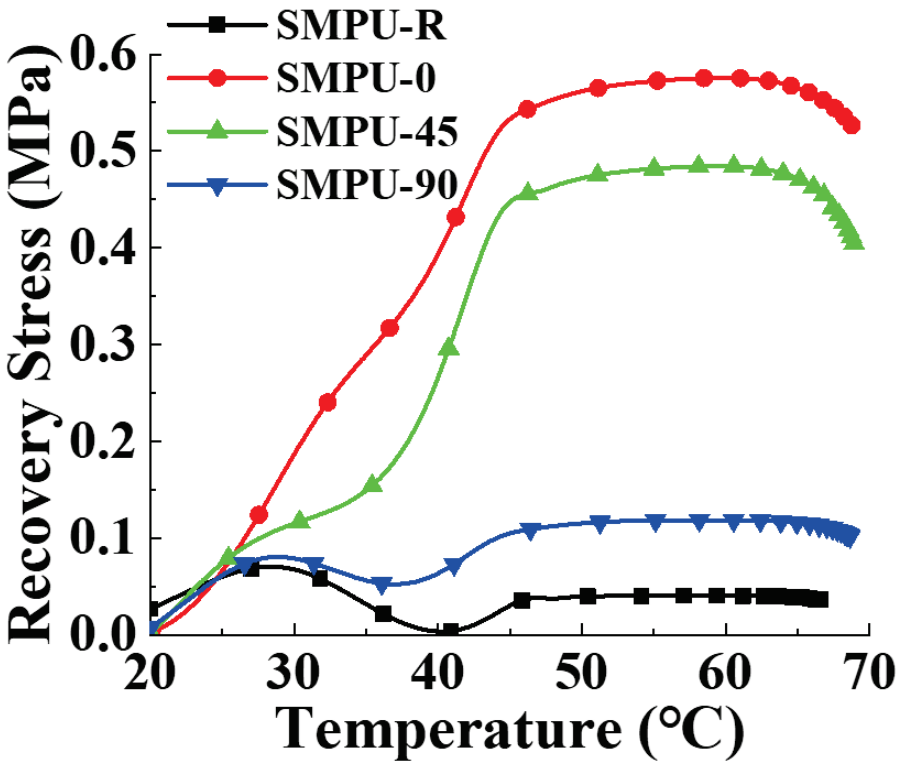

Figure 4-6. Recovery stresses versus time of random and aligned SMPU nanofibers

The shape recovery stress is a key parameter, especially for applications in the sensing and actuation fields. Figure 4-6 and Table 4-5 show the recovery stresses of random and aligned nanofibers, and the results demonstrate that the recovery stress significantly depends on the alignment degrees of the nanofibers. For the aligned nanofibers of SMPU-0 and SMPU 45), the shape recovery stress increases rapidly in the temperature region from 30 to 45 °C. Afterward, the curves become stable and reach the maximum recovery stress. However, for the random nanofiber (SMPU-R) and SMPU-90, the recovery stresses in the total temperature region are small. Especially, compared with the random nanofibers (SMPU-R), the recovery stresses of the aligned nanofibers reveal obvious enhancement, and increase when the alignment degree is 0°. The maximum recovery stress of SMPU-0 reaches 0.52 MPa, which is 7.4 times higher than that of SMPU-R.

Table 4-5. Maximum recovery stress of random and aligned nanofibers

Materials	**Maximum recovery stress** **Mpa**
SMPU-R	0.07
SMPU-0	0.58
SMPU-45	0.48
SMPU-90	0.12

The mechanism of recovery stress may depend on the change in the internal

deformation energy. The potential energy induced by high-temperature deformation can be stored "temporarily" during the cooling process after the SMPU is stretched to the temporary shape above T_g. This promotion of recovery stress can be attributed to two reasons: the initial part (20 °C to 35 °C) of recovery stress is related to the storage modulus, and the stored energy is released when the fixed samples are reheated again, leading to the promotion of recovery stress in the initial part [37]. Figure 3-8a shows the effects of alignment degree on storage modulus. SMPU-0 shows a larger change of storage modulus than those of other samples, which means that SMPU-0 stores more energy during deformation, resulting in the highest recovery stress during the initial part. In addition, increasing the slope of recovery stress is associated with alignment degrees of nanofibers. SMPU-0 has a larger volume of aligned nanofibers along the strain directions, which causes the rapid growth of recovery stress in the second part (at about 40 °C to 58 °C).

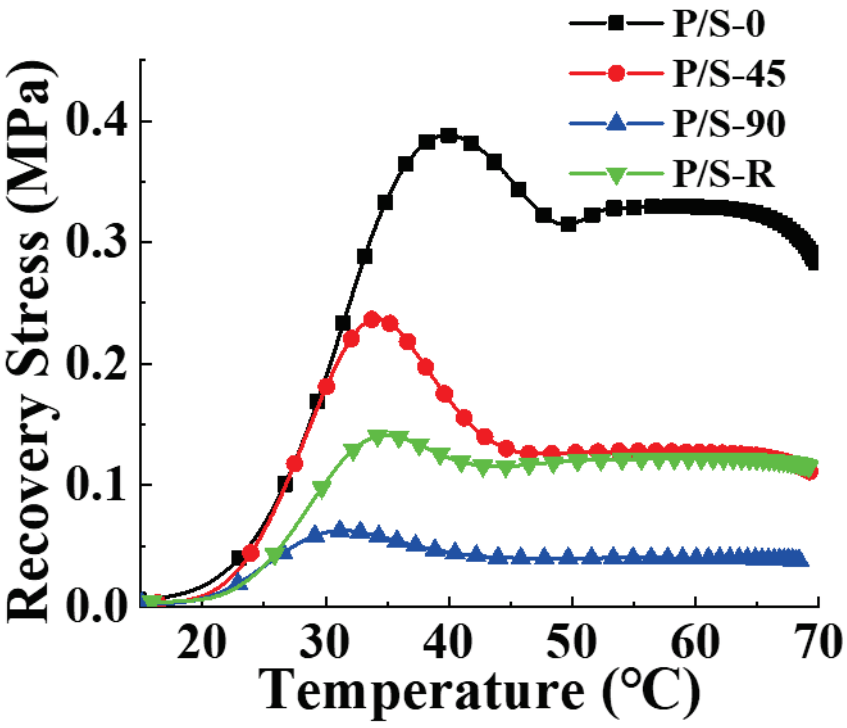

Figure 4-7. Recovery stress versus time for random and aligned PZT/SMPU nanofibers

As shown in Figure 4-7, the recovery stress of nanofibers rapidly increased in the initial part of the curves between 20°C to 35°C, and then reached the maximum recovery stress at about 35°C. With the temperature continuously being increased, the recovery stress decreased slightly and then stayed at a stable level when the temperature was in a range of about 50–70 °C (T_g range of SMPU).

Table 4-6. Maximum recovery stress of random and aligned nanofibers

Materials	Maximum recovery stress MPa
P/S-0	0.39
P/S-45	0.24
P/S-90	0.06
P/S-R	0.14

The rapidly increase of recovery stress in temperature range from 20°C to 35°C can be explained by the change in storage modulus[37]. The storage modulus in the nanofibers decreased as the nanofibers were heated, the release of stored energy led to the promotion of recovery stress, and affected the maximum recovery stress of nanofibers. This phenomenon was further revealed by the following dynamic mechanical analysis to investigate the initial increase of recovery stress. These data (Table 4-6) further demonstrate that storage modulus (Figure 3-9) affected recovery stress between 20°C to 35°C. In the T_g range, the recovery stresses of nanofibers depend on the shrinkage of the molecule chain along the fiber axis[38] in the nanoscale fibers. The fact that the P/S-0 has a greater number of nanofibers along the loading direction than that of other samples results in the P/S-0 giving the highest recovery stress in the T_g range. All of the analyses show that the PZT/SMPU nanofibers gain the highest recovery stress when the alignment angle is 0°, and increased by 1.8 times compared with random nanofibers.

4.3.3 Shape fixity

4.3.3.1 Effect of particles content and modification on the shape fixity of random nanofibers

The fixity ratio is a parameter indicates the ability to fix the temporary deformation. The fixity ratios of pristine SMPU and PZT/SMPU nanofibers are illustrated in Table 4-7. The fixity ratios for all the modified nanofibers are higher than 98% in all three cycles. Furthermore, with the increase of PZT contents, there is no obvious decrease in fixity ratios. These results clearly indicated that the modified PZT/SMPU nanofibers have good shape fixed properties.

Table 4-7. Shape fixity of pristine SMPU and PZT/SMPU nanofibers

Materials	Shape fixity (%)		
	1st cycle	2nd cycle	3rd cycle
Pristine SMPU	99.2	99.0	99.1
PZT 60%-U	98.6	98.5	98.1
PZT 60%-M	99.0	98.9	98.7
PZT 70%-U	98.7	98.6	99.3
PZT 70%-M	99.9	99.7	99.8
PZT 80%-U	98.8	98.0	98.2
PZT 80%-M	98.5	98.1	98.0

4.3.3.2 Effect of alignment degree on the shape fixity of SMPU and PZT/SMPU nanofibers

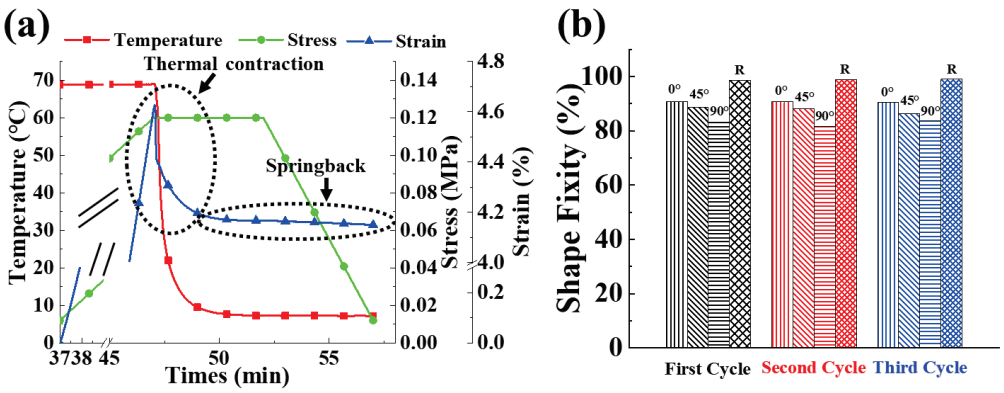

Figure 4-8. Shape fixity behavior of nanofibers, (a) stress vs strain curves of aligned SMPU nanofibers in thermal fixing processes, (b) shape fixity ratios of random and aligned SMPU nanofibers.

To understand the influence of alignment degree on the shape fixity at each recovery cycle, a comparison between the alignment degree and shape fixity ratios in each cycle is performed (Figure 4-8b and Table 4-8). The random nanofiber SMPU-R appears to have higher shape fixity than that of all the aligned nanofibers in three cycles, and the shape fixity ratios of SMPU-R are higher than 98% in each recovery process. For the aligned SMPU nanofibers, the shape fixities are increased to 7.6% and induced by the different alignment degrees (90° to 0°), and no obvious changes were observed as the test cycles were repeated.

Table 4-8. Shape fixity of random and aligned SMPU nanofibers.

Materials	Shape fixity (%)		
	1st cycle	2nd cycle	3rd cycle
SMPU-R	98.6	98.9	99.0
SMPU-0	90.8	90.7	90.5
SMPU-45	88.7	88.1	86.4
SMPU-90	83.2	81.7	83.8

Shape fixity is the ability to switch segments in shape memory material to fix the deformation and is determined by the movement of soft segments. The soft segment can be deformed freely under temperatures above T_g, and is determined to the temporary shapes. However, after cooling to room temperature, the soft segments are restricted and cannot easily recover from the strain after removing stress (Figure 4-3c), or endow the polymer chains with the ability to against the relaxation [39]. The shape fixing processes of nanofibers have two stages (Figure 4-8a), thermal contraction and springback. First, the strain on temporary shapes decrease sharply as the temperature decreases under a constant tensile stress, which is cause by thermal contraction in response to the temperature change. The wide range of alignment degrees of random nanofibers reduce the shrinkage along the tensile direction, resulting in longer retention of strain in the glassy stage. Compared with the random nanofibers, the oriented, rigid aligned nanofiber structure contracted along the direction of alignment and led to greater shrinkage. The soft segments of SMPU nanofibers are fixed in the glassy stage under the same stresses. Second, the loading applied to the SMPU nanofibers is released

when the nanofibers are cooled to room temperature (the glassy stage), at which time the nanofibers spring back during the low-temperature unloading process [40], which depends on the elastic modulus of the SMPU nanofibers. Because the springback represents elastic recovery at the removal of the applied stress, the higher elastic modulus of SMPU-0 indicates lower springback, leaving a larger strain after unloading at room temperature and resulting in higher shape fixity rates than that of aligned nanofibers. The shape fix ratios of aligned nanofibers increase with decreasing alignment degrees, which is a response to the promotion of the elastic modulus in aligned nanofibers in the glassy stage. The shape fixity of SMPU-0 is still higher than 90% when nanofibers become aligned, suggesting that the developed SMPU-0 has good shape fixity.

Table 4-9 Shape fixity of random and aligned PZT/SMPU nanofibers.

Materials	**Shape fixity (%)**		
	1st cycle	**2nd cycle**	**3rd cycle**
P/S-0	98.0	97.9	97.8
P/S-45	97.7	98.1	97.8
P/S-90	93.9	92.8	93.4
P/S-R	98.5	98.1	98.0

The shape fixity of aligned PZT/SMPU nanofibers (Table 4-9) have similar trend with the aligned SMPU nanofibers, the shape fixity of aligned PZT/SMPU nanofibers are increased with the decreasing of alignment degrees, and all the aligned nanofibers are lower than that of random PZT/SMPU nanofibers. But the shape fixity of aligned

PZT/SMPU nanofibers are promoted with the PZT fillers added and higher than those of aligned SMPU nanofibers, corresponding with the same alignment degrees. This phenomenon can be explained by the changes of thermal contraction. The PZT particles hinder the movement of SMPU molecular chain, restricts the thermal contraction resulting from the temperature change, leave a larger fixed deformation than that of pristine aligned SMPU nanofibers.

4.4 Conclusions

The SMPU and PZT/SMPU composite fibers show good shape recovery properties. The recovery rates of PZT 50%-M and PZT 60%-M reach 66.5% and 64.6% in the first cycles, respectively, and the recovery rates of composite fibers are increased with the increasing of test cycles.

The PZT 60%-M, PZT 70%-M and PZT 80%-M all show improvement in shape recovery rates and recovery stress after modification. The shape recovery rate of PZT 60%-M, PZT 70%-M and PZT 80%-M increases by 0.2%, 3.1% and 1.9%, respectively, compared with the unmodified nanofibers. The recovery stress of the PZT 60%-M, PZT 70%-M and PZT 80%-M increases by 26.15%, 76.99% and 21.2% in the first cycle, respectively, compared with the pristine SMPU nanofibers. All the modified and unmodified SMPU and PZT/SMPU nanofibers show excellent shape fixity more than 98.5S% in the first cycle.

The aligned nanofiber structures can store more energy from deformation above T_g owing to the higher elastic modulus from the larger volume of nanofibers along the

loading direction compared with the random structures. Because of these advantages, the aligned structures of SMPU nanofibers show excellent shape recovery and shape fixing ability. Especially, the shape recovery stress increased to 740% with an optimal structure design.

In terms of aligned PZT/SMPU nanofibers, the alignment angle of 0° in the loading direction endows the aligned nanofibers with superior recovery rates and recovery stress. Compared with the random PZT/SMPU nanofibers (P/S-R), the 0° aligned nanofibers (the nanofiber direction is parallel to the tensile direction) exhibit superior mechanical and shape recovery properties, including recovery stress (increased by 178%) and recovery rates (increased by 5.1%).

The shape fixity of aligned SMPU and PZT/SMPU nanofibers are decreased with the increasing of alignment degree, due to the increment of elastic modulus induced springback. All the aligned PZT/SMPU nanofibers have shape fixity than those of aligned SMPU nanofibers, resulting from the restriction of SMPU molecular chain.

It is suggested that by optimizing nanofiber alignment, the shape memory properties can be controlled and the shape memory effect and mechanical properties can be improved. Thus, the developed aligned SMPU and PZT/SMPU nanofibers, with both excellent shape recovery rates and recovery stress, suggesting widely potential applications in many fields.

Reference

[1] FS Senatov, KV Niaza, MY Zadorozhnyy, A Maksimkin, S Kaloshkin, Y Estrin

(2016) Journal of the mechanical behavior of biomedical materials 57: 139.

[2] J Wang, Z Wang, Z Song, L Ren, Q Liu, L Ren (2019) Advanced Materials Technologies 4: 1900293.

[3] K Watanabe, T Maeda, A Hotta (2018) Composites Science and Technology 165: 18.

[4] YJ Yun, WG Hong, N-J Choi, et al. (2014) Nanoscale 6: 6511.

[5] L Tan, J Hu, H Huang, J Han, H Hu (2015) International journal of biological macromolecules 79: 469.

[6] D Kai, MJ Tan, MP Prabhakaran, et al. (2016) Colloids and Surfaces B: Biointerfaces 148: 557.

[7] F Zhang, Y Xia, L Wang, L Liu, Y Liu, J Leng (2018) ACS applied materials & interfaces 10: 35526.

[8] M Bao, X Lou, Q Zhou, W Dong, H Yuan, Y Zhang (2014) ACS applied materials & interfaces 6: 2611.

[9] HM Pauly, DJ Kelly, KC Popat, et al. (2016) Journal of the mechanical behavior of biomedical materials 61: 258.

[10] L-F Tseng, PT Mather, JH Henderson (2013) Acta Biomater. 9: 8790.

[11] M Chen, L Li, L Xia, et al. (2019) Macromolecular Bioscience: 1900312.

[12] A Lendlein, R Langer (2002) Science 296: 1673. Doi:10.1126/science.1066102

[13] HY Du, LW Liu, FH Zhang, W Zhao, JS Leng, YJ Liu (2017) Polymer Testing 57: 119. Doi:10.1016/j.polymertesting.2016.11.011

[14] FL Ji, JL Hu, TC Li, YW Wong (2007) Polymer 48: 5133.

Doi:10.1016/j.polymer.2007.06.032

[15] HY Du, JH Zhang (2010) Soft Matter 6: 3370. Doi:10.1039/b922220k

[16] H Chen, W Liu, H Xia, Y Qiu, Q-Q Ni, Y Fu (2020) Composites Science and Technology 186: 107937.

[17] X Guan, H Chen, H Xia, Y Fu, Y Qiu, Q-Q Ni (2020) J. Intell. Mater. Syst. Struct.: 1045389X20906477.

[18] C Li, H Xia, J Yao, Q-Q Ni (2019) Polymer 180: 121678.

[19] GJH Melvin, QQ Ni, T Natsuki (2016) Polymer Composites 37: 262.

[20] Y Yan, H Xia, Y Qiu, Z Xu, Q-Q Ni (2019) Composites Science and Technology 172: 108.

[21] X Jin, Q-Q Ni, T Natsuki (2011) Journal of composite materials 45: 2547.

[22] J Yu, H Xia, A Teramoto, QQ Ni (2018) J. Biomed. Mater. Res. Part A 106: 244.

[23] J Yu, H Xia, A Teramoto, QQ Ni (2017) J. Biomed. Mater. Res. Part A 105: 1132.

[24] K Ma, H Xia, Q-Q Ni (2019) Journal of Biomaterials Science, Polymer Edition 30: 501.

[25] J Yu, H Xia, Q-Q Ni (2018) Journal of materials science 53: 4734.

[26] K Ma, S Rozet, Y Tamada, J Yao, Q-Q Ni (2019) Journal of Drug Delivery Science and Technology 53: 100900.

[27] H Tobushi, S Hayahi, A Ikai, H Hara, N Miwa (1996) Trans Jpn Soc Mech Eng A 62: 1291.

[28] IA Rousseau (2008) Polymer Engineering & Science 48: 2075.

[29] T Ohki, Q-Q Ni, N Ohsako, M Iwamoto (2004) Composites Part A: applied science

and manufacturing 35: 1065.

[30] IA Rousseau, PT Mather (2003) Journal of the American Chemical Society 125: 15300.

[31] T Xie (2011) Polymer 52: 4985.

[32] H Chen, H Xia, Y Qiu, Q-Q Ni (2018) Composites Science and Technology 163: 105.

[33] N Karak (2017) Biobased smart polyurethane nanocomposites: from synthesis to applications. Royal Society of Chemistry,

[34] T Ohki, QQ Ni, N Ohsako, M Iwamoto (2004) Compos. Pt. A-Appl. Sci. Manuf. 35: 1065. Doi:10.1016/j.compositesa.2004.03.001

[35] Q-Q Ni, C-s Zhang, Y Fu, G Dai, T Kimura (2007) Composite Structures 81: 176.

[36] W Zhang, F Zhang, X Lan, et al. (2018) Composites Science and Technology 160: 224.

[37] QQ Ni, CS Zhang, YQ Fu, GZ Dai, T Kimura (2007) Composite Structures 81: 176. Doi:10.1016/j.compstruct.2006.08.017

[38] LL Chen, SH Jiang, J Chen, et al. (2015) New J. Chem. 39: 8956. Doi:10.1039/c5nj01941a

[39] SA Abdullah, A Jumahat, NR Abdullah, L Frormann (2012) Procedia Engineering 41: 1641.

[40] Y Liu, K Gall, ML Dunn, AR Greenberg, J Diani (2006) International Journal of Plasticity 22: 279.

Chapter 5: Energy harvesting performance of PZT/SMPU composites

5.1 Introduction

Among the various kinds of piezoelectric energy harvesters, flexible energy harvesters have attracted much attention because of their flexibility, low density, and biocompatibility. Various microstructures designed for higher voltage output have been explored. These include aligned nanofibers [1], vertically aligned nanowire [2], porous film [3] and textiles [4], to meet the requirements of wearable devices [5] and soft electronics [6]. Owing to their high aspect ratio and large surface-area-to-volume ratio, aligned nanofibers are expected to enhance piezoelectricity in energy harvesting. In addition, the simplicity and low energy consumption of continuous nanofiber fabrication for electrospinning technology aids in the manufacture of flexible energy harvesters. Some approaches have been tried in piezoelectric nanofiber manufacturing to fabricate different fiber-based piezoelectric composites, but few studies have been reported on the relations between energy harvesting properties and aligned nanofibers and their fiber orientation dependence.

The main energy source in piezoelectric energy harvesting is mechanical energy (e.g., vibrations, stretching or bending) in ambient environments. Indeed, there are many objects around us that are not planar or simple structures but complicated or curved surfaces (e.g., a motor casing, the human body, or building structures) that provide mechanical energy. Thus, the ability of energy harvesters to conform to complex

structures is required [7]. In other words, a key issue for flexible energy harvesters is the ability to freely deform their shape. The development of a flexible energy harvester that is easily deformed and fixed into a curved shape to match complex surfaces is eagerly anticipated.

In this chapter, we developed flexible energy harvesters using PZT/SMPU. In addition to the PZT particles and SMPU matrix, random and aligned PZT/SMPU nanofibers were prepared by electrospinning technology in which the alignment angles between the PZT/SMPU nanofibers and interdigitated electrode were controlled. The flexible energy harvesters with nanofibers aligned randomly and at 0° (parallel), 45°, and 90° (perpendicular) to the tensile direction were designed and fabricated. The influence of the alignment angle of aligned and random nanofibers on mechanical, shape memory and energy harvesting properties was investigated. The mechanisms by which the alignment angle of nanofibers contributed more output voltage were discussed. By utilizing shape memory properties, the PZT/SMPU energy harvester was deformed and fixed into a designed shape to closely match a complex structure or surface for energy harvesting. The reason why the use of shape memory effect for shape matching enhanced output voltages from the aligned PZT/SMPU nanofiber energy harvester is analyzed. This may aid in progress toward a structural design for flexible energy harvesters for more efficient energy harvesting.

Further, PZT/SMPU composite fibers were compounded with PZT particles and the SMPU matrix, which were made into textiles. To improve the dispersion of PZT particles, their surfaces were modified by silane coupling agents. To investigate factors

influencing the energy harvesting properties of PZT/SMPU textiles, the output voltage of different samples is analyzed.

5.2 Materials and methods

5.2.1 Energy harvesting fabrication and measurement system

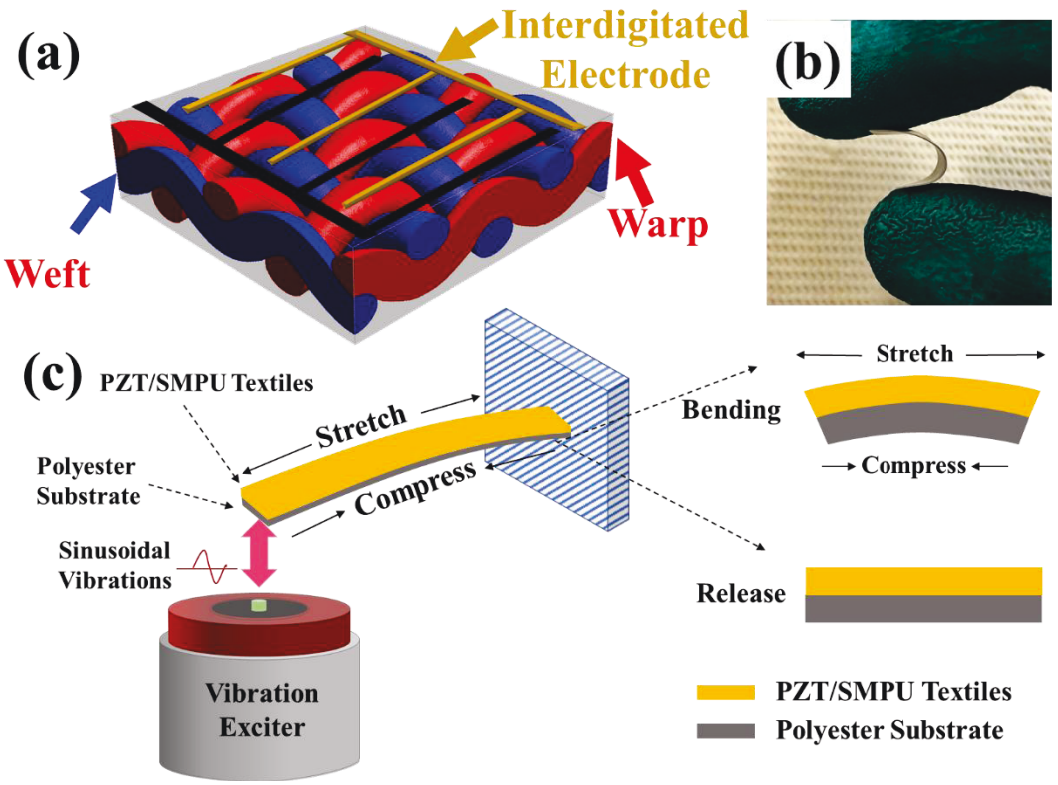

Figure 5-1. The schematic diagram of energy harvesting system for PZT/SMPU textiles, (a) the structure of PZT/SMPU textile-based energy harvester, (b) The image of PZT/SMPU textile-based energy harvester in bending stage, (c) The schematic diagram of energy harvesting system.

The schematic diagram of PZT/SMPU textile-based energy harvester is shown in Figure 5-1a, and energy harvester in bending stage is shown in Figure 5-1b. The

PZT/SMPU nanofibers were taped on the surface of polyester substrates with a thickness of 0.5 mm. The one end of samples was fixed and the other end was free. The sinusoidal vibrations applied to the free end were generated by a vibration exciter (SL-0105, Cybernavi Inc., Japan), and the excitation signal input into the vibration exciter were supplied by a signal generator (AD-8624A, A&D Company, Limited, Japan). The frequency was set at 800 Hz, and the acceleration from 10 to 233 m/s^2 was controlled by the power amplifier (APD-050FCA, Asahi Seisakusyo Co., Ltd, Japan). An accelerometer was mounted on the top of the vibration exciter to measure the acceleration. All the experimental data were also recorded by an oscilloscope (DS-5414A, Iwatsu electric co., ltd., Japan).

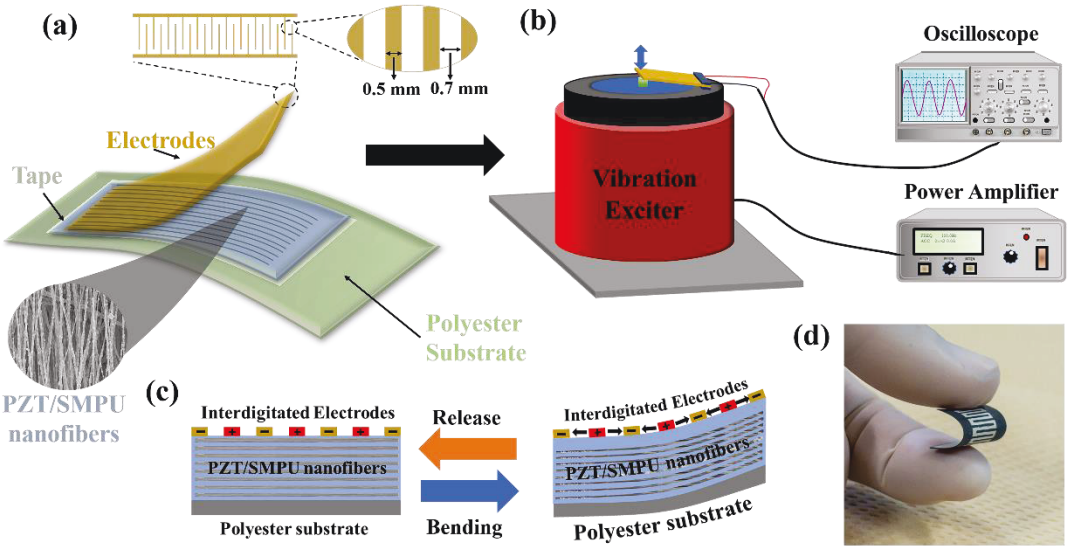

Figure 5-2. Schematic diagram of fabrication and use of the energy harvesting system of energy harvesters, (a) the structure of energy harvester and interdigitated electrodes, (b) the setup of the energy harvesting system, (c) the working principle of piezoelectric energy harvester, (d) image of an energy harvester in the bent state.

For the PZT/SMPU nanofibers-based energy harvester, the all the energy harvesters are made of PZT/SMPU nanofibers (Figure 5-2a). An aluminum mold was employed to make Pb-Pt alloy interdigitated electrodes on the surface of nanofibers using a sputtering machine. All the energy harvesters were polarized by an electric field of 10 kV/mm in silicone oil at 80 °C for 2 h.

The energy harvesting system is shown in Figure 5-2 (a-c). The energy harvesters were taped on the surface of polyester substrates with a thickness of 0.5 mm (Figure 5-3a). One end of samples was fixed, and the other end was taped to the vibration exciter (Figure 5-2b). The excitation signal, supplied by a signal generator, was inputted into the vibration exciter, with a vibration frequency ranging from 600 to 2000 Hz (for modified and unmodified analysis) or 70 to 300 Hz (for random and aligned structure analysis). Accelerations from 10 to 200 m/s^2 and displacements from 4 μm to 10 μm were controlled by a power amplifier. The displacement of the energy harvester was adjusted using the power amplifier and measured by a laser interferometer (SI-F01, Keyence Corp., Japan). All experimental data were recorded by an oscilloscope.

5.2.2 Energy harvesting measurement system for complex structures

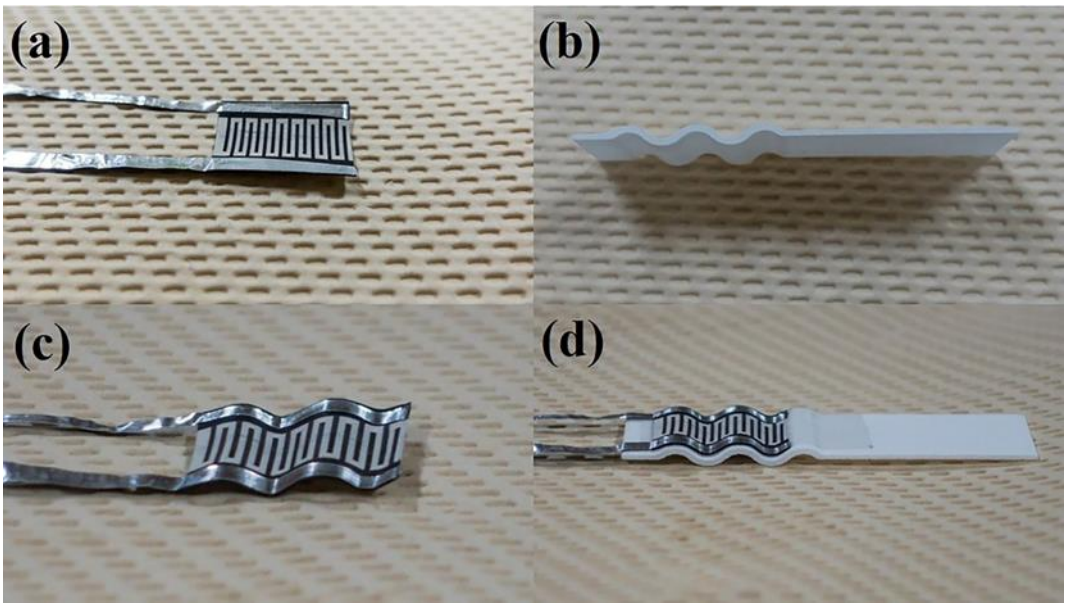

Figure 5-3. Energy harvesting for a complex structure. (a) The sample in its original shape. (b) The designed complex structure. (c) The sample deformed to conform to the structure. (d) The pre-deformed sample taped onto the surface of the complex structure.

To analyze the energy harvesting properties of the PZT/SMPU energy harvester in use with complex structures, two methods of fabricating energy harvesters, non-pre-deformed and pre-deformed, were employed. The pre-deformed energy harvester (Figure 5-3a) was heated to 65 °C (T_g of SMPU is 65°C), and deformed to match the shape of the designed complex surface (Figure 5-3b). It was then cooled down to room temperature to fix the temporary shape (Figure 5-3c) and taped onto the surface of the complex structure (Figure 5-3d). Another sample was taped on the complex surface directly without using the shape memory effect. This sample was named the non-pre-deformed energy harvester. The designed complex structures were fabricated with two 3D-printed materials (nylon and poly(methyl 2-methylpropenoate) (PMMA)) .

5.3 Results and discussion

5.3.1 Energy harvesting properties of textiles

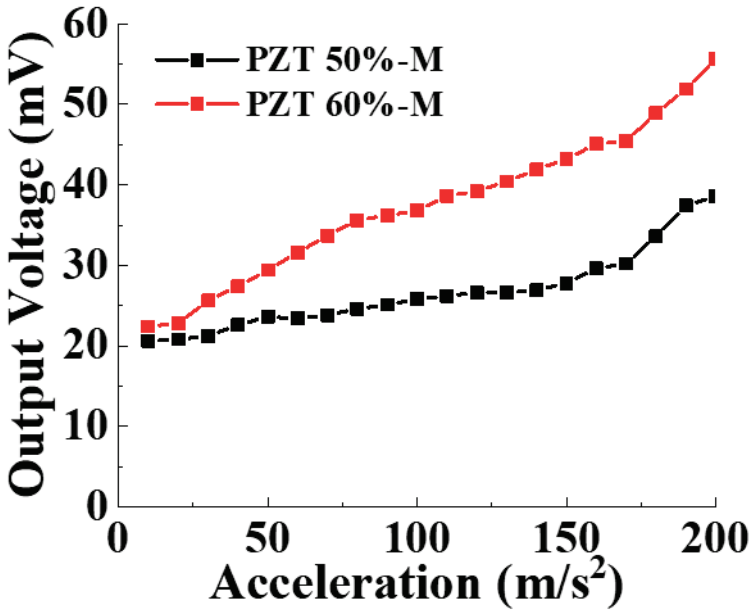

Figure 5-4. Output voltages of PZT/SMPU textile-based energy harvester at various acceleration at the frequency of 800 Hz.

Figure 5-4 reveals the output voltage of the PZT/SMPU textile-based energy harvester at various acceleration at 800 Hz. The output voltage is sine wave with the acceleration increased from 10 to 200 m/s^2, and the peak-to-peak voltage generated by PZT 50%-M nanofibers increases from 20.6 to 38.6 mv under the vibration of 800 Hz. Moreover, the output voltage of PZT 60%-M nanofibers increases from 22.4 to 55.6 mV. As expected from the results, the output voltage of PZT 60%-M at 200 m/s^2 increases by 2.48 times compared to that of PZT 60%-M at 10 m/s^2. The output voltage

of PZT 50%-M slightly changes with the increasing acceleration due to the lower content of PZT compared to that of PZT 60%-M.

5.3.2 Effect of acceleration and displacement on energy harvesting properties of PZT/SMPU nanofibers

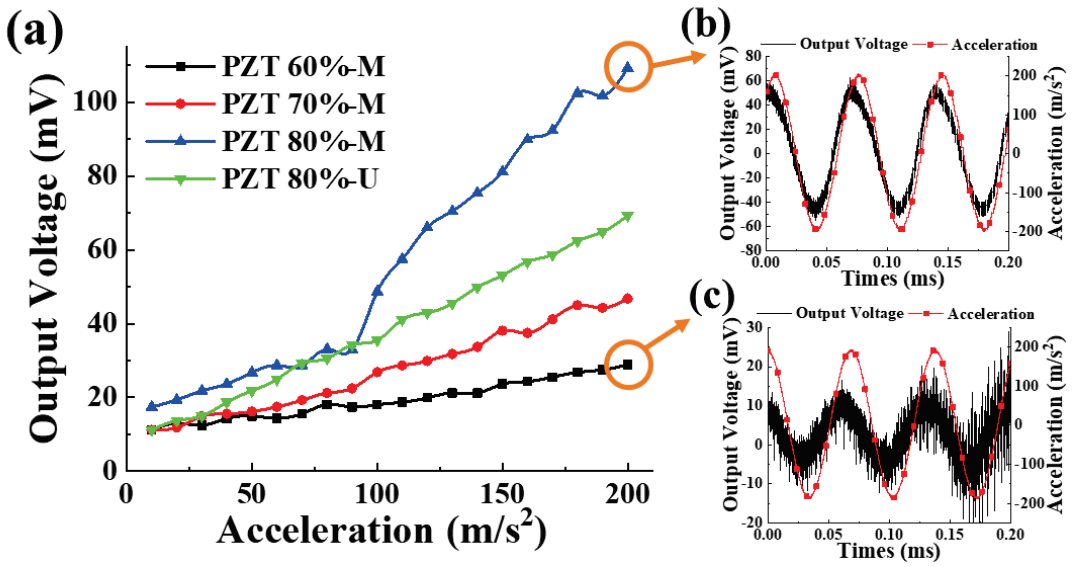

Figure 5-5. Energy harvesting performances of modified and unmodified PZT/SMPU nanofibers, (a) Output voltages of PZT/SMPU nanofibers at various acceleration at the frequency of 1450 Hz. (b-c) The output voltages of PZT/SMPU nanofibers with the acceleration of 200 $m/s^{2,}$ (b) PZT 60%-M, (c) PZT 80%-M.

The energy harvesters made of PZT/SMPU nanofibers were employed to harvest energy from external sinusoidal vibrations, Figure 5-5 show the harvesters are able to generate continuous sinusoidal voltages. The results indicate that the output voltages generated by the harvesters are repeatable. All the output voltages are peak-to-peak voltages.

Figure 5-5a shows the output voltages of harvesters with the variable acceleration (from 10 to 200 m/s^2) at the frequency of 1450Hz. With the increase of acceleration, the peak-to-peak voltages generated by the PZT 80%-M increase from 17.45 mV to 109.3 mv, the output voltages of the PZT 70%-M nanofibers increase from 11.24 mV to 46.8 mV, and the output voltages of the PZT 70%-M increase from 11.24 mV to 28.9 mV. The output voltages of PZT 80%-M at 200 m/s^2 are 6.26 times as high as the output voltages at 10 m/s^2. Because according to the Newton's second law of motion F = ma, where F is the force, m is the mass, and a is the acceleration, when the weight of an object is constant, the force is directly proportional to the acceleration. Therefore, the stress increase with the acceleration, which lead to the increment in output voltages.

Compared with the PZT 60%-M and PZT 70%-M, a greatly enhancement of output voltages of PZT 80%-M. The PZT 80%-M generate the output voltages of 109.3 mV when the acceleration reaches to 200m/s^2, which is 2.78 and 3.73 times higher than those of PZT 60%-M and PZT 70%-M. This phenomenon mainly results from different contents of PZT fillers. With increasing the volume fraction of PZT particles, the harvesters would become harder and absorb less energy when they are deformed. Therefore, more energy is transferred to PZT particles to generate voltages.

Additionally, Figure 5-5 show that the output voltages of PZT 80%-U are lower than that of PZT 80%-M, and the output voltage of PZT 80%-M is 1.58 times large than the voltage of PZT 80%-U at the acceleration of 200m/s^2. Because the weak interfaces in PZT 80%-U cause poor stress transmission between the PZT fillers and SMPU matrix, resulting in weaker stress transferred on the PZT fillers and lower output voltages. But

the modification helps the stress to be transferred to PZT particles more efficiently via improving the interfaces, leading to the increase of stress and higher voltages.

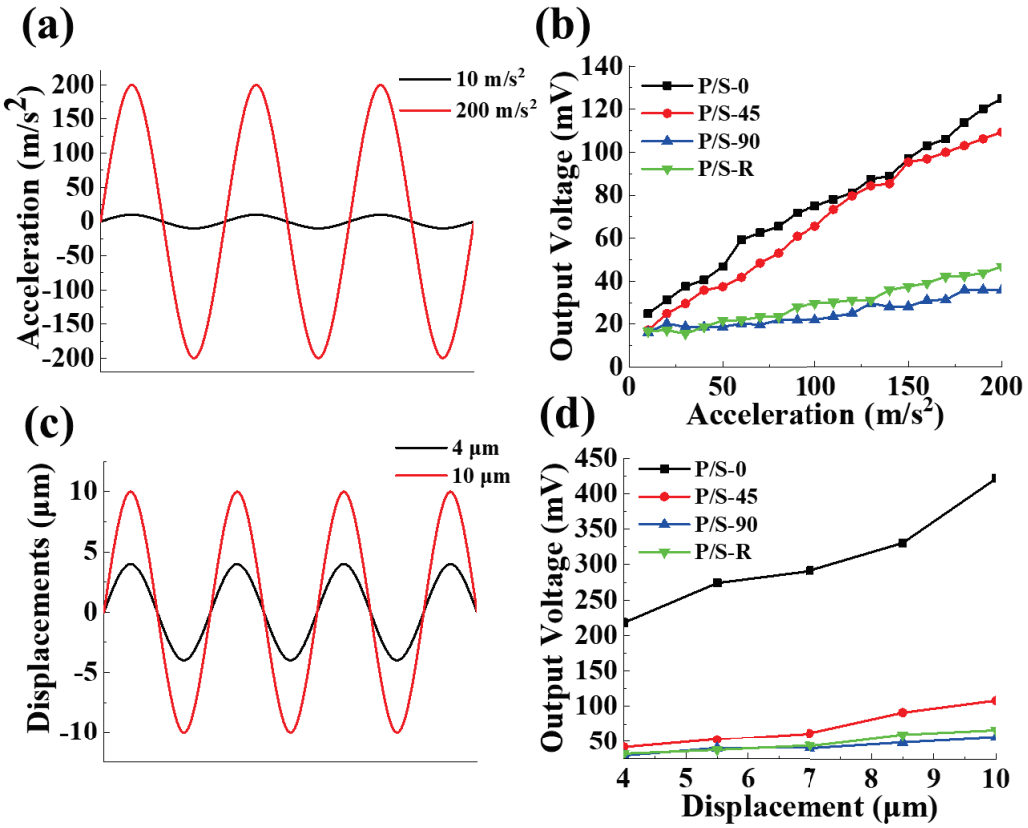

Figure 5-6. Energy harvesting performance of random and aligned PZT/SMPU nanofibers, (a-b) Output voltages of aligned PZT/SMPU nanofibers at various accelerations and a frequency of 300 Hz, (c-d) Output voltages of aligned PZT/SMPU nanofibers at various displacements and a frequency of 300 Hz.

As shown in Figure 5-6 (a-b), the output voltage of energy harvesters with different acceleration was from 10 m/s^2 to 200 m/s^2 (the frequency was fixed at 300 Hz). It can be seen that increasing the acceleration at the same frequency increased the output voltage generated by energy harvesters. With the increase of acceleration, the peak-to-peak voltages generated by the P/S-0 increased from 24.95 mV to 124.9 mV, which

increased by 5.01 times from 10 m/s^2 to 200 m/s^2, and increased by 1.7 times compared with that of random nanofibers P/S-R.

In a similar phenomenon to that observed in Figure 5-6 (c-d), three kinds of energy harvester generated different output voltages under various amplitudes of displacement (4 μm, 5.5 μm, 7 μm, 8.5 μm and 10 μm). Compared with the output voltages generated by P/S-0 at 4 μm, the output voltages increased to 421 mV at 10 μm, increased by 5.4 times compared with random nanofibers (65.6 mV). The increment of the acceleration and displacement both give rise to the higher output voltage resulting from the different stresses applied to the energy harvester. According to Newton's second law of motion and piezoelectric constitutive equations, the increasing accelerations result in enhancement of stresses, which results in the increment in output voltages. The displacement is directly proportional to the piezoelectric constant. Therefore, the increment of acceleration and displacement led to the increment in output voltages.

The results in Figure 5-6 indicate that the output voltages generated by P/S-0 grow more quickly than those of aligned samples with 45° and 0° orientation, whereas the output voltages increased by 2.5 times, 6.5 times, respectively, under identical conditions of acceleration, frequency. This phenomenon can be explained by two phenomena. One is the poling direction of energy harvester. Compared with the P/S-45 and P/S-90, the nanofibers in P/S-0 are perpendicular to the interdigitated electrode. Because the PZT filler is the source of the piezoelectricity, the aligned nanofibers along the poling direction induce the energy harvesters to generate higher voltage compared with samples with different alignment degrees[8]. The other phenomenon is that the

nanofibers oriented along the strain direction are more compliant to mechanical stresses than nanofibers in other alignment degrees[9], which leads to greater voltage generation. These results demonstrate that adjusting the nanofiber arrangement helps the energy harvester to improve the voltage, and that adjusting the orientation of the PZT/SMPU nanofibers to match the strain direction is an important idea for the structural design of piezoelectric nanofiber composites.

For random PZT/SMPU nanofibers, under the same vibration conditions, the output voltage of P/S-0 is higher than that of random nanofibers P/S-R, and provides evidence that aligned PZT/SMPU nanofibers are more efficient than random nanofibers for energy harvesting. The reason for this is that aligned nanofibers have a lower surface area and higher density than that of random nanofibers (Table 2-1). This indicates greater compactness and lower porosity of aligned nanofibers, which results in increased voltages. Figure 3-4 also provides evidence that the spaces between the nanofibers are decreased when the nanofibers are aligned. Therefore although they have the same content in terms of piezoelectric materials, the PZT materials in the aligned piezoelectric nanofibers have a higher specific density and induce increased energy harvesting properties.

5.3.3 Effect of frequency on energy harvesting properties of PZT/SMPU nanofibers

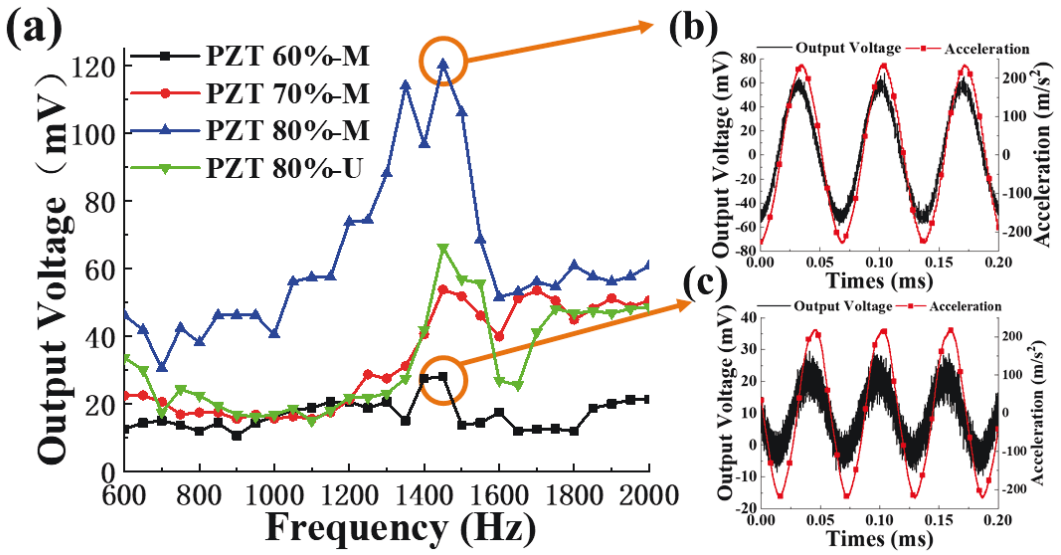

Figure 5-7. Energy harvesting performances of PZT/SMPU nanofibers, (a) Output voltages of PZT/SMPU nanofibers at various frequencies and acceleration of 233 m/s^2, The output voltages of PZT/SMPU nanofibers at the frequency of 1750Hz, (b) PZT 60%-M, (c) PZT 80%-M.

Figure 5-7a shows the output voltages harvested from the vibration with the frequency from 600 to 2000Hz (the acceleration is fixed at 233 m/s^2). The output voltages of harvesters change slightly under the frequency from 600 to about 1100Hz (Figure 5-7a). With the increment in vibration frequency, the output voltages rapidly increase and reach the maximum values at about 1450 Hz. The maximum output voltages of the PZT 60%-M, PZT 70%-M, and PZT 80%-M are 28.9 mV, 53.8 mV, and 120.3 mV, respectively. The output voltages of all samples increase with increasing frequency from about 1000 to 1500 Hz, because the increase in frequency induced the

increment in straining rate under the same applied acceleration [10]. When the output voltages of reach the maximum values, the output voltages decrease whereas the frequency increase. The reason is that when the frequency is relatively high, the soft polymer matrices could not respond to the vibration speed [11]. That's why the output voltages of PZT/SMPU nanofibers are initially increasing and then decreasing with the frequency increasing.

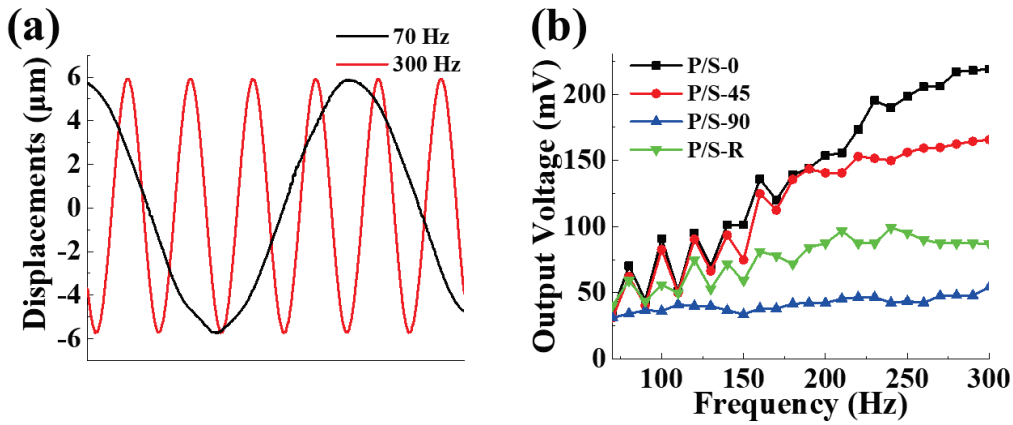

Figure 5-8. Energy harvesting performance of aligned PZT/SMPU nanofibers, (a-b) Output voltages of random and aligned PZT/SMPU nanofibers at various frequency and a displacement of 6 μm.

Figure 5-8 shows the output voltage harvested under different vibration frequencies from 60 Hz to 300 Hz (displacement is fixed at 6 μm). It is clear that the output voltage is proportional to the increment of frequency (Figure 5-8b). With increased frequency, the output voltages of waveforms in the P/S-0, P/S-45, P/S-90 and P/S-R samples rise and reach their maximum values of 219 mV, 164.4 mV, 48 mV and 87.3 mV, respectively. The output voltages are enhanced by 250% when the nanofibers are aligned (alignment angle of 0°). Enhancement of output voltage with increased

frequency is associated with a strain rate that is proportional to the output voltages [12]. Under a constant strain, increasing the cycling frequency induced the increment of strain rate and attributed to the piezoelectric effect, and led to enhanced output voltages. The output voltages of P/S-0 increased by 3.3 times than those of aligned samples with 45° and 0° orientation, under the same displacement.

5.3.4 Energy harvesting properties of complex structures

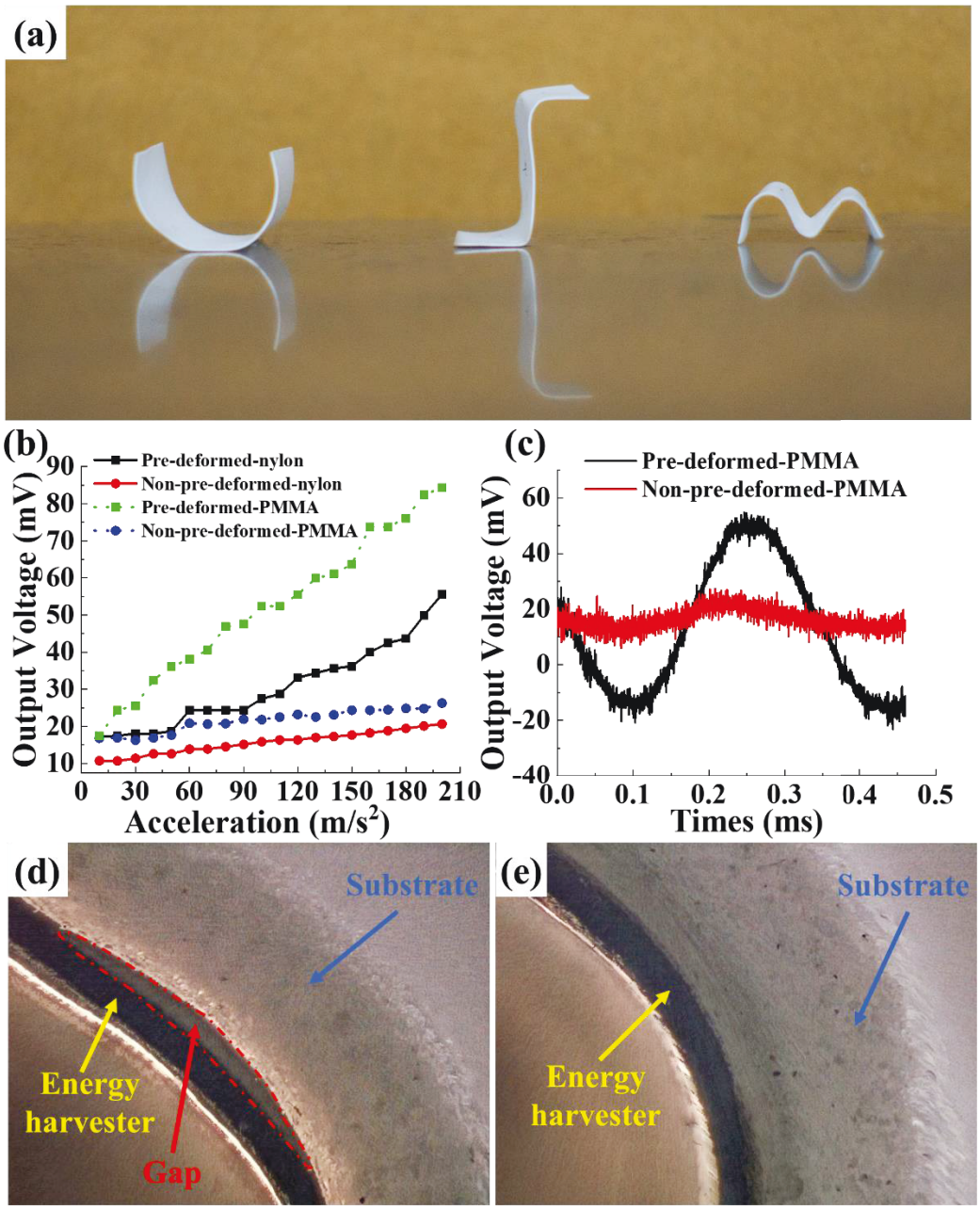

Figure 5-9. (a) PZT/SMPU nanofibers are deformed to a designed shape by changing temperature, including a "U" shape, a "Z" shape, and an "M" shape. (b) The output voltage of pre-deformed and non-pre-deformed energy harvesters at various accelerations and a frequency of 300 Hz, (c) Comparison of the output voltage generated by pre-deformed and non-pre-deformed energy harvesters taped on the

PMMA substrate at an acceleration of 200 m/s2. Images of the structure between the energy harvester and the nylon substrate after vibration, (d) Non-pre-deformed sample, (e) Pre-deformed sample.

Because of the shape memory effect, the PZT/SMPU nanofibers can be deformed easily into any shape by changing the temperature to about 65°C (T_g temperature of SMPU is 65°C, which is lower than the depolarization temperature of PZT fillers), and fixing their designed shape at room temperature (Figure 5-9a), which ensures the energy harvester performance for curved or complex surfaces. Owing to its higher piezoelectricity compared with other samples, the P/S-0 energy harvester was used to analyze energy harvesting performance in complex structures. Figure 5-9(b-c) shows the output voltage of a harvester for a complex structure made by two different fabrication methods, pre-deformed and non-pre-deformed. The pre-deformed energy harvester (taped on the nylon substrate) achieves higher voltages than the non-pre-deformed sample, and the maximum output voltage reaches 55.6 mV, which is 2.7 times as high as a non-pre-deformed sample. The same phenomenon was also observed in PMMA complex substrate; after the shape was changed to adapt the curved structure, the pre-deformed energy harvester gained a voltage of 84.3 mV, 3.2 times higher than that of the non-pre-deformed sample.

The difference in output voltage between these two methods is attributed to the harvester's ability to conform to complex structures. The shape of the pre-deformed energy harvester closely matches the complex surface, resulting in closer matching than in the non-pre-deformed sample. The higher matching performance helps transferred

the strain to the energy harvester more effectively, thus enhancing output voltages. When the acceleration is increasing, the output voltage generated by the pre-deformed energy harvester is higher than that of the non-pre-deformed sample, resulting from the debonding of the non-pre-deformed energy harvester and complex surfaces. Figure 5-9d clearly shows that debonding was found between the non-pre-deformed energy harvester and substrate after 1 hour of vibration (300 Hz and 200 m/s^2) because the elastic recovery of the material allows the energy harvester return to its original shape (flat film) after deformation. However, high frequency vibration accelerates the debonding process. However, owing to the shape matching before vibration, the pre-deformed energy harvester (Figure 5-9e) was still firmly attached to the complex structure, even under high acceleration. Therefore, utilizing the shape memory effect, the PZT/SMPU energy harvester deformed into designed shapes to closely match complex structures, and may aid in harvesting energy more efficiently.

The output voltage was also associated with the substrate materials. Figure 5-9b shows the difference in output voltages between the nylon substrate (55.6 mV) and the PMMA substrate (84.3 mV) applied with same vibration parameters (300 Hz in frequency and 200 m/s^2 in acceleration). Compared with the nylon substrate, the output voltages of the PMMA substrate increased to 1.5 times at the acceleration of 200 m/s^2, and the curve of output voltages of the pre-deformed PMMA substrate grows more quickly than that of the nylon substrate with increasing acceleration. Differing softness of the substrate materials (nylon and PMMA) leads to differences in strain during the vibration process, resulting in various output voltages, even though all the samples

closely conformed to the substrates.

5.4 Conclusions

The PZT/SMPU textiles-based energy harvester show the ability to generate output voltages responding to the external stimuli, and the output voltages promoted with the increasing of acceleration. The maximum output voltage of PZT 50%-M and PZT 60%-M reach to 38.6 mV and 55.6 mV at 200 m/s^2, respectively.

The results show that the output voltages of the random PZT/SMPU nanofibers first increased and later decreased as the frequency increased from 600 to 2000 Hz at an acceleration of 233 m/s^2, and increased with the increasing of acceleration from 10 to 200 m/s^2 under the vibration frequency of 1450 Hz. The modification of PZT particles improve the output voltages, because the better interfaces leading to the increase of stress and higher voltages. PZT 80%-M generated higher output voltages than those of PZT 80%-U at the acceleration from 10 to 200 m/s^2 and vibration of 1450 Hz. The output voltage of PZT 80%-M is 1.58 times large than the voltage of PZT 80%-U at the acceleration of 200 m/s^2 and frequency of 1450 Hz

For the aligned PZT/SMPU nanofibers, experiments demonstrated that optimizing the alignment angles of aligned nanofibers gave rise to higher output voltages. The output voltage generated by aligned PZT/SMPU nanofibers are increased wi the decreasing of alignment degrees. The flexible energy harvester based on 0° aligned PZT/SMPU nanofibers (P/S-0) showed higher energy harvesting efficiency during vibration as compared with the random nanofibers. The P/S-0 generated 421 mV

voltage at displacements of 10 μm, which increased by 5.4 times compared with the P/S-R.

Taking advantage of the shape memory effect, the PZT/SMPU energy harvester can be deformed to fit curved or complex structured surfaces and fixed at room temperature. This effect can be used to closely match harvester to curved surfaces for better energy harvesting. Our results showed that a pre-deformed energy harvester with a curved shape generated an output voltage of 84.3 mV, which is 3.21 times as high as that of a non-pre-deformed energy harvester (taped on the PMMA substrate). Our results confirm that the combination of shape memory and piezoelectric properties is very promising for potential application in flexible PZT/SMPU energy harvesters in a wide variety of fields for mechanical energy harvesting in sensors and wearable devices.

Reference

[1] ZH Liu, CT Pan, LW Lin, JC Huang, ZY Ou (2014) Smart Materials and Structures 23: 11. Doi:10.1088/0964-1726/23/2/025003

[2] A El Kacimi, E Pauliac-Vaujour, J Eymery (2018) Acs Applied Materials & Interfaces 10: 4794. Doi:10.1021/acsami.7b15649

[3] L Chen, JL Cao, GL Li, P Fang, XS Gong, XQ Zhang (2019) IEEE Sens. J. 19: 11262. Doi:10.1109/jsen.2019.2933356

[4] A Talbourdet, F Rault, G Lemort, C Cochrane, E Devaux, C Campagne (2018) Smart Materials and Structures 27: 7. Doi:10.1088/1361-665X/aab865

[5] CX Zhao, J Niu, YY Zhang, C Li, PH Hu (2019) Compos. Pt. B-Eng. 178: 8.

Doi:10.1016/j.compositesb.2019.107447

[6] M Ha, S Lim, J Park, DS Um, Y Lee, H Ko (2015) Adv. Funct. Mater. 25: 2841. Doi:10.1002/adfm.201500453

[7] Y Qi, J Kim, TD Nguyen, B Lisko, PK Purohit, MC McAlpine (2011) Nano Letters 11: 1331. Doi:10.1021/nl104412b

[8] PG Kang, TK Lee, CW Ahn, et al. (2015) Nano Energy 17: 261. Doi:10.1016/j.nanoen.2015.09.004

[9] J Yan, YG Jeong (2016) Acs Applied Materials & Interfaces 8: 15700. Doi:10.1021/acsami.6b02177

[10] LB Kong, T Li, HH Hng, F Boey, T Zhang, S Li (2014) Waste energy harvesting. Springer,

[11] S Xu, BJ Hansen, ZL Wang (2010) Nature communications 1: 93.

[12] CE Chang, VH Tran, JB Wang, YK Fuh, LW Lin (2010) Nano Letters 10: 726. Doi:10.1021/nl9040719

Chapter 6: Nanofiber-based wearable devices for energy harvesting in different motions

6.1 Introduction

Energy harvesting technology that converts energy like mechanical, solar, thermal energies into electric charges from surrounding environments has become one of important fields of research[1-3]. Energy harvesters meet the increasing demands of renewable energy sources, eco-friendly requirements, and can be used to power wearable electronics and so on. Among various kinds of energy harvesters, flexible wearable energy harvesters have attracted considerable research attention for improving their energy harvesting efficiency based on human body movements while ensuring flexibility. These harvesters offer the possibility of controlling electronics at any time and thus have a wide potential for application as health monitors[4], soft robotics[5], flexible solar cells[6], electric skins[7], and flexible energy harvesters[8]. Among these devices, wearable energy harvesters are of significance considering their energy conversion and motion detection capabilities. They are suitable for application as energy harvesters and sensors for harvesting waste mechanical energy or for monitoring human body part motions[9]. These wearable energy harvesters are based on piezoelectric[10], triboelectric[11], and electrostatic effects[12] that offer the possibility of converting mechanical movements from human motions to electricity. This harvested energy not only serves the device, it can also act as a power supply source for low power consumption electronic devices[13] and facilitate the

development of increasingly efficient energy storage technologies.

With the development of wearable energy harvesters, there has been a shift in requirements for flexible, lightweight, and durable materials[14] that provide the right feel[15], which is similar to that of clothing on the human skin; the balance between energy harvesting properties and flexibility has become increasingly important. Owing to the inherent flexibility of polymers, polymer-based energy harvesters, which can be used in many portable and light-weight applications[16], have solved the flexibility problem associated with piezoelectric ceramics. Electrospinning, which allows the deposition and formation of polymer-based nanofibrous mats in random or aligned network structures, is an attractive low-cost and easy processing method for fabricating wearable energy harvesters. These polymer-based nanofibrous mats have a 1-D nanostructure and play a vital role in the design of new nanomaterials including in nanofabrication[17], biomaterials[18], and microelectromechanical systems[19]. In particular, because of their high aspect ratio and large surface area to volume ratio, the aligned nanofibers are used to enhance piezoelectricity in piezoelectric composites[20]. Nanofiber-based wearable energy harvesters exhibit excellent resistance to fatigue and repeatability, and they provide the wearable energy harvester with structural flexibility and wearing comfort. Most nanofiber-based wearable energy harvesters are designed to have aligned structures distributed along the body-length direction or aligned with the warp directions[21, 22].

Although the movable connections for the human body—joints—allow stretching, bending, or twisting, the motion of some joints including those of the fingers and the

knees is limited to one direction. Other joints and body parts are not only bendable, but are also twistable, and they can move in different directions, e.g., the forearm, neck, and the wrist. For the bending deformation induced by the joints, as the arm or finger angle is changed from 180° (full extension) to 90° (flexion), the upper skin layers are stretched, causing a significant increase of strain. That is why many researches focus on the wearable energy harvesters using human bending motion to improve the energy harvesting efficiency[23, 24]. Because of the characteristics of human structure, the skin is connected with each other and attached to the skeleton via muscle and fascia. Thus, the skin is stretched during the movement of human body, and the strain of skin stretching induced by various body motions will cause changes of strain orientation to a certain degree. Therefore, it is still challenging to harvest mechanical energy from different directions efficiently for various types of motions and optimize nanofiber alignment in developing energy harvesters. This research aims to investigate the influence of nanofiber alignment degree on the piezoelectricity and energy harvesting properties from the aligned structures and efficiently improve the energy harvesting properties in response to the deformation generated by various types of human body motions in the wearable energy harvester.

In this study, nanofiber-based flexible piezoelectric energy harvesters were prepared via electrospinning and fabricated into wearable energy harvesters. Different alignment angles were selected for the nanofibers, i.e., random, 0°, 45°, and 90°, and the corresponding energy harvesters were fabricated with external vibrations generated by a square wave at a frequency of 1 Hz, which simulate the bending or twisting behaviors

derived from human motions at low frequency. The influence of the vibration directions and alignment angles on the energy harvesting performance of the harvesters were investigated by changing the angles between the samples and vibration direction. In addition, strain variations in the energy harvesters were simulated at different alignment angles, and the mechanism of energy harvesting at the optimal alignment angles were discussed. Because of the flexibility from the shape memory polyurethane (SMPU) matrix, the lead zirconate titanate (PZT)/SMPU nanofiber-based energy harvesters could be taped onto the joint parts of the human body as wearable energy harvesters to harvest mechanical energy, and the alignment angles of the nanofibers could be optimized to promote the output voltages resulting from the twisting and bending motions. The results obtained may provide a new strategy for the structural design of aligned nanofiber-based wearable energy harvesters for harvesting mechanical energy from human motions efficiently.

6.2 Materials and methods

6.2.1 Materials and preparation

To improve the distribution of piezoelectric (PZT) particles in the SMPU matrix, the surfaces of PZT particles (HIZIRCO ALT, Hayashi Chemical Industry Co., Ltd., Japan) were modified[25], i.e., the PZT particles were mixed with an acetone and silane coupling agent (KBM-503, Shin-Etsu Chemical Co., Ltd., Japan) in a certain ratio, and they were dispersed using an ultrasonic device (Sonifier 250, Branson Ultrasonics

Corp., USA.). Finally, the mixture was dried at 70 °C to completely remove the acetone.

The modified PZT particles were mixed with a solution of tetrahydrofuran /dimethylformamide (6/4 wt.%) and dispersed using an ultrasonic device for 16 min. After dispersion, the SMPU pellets (MM6520, SMP Technologies Inc., Japan) were added to the mixture while stirring; the PZT particle content was 80 wt.%. To prepare random and aligned PZT/SMPU nanofibers via electrospinning, the PZT/SMPU solution was delivered into a syringe and applied at 20 kV. The collector was rotated at a speed of 19.63 m/min (for the aligned nanofibers) or 3.93 m/min (for random nanofibers), and it was placed at a distance of 7.5 cm from the syringe.

6.2.2 Fabrication of wearable energy harvesters

Based on alignment angles, four random and aligned PZT/SMPU nanofibers types were cut from the nanofiber mats and divided into four groups: random (Wear-R), 0° (Wear-0), 45° (Wear-45), and 90° (Wear-90), depending on the alignment angles between the nanofiber and longitudinal directions. These four nanofibers groups were then fabricated into wearable energy harvesters (Fig. 6-1(a) and (c)). Pb-Pt alloy interdigitated electrodes were coated on the surface of the nanofibers using a designed aluminum mold and a sputtering machine (Fig. 6-1(b)); all samples were polarized in a 10 kV/mm electric field in silicone oil at 80 °C for 2 h.

The X-ray diffraction analyses (XRD) (MiniFlex 300, Rigaku Corporation, Japan) were employed to record the profiles of SMPU at 40 kV and 20 mA. The measurements

were operated in the range of 2θ from 10° to 90° at a rate of 0.04 deg/step and 5 deg/min.

The surface morphology of nanofibers was observed by a scanning electron microscopy (SU1510, Hitachi Co., Ltd., Japan), and Energy-dispersive X-ray spectroscopy (EDS) was done to obtain the chemical compositions of the PZT/SMPU nanofibers.

6.2.3 Energy harvesting from different vibration directions

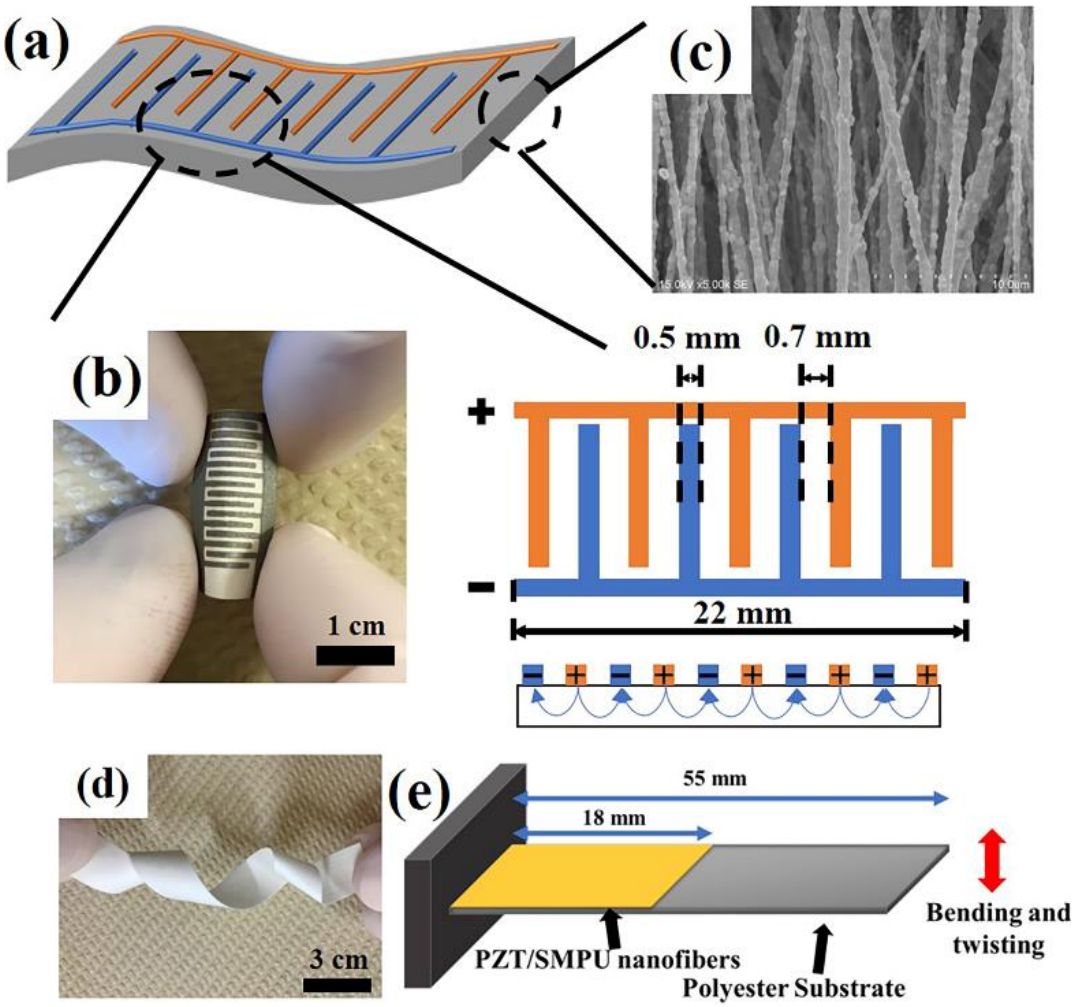

Figure. 6-1 PZT/SMPU nanofiber-based energy harvesters. (a) Structural diagram of the PZT/SMPU nanofiber energy harvester; (b) Actual image and schematic of

interdigitated electrode; (c) SEM image of aligned PZT/SMPU nanofibers; (d) Image of PZT/SMPU nanofibers in the twisted state; and (d) Schematic of energy harvesting system for bending and twisting.

The energy harvesting system is shown in Fig. 6-1(e). The energy harvesters were taped to the surface of a 0.5-mm-thick polyester substrate. One end of the substrate was taped to the top of a vibration exciter (SL-0105, Cybernavi Inc., Japan), and the other end was fixed. The substrate was vibrated using a square wave supplied by a signal generator (AD-8624A, A&D Company, Limited, Japan) with input at a frequency of 1 Hz. The determination of the energy harvesting performance was performed in the bending and twisting modes with displacements of 0.4, 0.8, 1.2, and 1.6 mm, and at turning angles of 1.4°, 2.9°, 4.3°, and 5.7°, which were adjusted using a power amplifier (APD-050FCA, Cybernavi Inc.) and measured using a laser interferometer (SI-F01, Keyence Corp., Japan). All experimental data were recorded using an oscilloscope (DS-5414A, Iwatsu Electric Co., Ltd., Japan), and all output voltages were peak-to-peak open circuit voltages.

6.3 Results and discussion

6.3.1 Effect of alignment angles on piezoelectric properties

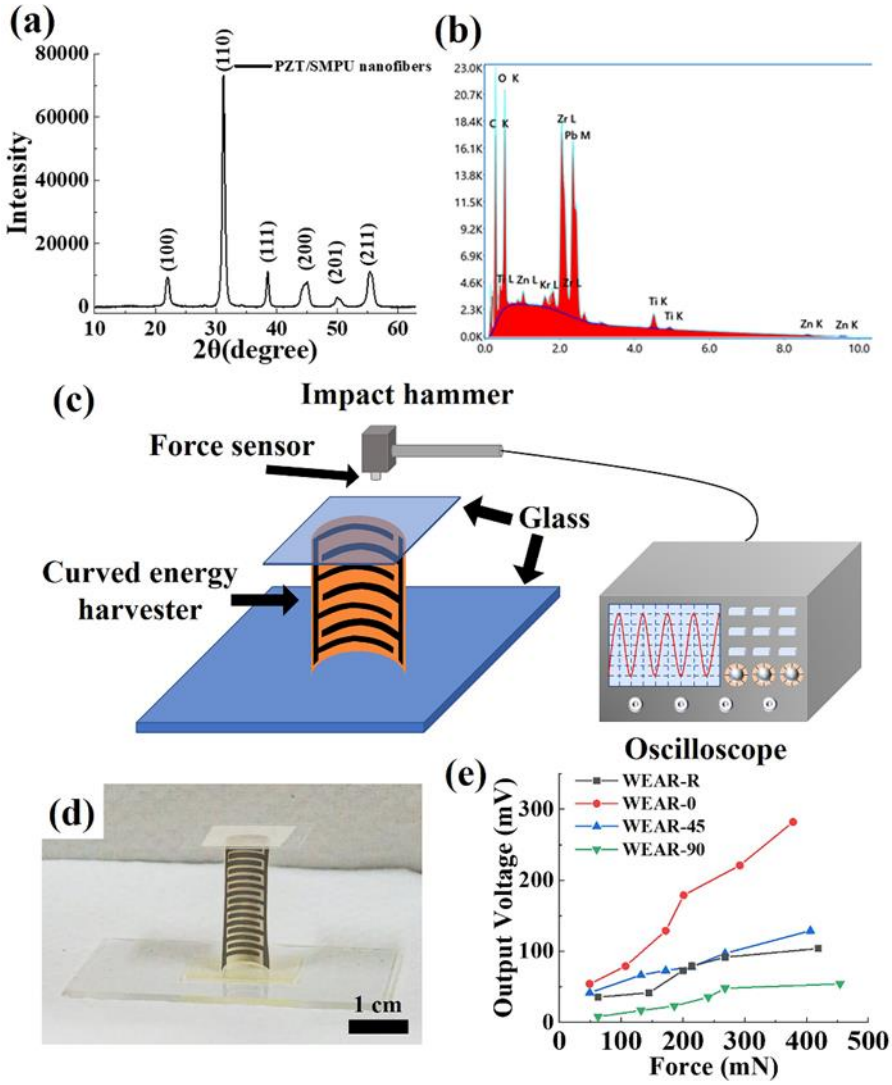

Figure. 6-2 (a) XRD patterns and (b) EDS spectrum of the of PZT/SMPU nanofiber. (c) Schematic illustration of the experimental system for the PZT/SMPU energy harvester in the nanofiber direction. (d) Actual image of the experimental setup of the U-shaped PZT/SMPU energy harvester. (e) Voltage–force relationship based on the experimental results corresponding to the random and aligned PZT/SMPU energy harvesters.

Fig.6-2a shows the x-ray diffraction spectrum of the PZT/SMPU nanofibers. The

diffraction peaks of perovskite phase are observed in the figure and the peak of (110) is perfectively oriented. The EDS of PZT/SMPU nanofibers is shown in the Fig. 6-2b. The results confirmed that the PZT/SMPU nanofibers contains lead (Pb), titanium (Ti), zirconium (Zr), oxygen (O) and carbon (C). The PZT/SMPU nanofibers are deposited along the longitudinal direction of the energy harvesters at different orientation. To evaluate the piezoelectric properties of these energy harvesters, impact hammer tapping tests are conducted, and the energy harvester are vertically placed and deformed to have a "U" shape (Fig. 6-2(c)). Exploiting the shape memory effect, the SMPU-based energy harvesters were curved and deformed to be U-shaped at ~70 °C (T_g of the SMPU was 65 °C). Thereafter, the sample was cooled to room temperature to fix the temporary shape, and both ends of the energy harvesters were tapped on glass. Compared with a plate film, the energy harvesters could stand in a stable manner in the vertical direction because of the U-shaped structure (Fig. 6-2(d)). To activate energy harvesters, an impact hammer (Type 8204 Impact hammer, Brüel & Kjær Sound & Vibration Measurement, Denmark) was used to knock the upper glass. The impulsive force was measured using the force sensor, and the resulting output voltages were recorded using an oscilloscope.

Fig. 6-2(e) shows the results of the hammer tapping test for both the random and aligned energy harvesters. From the figure, it is evident that output voltages generated by the piezoelectric effect were promoted when the impulse forces were increased. The PZT/SMPU nanofibers were orderly or randomly arranged along the longitudinal direction of the energy harvesters, and they could generate voltages in response to the impulse forces from the top to the bottom. Further, it was evident that the output

voltages increased at a faster rate as the alignment angle changed from 90° to 0°. In particular, Wear-0 generated 221 mV when a force impulse of 292 mN was applied, and it showed a greater performance when generating output voltages in the range of 49–378 mV compared to other energy harvesters.

The different output voltages observed under the influence of different impulsive forces could be attributed to two factors, the orientation of nanofibers and the force. The piezoelectric properties of the nanofibers were estimated via the direct measurement of the piezoelectric effect associated with energy harvesters. The piezoelectric coefficient is a constant that represents piezoelectric properties, and it is estimated using stress-induced charges resulting from the direct piezoelectric effect, which is measured using

$$d = \frac{\Delta Q}{\Delta N} \quad (1)$$

where d represents the piezoelectric coefficient, ΔQ represents the induced charge, and ΔN represents the stress applied on the energy harvesters.

According to Equation (1), the piezoelectric coefficient is proportional to the output voltage under the same loading. A comparison of the energy harvesters showed that Wear-0 could generate higher output voltages under the same applied stress compared to others, thereby indicating higher piezoelectric properties. Given that the nanofibers are the main load-bearing objects in the energy harvesters, an increase in their proportion leads to superior piezoelectric properties in the longitudinal direction. Thus, it is reasonable that Wear-0 showed superior energy harvesting performance with nanofibers aligned in the longitudinal direction.

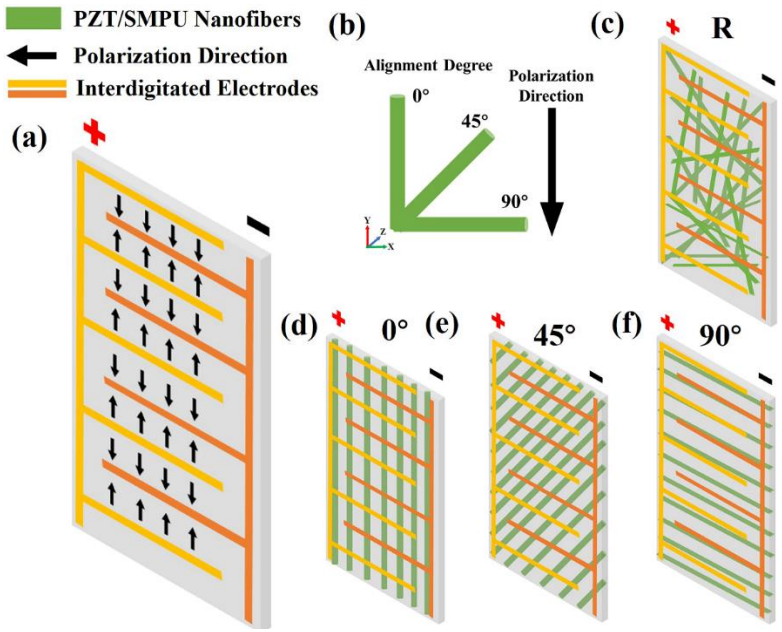

Fig. 6-3. (a) Polarization direction on nanofibers with an interdigitated electrode. (b) Polarization direction on different alignment angles of nanofibers. Schematic of the polarization direction on the different alignment angles of the nanofibers, the structure of the wearable energy harvesters, and the interdigitated electrodes with (c) Randomly-, (d) 0°-, (e) 45°-, and (f) 90°-aligned nanofibers.

The polarization direction of the piezoelectric nanofibers also affects piezoelectric properties. The interdigitated electrodes utilized the piezoelectric effect along the length direction (1.8 cm) rather than along the thickness (200 μm). The anisotropic (aligned) and isotropic (random) PZT/SMPU nanofibers with the polarization direction along the longitudinal direction of the samples are shown in Fig. 6-3(a). The PZT/SMPU nanofiber-based energy harvesters consisted of network structures made from high-permittivity ceramic phase (PZT) and low-permittivity polymer and pore phases (SMPU and air). Such random or aligned network structures are influenced by the distribution of the electric field during the polarization process.

Nanofibers with dielectric inclusions parallel to the axis of the polarization direction (Fig. 6-3(b)) generate electric fields with higher field strengths compared to those generated by permittivity phases close to the pore caused by the desirable distribution of the local electric field in the polarization system[26, 27]. Thus, Wear-0 showed more promising piezoelectric properties, and it was characterized by a more effective polarization process compared with randomly, slantingly, or transversely aligned materials (Fig. 6-3(c–f)), which resulted in higher responding voltages under the same impulsive force.

6.3.2 Effect of alignment angles on the energy harvesting properties with respect to bending and twisting motions

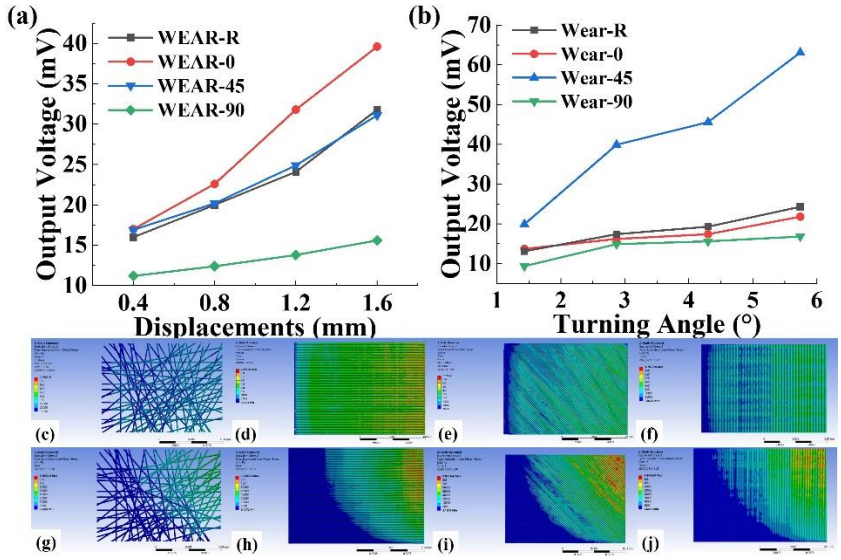

Fig. 6-4. Output voltage vs. (a) Displacement (mm) and (b) Twist angle (°) of the PZT/SMPU energy harvesters. Finite element analysis of various nanofiber alignments in bending motion: (c) Random, (d) 0°, (e) 45°, and (f) 90°, and in twisting motion: (g) Random, (h) 0°, (i) 45°, and (j) 90°.

As shown in Fig. 6-1(d), the developed PZT/SMPU nanofiber energy harvesters showed good flexibility, and therefore, they could be deformed easily and repeatedly. Fig. 6-4(a-b) show the output voltages of the random and aligned PZT/SMPU nanofiber energy harvesters obtained from bending and twisting motions at different displacements and twist angles.

The strain induced by the bending or twisting motion was transmitted to the energy harvesters along the substrates (Fig. 6-1(e)) at certain directions, thereby producing stresses on the energy harvesters and thus leading to a closer molecular dipole moment that generated voltage. During the bending tests, four energy harvester types generated different voltages under different displacements (0.4, 0.8, 1.2, and 1.6 mm). All output voltages generated from the energy harvesters increased as the displacement increased (Fig. 6-4(a)). In addition, a comparison of the harvested energies showed that Wear-0 achieved the maximum output voltage of 39.6 mV. However, that generated by Wear-90 was relatively lower compared with those of the other samples. There was no significant difference between the output voltage trends corresponding to Wear-45 and Wear-R. The waveform of the output voltages corresponding to Wear-45 and Wear-R showed an increasing trend as the displacement increased, reaching maximum values of 31.1 and 31.8 mV at 1.6 mm, respectively.

When energy harvesters were evaluated during the bending tests, the nanofibers along the longitudinal direction of the samples were the primary load-bearing components that significantly determined the bending behavior. Compared with other energy harvesters, Wear-0, which was positioned parallel to the vibration direction,

showed higher output voltages that resulted from the application of higher stresses on the nanofibers. Therefore, there is a link between increments in output voltage and the angle between the nanofibers and strain directions. For the other harvesters (Wear-45, Wear-90, and Wear-R), the contributions of the nanofibers to the output voltage were less significant.

To illustrate the stress distribution in the nanofibers visually, ANSYS code was used for simulation under the following conditions: one end of the energy harvester and the polyester substrate were fixed, while a displacement of 1.6 mm was applied to the other end of the substrate. Fig. 6-4(c–f) show the stress distributions in the energy harvesters caused by the bending motion. The stresses induced by the vibration displacement at the top of the substrate were transferred to the energy harvesters along the substrate; thus, all energy harvesters showed continuous stress distribution. The highest stress applied on Wear-0 reached 2.46 MPa, and it increased by at least 7.4% compared with those applied on Wear-45, Wear-90, and Wear-R. This observation could be attributed to the increase in the elastic modulus of the nanofibers. Wear-0 showed a higher elastic modulus, which was linked to the stiffness of the material compared with the other samples. This increment indicated that Wear-0 has a greater potential to resist plastic deformation, thereby enabling nanofibers to endure more stress under the influence of the bending motion.

As illustrated in Fig. 6-4(b), twist experiments showed a different phenomenon. The torsion in the energy harvesting system could be resolved into stress and compression applied on the energy harvesters at certain angles along the substrate. In

addition, the figure shows output voltages harvested under different twist angles because of the twisting motion from 1.4–5.7°. Indeed, the output voltage was proportional to the increase in the twist angle, and those corresponding to Wear-R, Wear-0, Wear-45, and Wear-90 increased, and reached the maximum values of 24.3, 21.8, 63.1, and 16.8 mV, respectively, as the twist angle increased. There was a 3.75-fold increase in the output voltages when the alignment angle changed from 90° to 45°.

Unlike the bending motion, the twisting motion rotated the substrate at a certain angle, transmitting strain to the energy harvesters. Thus, the effect of the 45°-aligned nanofibers, which were predominantly controlled by the twisting motion of the energy harvesters on the output voltages was greater than those of the 0°-, 90°-, and randomly-aligned nanofibers. The results of the finite element analysis performed using ANSYS code (Fig. 6-4(g–j)) demonstrated the maximum stresses applied on Wear-45 were higher than those corresponding to the other nanofiber alignments. It reached 2.03 MPa, which represents a 1.48-, 4.72-, and 1.15-fold increase relative to the randomly-, 0°-, and 90°-aligned nanofibers, respectively. The applied stresses were mostly directed to the 45°-aligned nanofibers, which represent the group with the most significant influence considering the energy harvester.

Thus, output voltages were associated with the alignment angle of the nanofibers. When the nanofibers and vibration source were aligned in the same direction, the stresses applied on the energy harvesters were enhanced. Given that there was a strain in the structure of the PZT crystal when it was subjected to stress, which pushed some of the molecular dipole moments closer or further apart, it resulted in the generation of

external electrical charges. Thus, increments in stress led to increments in the output voltage.

6.3.3 Energy harvesting in different human motions

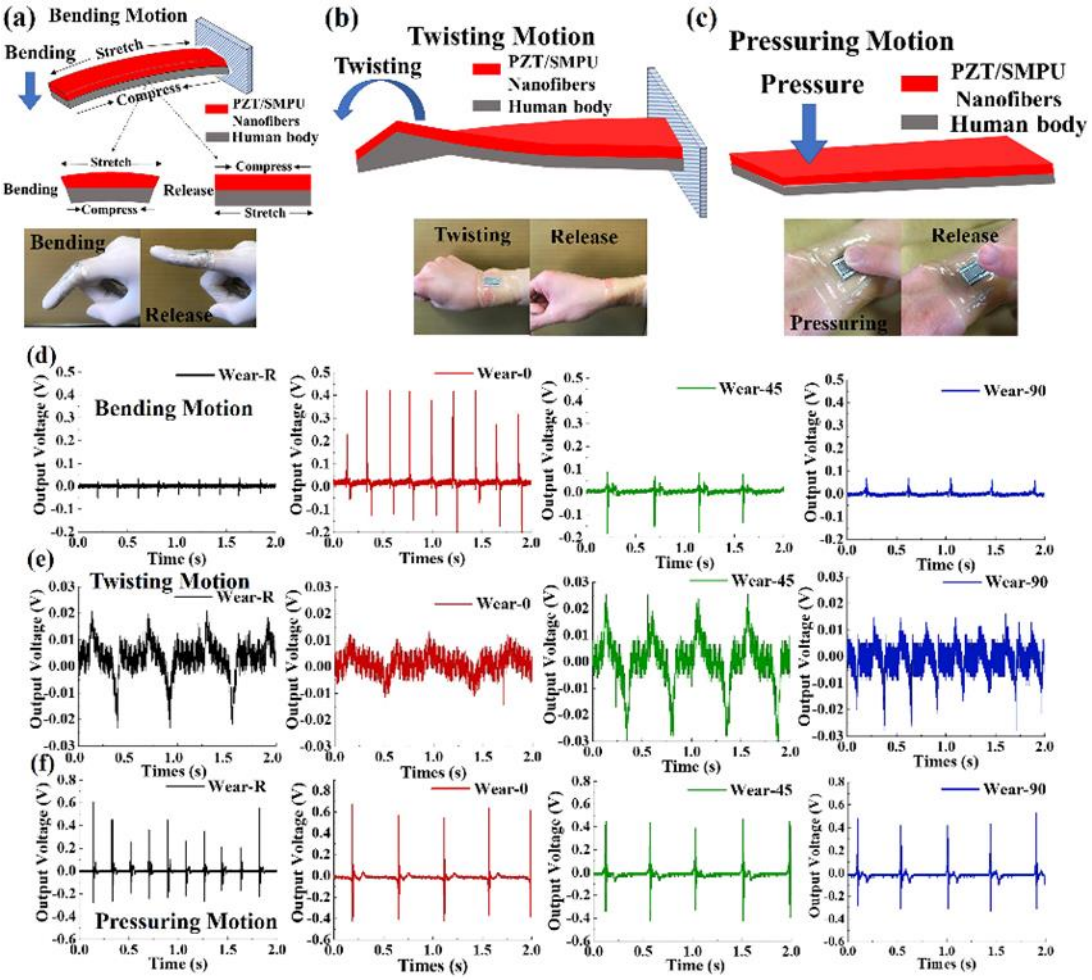

Fig. 6-5 Schematic of the deformation of energy harvesters and nanofibers because of different human movements: (a) Bending, (b) Twisting, and (c) Applying pressure. Output voltages generated by the PZT/SMPU nanofiber-based wearable energy harvester under different human movements: (d) Bending, (e) Twisting, and (f) Applying pressure.

The main motions associated with human movements can be classified as bending, twisting, and pressuring motions, which correspond to tension and compression in different directions. The deformations of the wearable energy harvesters caused by finger bending are shown in Fig. 6-5(a). The bending motion resulted in the displacement of the aligned nanofibers, which were stretched along the x-direction (longitudinal direction of the samples). Under the influence of the twisting motion, the energy harvesters underwent twisting. The torsion tended to twist the parts of the energy harvester to one side, while the other parts remained intact (Fig. 6-5(b)). The shear stress in the shaft of the energy harvester and human body could be resolved into two groups of principal stresses, i.e., tension and compression. The stress was oriented at a certain degree around the shaft along the direction of the maximum principal stress. In addition, the twisting motion strengthened and compressed the energy harvesters at a certain angle. The quasi-static compression exerted a compressive force in the z-direction, which is parallel to the thickness of the energy harvester and perpendicular to the PZT/SMPU nanofibers.

Owing to their high flexibility, the PZT/SMPU energy harvesters can be potential employed as wearable energy harvesters to harvest waste mechanical energy resulting from human motion. To investigate the energy harvesting properties of nanofibers and the effect of their alignment angles on their energy harvesting function, the PZT/SMPU wearable energy harvesters were taped to different parts of the human body, and they were subjected to bending (by a finger), twisting (by a wrist), and application of pressure (by a finger). The resulting output voltages corresponding to these different

body movements were then determined. Because human motions are primarily in the low-frequency range, the movement frequency of the body was controlled in the range 1–5 Hz.

To evaluate the performance of the energy harvesters under the influence of bending motion, they were taped on the top of the proximal interphalangeal joint and bent at 90°. The output voltages corresponding to the random and aligned PZT/SMPU wearable energy harvesters resulting from the bending motion of a finger are shown in Fig. 6-5(d). The energy harvesters were firmly taped on the surfaces of the fingers, and output voltages were generated as the fingers were bent. The randomly-, 0°-, 45°-, and 90°-aligned energy harvesters generated the average maximum output voltages of 78, 537, 231, and 78 mV, respectively. In addition, the output voltage corresponding to Wear-0 was 6.88-fold higher than those corresponding to Wear-R and Wear-90. For bending joints, such as the fingers and toes, the bending load was applied parallel to the joint surfaces, thereby stretching the surfaces. Compared with other nanofiber samples, the nanofibers in Wear-0 were parallel to the direction of the bending, and this resulted in higher output voltages. These results are consistent with the simulation results shown in Fig. 6-4(c-f).

The output voltages of the wearable energy harvesters for the twisting motion are shown in Fig. 6-5(e). To determine the performance of wearable energy harvesters subjected to twisting motions, they were taped onto the arm above the radius, and the arm was twisted at an angle of 90°. It was observed that the energy harvesters could generate voltages because of this mechanical motion of the human arm. With respect to

the alignment of the energy harvesters, Wear-45 showed excellent output voltages (55 mV), which reduced when the alignment angles change to 0° and 90° (i.e., 23 and 36 mV, respectively). Wear-R also exhibited good energy harvesting properties (43 mV) compared with those for Wear-0 and Wear-90. These results indicate that the voltages generated by Wear-0 are lower than those generated by Wear-45 and Wear-90. This difference can be attributed to the different deformations resulting from twisting and bending motions. Compared with the twisting deformation, the bending of a joint, such as the knee or the fingers, can extend to more than 90°, leaving a large amount of stretch deformation on the human skin. However, arm twisting, which is limited by the bone, muscles, as well as blood vessels, results in less skin deformation in the transverse direction. Thus, the voltages generated as a result of the twisting motions were lower than those resulting from the bending motions. Further, the human skin followed the twisting direction of the forearm, and applied the generated deformation onto the wearable energy harvesters; however, the twisting did not align with the longitudinal direction of the arm. Rather, it aligned with the twisting in the transverse direction as shown in Fig. 6-5(b). Therefore, based on the angle of the principal stresses associated with the twisting motion, adjusting the alignment angles to ∼45° will result in the deformation of the wearable energy harvesters, which enhances their energy harvesting performance under the influence of twisting motions.

The effects of the motion of applying pressure on the performance of energy harvesters was different compared to those of the bending and twisting motions. The large force—regarded as a fast-acting impact or impulse force resulting from human

pressure—applied on the energy harvesters for a short duration (Fig. 6-5(c)) pushed some of the molecular dipole moments closer or further apart, thereby resulting in impulse voltage generation. The mechanical energy from the pressure was harvested by the wearable energy harvesters as shown in Fig. 6-5(f). The developed wearable energy harvesters were firmly attached on the wrist, and mechanical pressure was applied via a compression cycle of a finger. These dynamic impact forces caused the wearable energy harvesters to generate impulse voltages in the range 1–5 Hz. The results obtained showed that there were no significant differences between the output voltages corresponding to the four types of wearable energy harvesters, suggesting that there is no relationship between the alignment angle of the nanofibers and the output voltages generated under the influence of impact pressure. These impulse voltages were primarily generated as a result of deformation in the thickness direction, which depends on the density of the PZT materials. These results indicate that aligned nanofiber-based wearable energy harvesters are suitable for harvesting energy from human movements such as finger and arm joint movements, and they have potential for application in the detection of the direction of vibration sources, which is suitable for motion monitoring.

6.4 Conclusions

In this study, well-aligned PZT/SMPU-based electrospun nanofibers were prepared and fabricated into wearable energy harvesters. By adjusting the alignment angle of the nanofibers, which acted as the main load-bearing object, the proportion of the nanofibers was optimized to improve energy harvesting efficiency under the influence

of bending and twisting motions. The results obtained revealed that Wear-0 and Wear-45 had higher energy harvesting efficiencies, and their maximum output voltages were 39.6 and 63.1 mV owing to the bending and twisting motions, respectively. The ANSYS code was used to stimulate the stress distribution in the energy harvesters and clarify the mechanism by which the alignments angles of the nanofibers enhanced the output voltages corresponding to different motions. The simulation results showed that the maximum stresses applied on Wear-0 and Wear-45 were increased by at least 7.4% and 11.5%, respectively, because of the bending and twisting motions. The consistency between the nanofiber alignment and strain directions enabled Wear-0 and Wear-45 energy harvesters to be identified as optimal structures based on their output voltages.

For practical tests, flexible energy harvesters were taped onto the human body to convert mechanical energy into electricity. Relative to the random nanofiber-based energy harvesters, the aligned PZT/SMPU nanofibers-based wearable energy harvesters showed different performances under different types of human movements. Wear-0 and Wear-45 showed higher energy harvesting efficiencies under finger bending and wrist twisting motions, and their maximum output voltages were 537 and 55 mV, respectively, and this represents an increase of at least 27.9% compared with those of other samples. These results demonstrate that adjusting the alignment angle according to the bending or twisting directions from the joints has an effect on the performance of the energy harvesters. However, under tests for applying pressure, there were no obvious differences between the random and aligned energy harvesters.

In addition, the effect of the alignment angle on the piezoelectric properties of the

energy harvesters in the longitudinal direction was investigated. Wear-0 showed better piezoelectric properties, and under the same impulse force, they generated an output voltage higher than those of other samples, i.e., 282 mV, which was 4.2-folds higher than that generated by Wear-90. This enhanced output voltage generation could primarily be attributed to the desirable distribution of dielectric inclusions, which induced high local electric fields along the polarization direction. This enhanced the performance of the energy harvesters and their ability to act as sensors considering their high efficiency and sensitivity.

This study provides insight into the control and design of the alignment angle of nanofibers in wearable energy harvesters based on the movement directions of different joints to improve energy harvesting properties.

Reference

[1] C.-M. Wu, M.-H. Chou, T.F. Chala, Y. Shimamura, R.-i. Murakami, Infrared-driven poly (vinylidene difluoride)/tungsten oxide pyroelectric generator for non-contact energy harvesting, Composites Science and Technology 178 (2019) 26-32.

[2] K. Liu, H.J. Choi, B.K. Kim, D.B. Kim, C.S. Han, S.W. Kim, H.B. Kang, J.-W. Park, Y.S. Cho, Piezoelectric energy harvesting and charging performance of Pb (Zn1/3Nb2/3) O3–Pb (Zr0. 5Ti0. 5) O3 nanoparticle-embedded P (VDF-TrFE) nanofiber composite sheets, Composites Science and Technology 168 (2018) 296-302.

[3] A. Alsaadi, Y. Shi, L. Pan, J. Tao, Y. Jia, Vibration energy harvesting of multifunctional carbon fibre composite laminate structures, Composites Science and

Technology 178 (2019) 1-10.

[4] K. Takei, W. Honda, S. Harada, T. Arie, S. Akita, Toward flexible and wearable human-interactive health-monitoring devices, Adv Healthc Mater 4(4) (2015) 487-500.

[5] H.K. Yap, N. Kamaldin, J.H. Lim, F.A. Nasrallah, J.C.H. Goh, C.-H. Yeow, A magnetic resonance compatible soft wearable robotic glove for hand rehabilitation and brain imaging, IEEE transactions on neural systems and rehabilitation engineering 25(6) (2016) 782-793.

[6] S. J. Varma, K. Sambath Kumar, S. Seal, S. Rajaraman, J. Thomas, Fiber-type solar cells, nanogenerators, batteries, and supercapacitors for wearable applications, Advanced Science 5(9) (2018) 1800340.

[7] Y.C. Lai, J. Deng, S. Niu, W. Peng, C. Wu, R. Liu, Z. Wen, Z.L. Wang, Electric eel-skin-inspired mechanically durable and super-stretchable nanogenerator for deformable power source and fully autonomous conformable electronic-skin applications, Advanced Materials 28(45) (2016) 10024-10032.

[8] X. Guan, H. Chen, H. Xia, Y. Fu, J. Yao, Q.-Q. Ni, Flexible energy harvester based on aligned PZT/SMPU nanofibers and shape memory effect for curved sensors, Composites Part B: Engineering (2020) 108169.

[9] Y. Cha, Energy harvesting using flexible piezoelectric materials from human walking motion: Theoretical analysis, J. Intell. Mater. Syst. Struct. 28(20) (2017) 3006-3015.

[10] M. Pozzi, M. Zhu, Characterization of a rotary piezoelectric energy harvester based on plucking excitation for knee-joint wearable applications, Smart Materials and

Structures 21(5) (2012) 055004.

[11] M. Matsunaga, J. Hirotani, S. Kishimoto, Y. Ohno, High-output, transparent, stretchable triboelectric nanogenerator based on carbon nanotube thin film toward wearable energy harvesters, Nano Energy 67 (2020) 104297.

[12] T. Ghomian, S. Mehraeen, Survey of energy scavenging for wearable and implantable devices, Energy (2019).

[13] Z. Liu, C. Pan, C. Yen, L. Lin, J. Huang, C. Ke, Crystallization and mechanical behavior of the ferroelectric polymer nonwoven fiber fabrics for highly durable wearable sensor applications, Appl. Surf. Sci. 346 (2015) 291-301.

[14] X. Mo, H. Zhou, W. Li, Z. Xu, J. Duan, L. Huang, B. Hu, J. Zhou, Piezoelectrets for wearable energy harvesters and sensors, Nano Energy (2019) 104033.

[15] W. Zeng, X.-M. Tao, S. Chen, S. Shang, H.L.W. Chan, S.H. Choy, Highly durable all-fiber nanogenerator for mechanical energy harvesting, Energy & Environmental Science 6(9) (2013) 2631-2638.

[16] F. Gao, G. Liu, B.L.-H. Chung, H.H.-T. Chan, W.-H. Liao, Macro fiber composite-based energy harvester for human knee, Applied Physics Letters 115(3) (2019) 033901.

[17] S. Vigneswari, V. Murugaiyah, G. Kaur, H.A. Khalil, A. Amirul, Simultaneous dual syringe electrospinning system using benign solvent to fabricate nanofibrous P (3HB-co-4HB)/collagen peptides construct as potential leave-on wound dressing, Materials Science and Engineering: C 66 (2016) 147-155.

[18] N.H.A. Ngadiman, A. Idris, M. Irfan, D. Kurniawan, N.M. Yusof, R. Nasiri, γ-Fe2O3 nanoparticles filled polyvinyl alcohol as potential biomaterial for tissue

engineering scaffold, Journal of the mechanical behavior of biomedical materials 49 (2015) 90-104.

[19] R. Ramachandramoorthy, A. Beese, H. Espinosa, In situ electron microscopy tensile testing of constrained carbon nanofibers, International Journal of Mechanical Sciences 149 (2018) 452-458.

[20] D.-N. Nguyen, Y. Hwang, W. Moon, Electrospinning of well-aligned fiber bundles using an End-point Control Assembly method, European Polymer Journal 77 (2016) 54-64.

[21] S.B. Kang, S.H. Won, M.J. Im, C.U. Kim, W.I. Park, J.M. Baik, K.J. Choi, Enhanced piezoresponse of highly aligned electrospun poly (vinylidene fluoride) nanofibers, Nanotechnology 28(39) (2017) 395402.

[22] C. Jin, H. Fan, Y. Wang, H. Hwang, Y. Zhang, Q. Wang, Electrospinning aligned and random environmental-friendly BCTZ nanowires for high-performance energy harvester, Ceramics International 43(16) (2017) 14476-14480.

[23] L. Zhang, J. Gui, Z. Wu, R. Li, Y. Wang, Z. Gong, X. Zhao, C. Sun, S. Guo, Enhanced performance of piezoelectric nanogenerator based on aligned nanofibers and three-dimensional interdigital electrodes, Nano Energy 65 (2019) 103924.

[24] M. Ren, Y. Zhou, Y. Wang, G. Zheng, K. Dai, C. Liu, C. Shen, Highly stretchable and durable strain sensor based on carbon nanotubes decorated thermoplastic polyurethane fibrous network with aligned wave-like structure, Chemical Engineering Journal 360 (2019) 762-777.

[25] X. Guan, H. Chen, H. Xia, Y. Fu, Y. Qiu, Q.-Q. Ni, Multifunctional composite

nanofibers with shape memory and piezoelectric properties for energy harvesting, J. Intell. Mater. Syst. Struct. (2020) 1045389X20906477.

[26] Y. Zhang, M. Xie, J. Roscow, Y. Bao, K. Zhou, D. Zhang, C.R. Bowen, Enhanced pyroelectric and piezoelectric properties of PZT with aligned porosity for energy harvesting applications, Journal of Materials Chemistry A 5(14) (2017) 6569-6580.

[27] L. Padurariu, L.P. Curecheriu, L. Mitoseriu, Nonlinear dielectric properties of paraelectric-dielectric composites described by a 3D Finite Element Method based on Landau-Devonshire theory, Acta Mater. 103 (2016) 724-734.

Chapter 7: General conclusions

PZT/SMPU composite fibers and nanofibers are prepared with two combined smart effects (piezoelectric and shape memory effects). The developed PZT/SMPU composite fibers and nanofibers not only exhibit excellent shape memory properties but also show superior energy harvesting properties from external vibration. The remarkable performance ensures that the resultant composites can be applied in a wide range of applications due to the piezoelectric or shape memory effect. This would facilitate the development of the flexible energy harvester and harvesting energy from complex surfaces. The main conclusions of this study are given below.

In the Chapter 2, the optimal method to prepare PZT/SMPU composites was proposed and the characterization of the developed materials was clarified. The proposed surface modification significantly improved the dispersion of PZT particles in the SMPU matrix, and enhanced the interactive force between particles and the polymer matrix， while PZT particles aggregate together before modification and showed weak interfacial bonding between fillers and the polymer matrix due to the poor dispersion. The results proved that the silane coupling agents are coated on the surface of PZT particles, as a bridge to bind the SMPU matrix and particles. Thus, the saline coupling agents improve the dispersion and interfaces between the fillers and polymer matrix. The aligned SMPU and PZT/SMPU nanofibers are distributed in the rotation direction with alignment degrees of 0°, 45° and 90°, leading to the formation of high-density PZT/SMPU nanofiber mats, while the random nanofibers were disordered in spatial orientation and exhibited a wide range of alignment degrees. The results from

BET surface area and density show that the aligned nanofibers (including SMPU and PZT/SMPU nanofibers) have lower BET surface area and higher density, compared with the random nanofibers, indicated that the aligned nanofibers have higher volume of nanofibers and more compact in the same area.

In the Chapter 3, the static and cyclic mechanical measurements were conducted and their mechanical properties were clarified. The influence of the filler content and the effect of modification on their mechanical properties were also studied. The results showed that compared to unmodified samples, random PZT/SMPU nanofibers exhibited superior mechanical properties, including yield stress, tensile stress and elastic modulus. The enhanced performance is considered as a result of from the increased interfacial interactions enhanced by silane coupling agents. Additionally, the recovery rate and recovery stress of modified PZT/SMPU nanofibers are higher than those of unmodified nanofibers because of the increased storage modulus by modification. Even the content of PZT reaches 80%, the shape recovery rates are still no less than 84.8%, revealing a good shape recovery ability of modified nanofibers. The strong interface also helps the stress transmission between PZT fillers and the SMPU matrix, leading to the higher energy harvesting properties than those of unmodified nanofiber.

According to the optimal alignment degree of nanofibers, the mechanical properties of aligned nanofibers show higher yield stress, elastic modulus, tensile strength and breaking strain than those of randomly oriented nanofibers. The alignment angles play an important role in mechanical properties. This is because the volume of nanofibers

along the strain direction determines overall mechanical properties, which bears the main applied load during the tensile process. The aligned nanofibers are drafted and stretched along the longitudinal direction during the preparation process, which endows aligned nanofiber with higher stored energy than that of random nanofibers and enhance elasticity and stiffness.

In the Chapter 4, the excellent shape memory properties of pristine SMPU and PZT/SMPU composite nanofibers were investigated, and the mechanism of shape recovery and fixing were clarified. With the increasing content of PZT fillers, the improvement of storage modulus gives rise to the shape recovery stress, while such high-content particles hinder the movement of the SMPU molecular chain and decrease the shape recovery rate. Compared with random SMPU nanofibers, aligned SMPU nanofibers have more orientation ratio of nanofibers along the loading direction and higher stiffness, which may cause the less polymer chain slippage of soft segments during tensile and the low strain above T_g. This can explain why aligned nanofibers have a higher shape recovery rate than that of random nanofibers. Furthermore, the aligned SMPU and PZT/SMPU nanofibers with higher elastic modulus are more easily to recover from the strain after removing stress than restricted ones, leaving longer strain retention and lower shape fixity than those of random nanofibers.

In the Chapter 5, the piezoelectric effect of PZT/SMPU composite fibers and nanofibers were discussed relative to the output voltage generation in response to applied external stress. The influence and mechanism of the alignment degree on the energy harvesting performance at various acceleration, frequency and displacements

were systemically investigated. With the increasing vibration frequency, the output voltages rapidly increased and reached the maximum value, because the increasing frequency can boost the straining rate under the same applied acceleration. With the increasing acceleration and displacements, the peak-to-peak voltages generated by the aligned nanofiber-based energy harvester increased, because the increasing accelerations can improve stresses. The energy harvesting properties are associated with the alignment degree of the nanofiber. The aligned nanofibers along the poling direction and strain direction can augment the strain rate and mechanical stress, thus enhance output voltages. The aligned PZT/SMPU nanofibers can generate more output voltages compared with random nanofibers. Even at the same content of piezoelectric materials, the higher specific density of aligned nanofibers increased energy harvesting properties.

In the Chapter 6, the developed PZT/SMPU nanofibers were endowed to a promising potential in the energy harvesting for curved surfaces due to shape memory effect and easy deformation of SMPs. The PZT/SMPU nanofiber-based energy harvester can be deformed to match the shape of the designed complex surface, and then fix the temporary shape after cooling down to room temperature. This kind of intimate attachment facilitates energy harvester to closely match complex structures, resulting in higher output voltages, even under high acceleration.

In summary, PZT/SMPU composites possess both piezoelectric and shape memory effects. The prepared multifunctional smart composite material can be applied in various fields. More efforts should be made to continuously address technical problems

and develop more applications in future works.

List of Publications

Guan, X., Chen, H., Xia, H., Fu, Y., Qiu, Y., & Ni, Q. Q. (2020). Multifunctional composite nanofibers with shape memory and piezoelectric properties for energy harvesting. Journal of Intelligent Material Systems and Structures, 1045389X20906477.

Guan X, Chen H, Xia H, et al. Flexible energy harvester based on aligned PZT/SMPU nanofibers and shape memory effect for curved sensors[J]. Composites Part B: Engineering, 2020: 108169.

Guan X, Dong Y, Xia H, et al. Mechanical and shape memory performance of shape memory polyurethane-based aligned nanofibers[J]. Polymer Testing, 2020: 106778.

Ni, Q. Q., **Guan, X**., Zhu, Y., Dong, Y., & Xia, H. (2020). Nanofiber-based wearable energy harvesters in different body motions. Composites Science and Technology, 108478. (co-first author)

Scientific Presentation

- **International conference**

1. **Xiaoyu Guan**, Hairong Chen, Xia Hong and Qing-Qing Ni, Shape memory and piezoelectric composites for energy harvesting, SYMPOSIUM OF ADVANCED COMPOSITES in Sapporo, Hokkaido, Japan.
2. **Xiaoyu Guan**, Hairong Chen and Qing-Qing Ni, Multifunctional Composites for Energy Harvesting, The 22nd International Conference on Composites Materials (ICCM22), Melbourne, Australia.
3. **Xiaoyu Guan**, Hairong Chen and Qing-Qing Ni, Smart Composites with shape memory effect and piezoelectric effect for energy harvesting, Sixth International Conference on Multifunctional, Hybrid and Nanomaterials 2019, 2019, Sitges, Spain.
4. **Xiaoyu Guan**, Hairong Chen and Qing-Qing Ni, Smart composites of Piezoelectric and shape memory properties for Energy Harvesting, The Second International Forum on Textiles for Graduate Students (IFTGS), 2018, Tianjin, China.
5. **Xiaoyu Guan**, Hairong Chen and Qing-Qing Ni, The preparation of SMPU/PZT piezoelectric fibers, Workshop of Advanced Composites, 2017, Ueda, Japan.
6. **Xiaoyu Guan**, Hairong Chen and Qing-Qing Ni, The preparation of SMPU/PZT piezoelectric fibers, The First International Forum on Textiles for Graduate Students (IFTGS), 2017, Tianjin, China.
7. **Xiaoyu GUAN**, Qing-Qing Ni, Preparation and Research of Wet-laid Thermo-

Bonded Nonwovens, 4th International Symposium on Advanced Textile Science and Technology cum the International Seminar on Silk Fashion Design and Development Trend, 2016, Hangzhou, China.

- **Domestic conference**

1. **Xiaoyu Guan**, Hairong Chen, Xia Hong and Qing-Qing Ni, Multifunctional Smart Textile For Energy Harvesting, 繊維学会秋季研究発表会, 2019, Nagano.
2. **Xiaoyu Guan**, Hairong Chen, Xia Hong and Qing-Qing Ni, Smart Composites for two different kinds of energy harvesting, 第 10 回日本複合材料会議(JCCM-10), 2019, Tokyo.
3. **Xiaoyu Guan**, Kazuki HIBINO, Yuichiro ITO and Qing-Qing Ni, The development of multi-layer and 3d dimensional fabric structures and its application, 第 9 回日本複合材料会議(JCCM-9), 2018, Kyoto.
4. **Xiaoyu Guan**, Hairong Chen and Qing-Qing Ni, The Preparation of SMPU/PZT Piezoelectric Fibers, 第 8 回日本複合材料会議(JCCM-9), 2017, Tokyo.

Acknowledgements

I would like to appreciate my supervisor Prof. Qing-Qing Ni for his continuous support and encouragement. He not only guides me in the research to overcome various problems but also encourages me to struggle for anything. Thanks to his guidance, I can successfully obtain a PhD degree.

It is my pleasure to get assistance from many people during my research. I would like to express my most sincere gratitude to all of them.

Many thanks also to Prof. Toshiaki Natsuki and Prof. Yasuo Gotoh for the help in experiments. We deeply discussed mechanical and chemical work.

I also want to thank Dr. Hong Xia who gives me a lot of help in experiments. Without her assistance, I could not make huge progress in my research.

I gratefully acknowledge the funding received towards my PhD from the Interdisciplinary Graduate School of Science and Technology (Shinshu University) to give me financial support.

I greatly appreciate the support received from technicians in Shinshu University, Okada Yusuke, Adachi Etsuko, Shinozuka Makiko, Takeda Masaaki, Nakamura Miho, Yoshioka Sachiko, Nakamura Isao, Nishida Ayako, Hayashi teruhiko, Shinohara chiburi for their kindness and help. Their suggestions are conducive to my experiments.

My colleagues, Ran Li, Juhong Yu, Jian Xing, Wanwan Liu, Zhe Yang, Ke Ma, Zhong Wang, Xiangdong Xiong, Yongjie Yan, Jun Hong, Jing Hui, Yinan Jing, Yajun Liu, Xiaojuan Li, Canyi Huang, Lina Cui, Fengyu Li, Baoji Hu, Jingyan Qu, Ping Xu, Wendan Yang, Chongchao Li, Si Chen, Guangyu Su, Peng Zhu, Chuanfang Xie, Ye Sun,

Kailun Chen, Jian Yang, Bing Liu, Jiaping Zhang, Yuan Wen, Xu Wang, Li Yang, Wei Li, Caiqian Zhang, DO VIET TIEN and Heng Zhang, kindly support all the time. I am also very grateful to Hairong Chen who helps a lot in my research.

I also need to thank someone. Even though your forsaking depresses me, I finally cheer myself up. This mistake inspires me and lets me know that the world is not worth it. I become more positive and move on.

Finally, I need to thank my parents who encouraged and supported me completely at every stage of my personal and academic life.